DNA 5531F

MITIGATION OF EXPLOSION BUBBLE PULSATION CAUSED BY THE DEEP UNDERWATER DETONATION OF A TAPERED CHARGE

Physics International Company
2700 Merced Street
San Leandro, California 94577

31 October 1980

Final Report for Period 21 April 1980—31 October 1980

CONTRACT No. DNA 001-80-C-0125

THIS WORK SPONSORED BY THE DEFENSE NUCLEAR AGENCY
UNDER RDT&E RMSS CODE B344080464 Y99QAXSD07059 H2590D.

Prepared for
Director
DEFENSE NUCLEAR AGENCY
Washington, D. C. 20305

Destroy this report when it is no longer needed. Do not return to sender.

PLEASE NOTIFY THE DEFENSE NUCLEAR AGENCY, ATTN: STTI, WASHINGTON, D.C. 20305, IF YOUR ADDRESS IS INCORRECT, IF YOU WISH TO BE DELETED FROM THE DISTRIBUTION LIST, OR IF THE ADDRESSEE IS NO LONGER EMPLOYED BY YOUR ORGANIZATION.

UNCLASSIFIED

SECURITY CLASSIFICATION OF THIS PAGE (When Data Entered)

REPORT DOCUMENTATION PAGE		READ INSTRUCTIONS BEFORE COMPLETING FORM
1 REPORT NUMBER DNA 5531F	2. GOVT ACCESSION NO. AD-A107804	3. RECIPIENT'S CATALOG NUMBER
4 TITLE (and Subtitle) MITIGATION OF EXPLOSION BUBBLE PULSATION CAUSED BY THE DEEP UNDERWATER DETONATION OF A TAPERED CHARGE		5. TYPE OF REPORT & PERIOD COVERED Final Report for period 21 April 1980-31 October 1980
		6. PERFORMING ORG. REPORT NUMBER PIFR-1426
7 AUTHOR(s) J. M. Thomsen S. F. Ruhl		8. CONTRACT OR GRANT NUMBER(s) DNA 001-80-C-0125
9. PERFORMING ORGANIZATION NAME AND ADDRESS Physics International Company 2700 Merced Street San Leandro, California 94577		10. PROGRAM ELEMENT, PROJECT, TASK AREA & WORK UNIT NUMBERS Subtask Y99QAXSD070-59 62704H
11 CONTROLLING OFFICE NAME AND ADDRESS Director Defense Nuclear Agency Washington, D.C. 20305		12 REPORT DATE 31 October 1980 13 NUMBER OF PAGES 212
14. MONITORING AGENCY NAME & ADDRESS(if different from Controlling Office)		15. SECURITY CLASS. (of this report) UNCLASSIFIED 15a. DECLASSIFICATION/DOWNGRADING SCHEDULE N/A

16 DISTRIBUTION STATEMENT (of this Report)

Approved for public release; distribution unlimited.

17. DISTRIBUTION STATEMENT (of the abstract entered in Block 20, if different from Report)

18. SUPPLEMENTARY NOTES

This work sponsored by the Defense Nuclear Agency under RTD&E RMSS Code B344080464 Y99QAXSD07059 H2590D.

19. KEY WORDS (Continue on reverse side if necessary and identify by block number)

Underwater Shock	TNT
Explosion Bubbles	HBX-1
NWE Simulation	Propellants
Tapered Charge	Bubble Pulsation

20. ABSTRACT (Continue on reverse side if necessary and identify by block number)

The dynamics of the explosion bubble growth and collapse due to the underwater detonation of a 5.3-m-long (17.5-ft) tapered charge containing 454 kg (1000 lb) of TNT are examined calculationally. The burst was 305 m (1000 ft) below the sea surface in deep water. The calculational method, using a coupled Eulerian-Lagrangian finite-difference hydrodynamics computer code, was made credible by successfully calculating the explosion bubble dynamics of spherical TNT charges detonated at the same depth of burst.

(cont.)

DD FORM 1 JAN 73 1473 EDITION OF 1 NOV 65 IS OBSOLETE

UNCLASSIFIED

SECURITY CLASSIFICATION OF THIS PAGE (When Data Entered)

20. ABSTRACT (cont.)

Results show that the tapered charge explosion bubble exhibits characteristics that are very similar to an equal-weight spherical charge over the first bubble period. This implies that bubble pulses will be produced by tapered charge detonations at this depth and deeper.

The bubble pulses emitted by deep tapered charge detonations are not characteristic of the underwater nuclear detonation that these charges are designed to simulate. In fact, for conventional charges, bubble reloading of models is severe, and can lead to their (unplanned) collapse. Three methods of tapered charge bubble pulse mitigation were examined: (1) injection of propellant gas into the bubble to prevent/cushion collapse, (2) dissipation of bubble energy through enhancement of turbulence at the first minimum by creating an asymmetric bubble, and (3) using an explosive that produces condensible/soluble detonation products, thereby allowing more rapid transfer of bubble energy to the water and preventing the creation of a substantial bubble pulse. Results show that (2) and (3) are promising methods of bubble pulse mitigation. Additional computational and experimental work must be done to quantify the effectiveness of these methods, and to produce specific test designs.

PREFACE

The authors would like to thank Dr. Andrew P. Misovec of Weidlinger Associates, Chesapeake, VA, and Mr. John R. Krezel and Mr. John D. Gordon of the Underwater Explosions Research Division of the David Taylor Naval Ship Research and Development Center, Portsmouth, VA for their contributions throughout the program. We would also like to thank Dr. W. Conley, Dr. D. Phillips, Dr. L. Roslund, Dr. A. Van Tuyl, Dr. H. Sternberg, Dr. W. Walker, and Mr. M. Swisdak of the Naval Surface Weapons Center, White Oak, MD, and Dr. M. Finger and Dr. T. Butkovich of the Lawrence Livermore National Laboratory, Livermore, CA, for the useful conversations held with them. Mr. Fred M. Sauer, Senior Staff Scientist of the Nuclear Effects Division of Physics International Company, provided overall technical direction of the effort.

During the program, CDR Thomas J. Deevy, USN, was the DNA Contracting Officer's representative; Lt. Col. John Galloway was the Acting Chief of the Strategic Structures Division.

TABLE OF CONTENTS

TABLE OF CONTENTS (cont.)

LIST OF ILLUSTRATIONS

LIST OF ILLUSTRATIONS (cont.)

LIST OF ILLUSTRATIONS (cont.)

LIST OF ILLUSTRATIONS (cont.)

LIST OF TABLES

SECTION 1

INTRODUCTION

Using tapered charges is currently the best way to simulate the pressure pulse generated by an underwater nuclear detonation (Reference 1). At depths less than approximately 30 m (100 ft) the simulation is quite good, if the pressure pulse is sufficiently planar at the model location, and if the explosion bubble vents through the surface.

Recent survivability requirements (Reference 2) demand exposure of models to simulated nuclear pressure pulses at depths of 300 to 600 m (1,000 to 2,000 ft). As part of the current Underwater Explosion (UNDEX) Test Series, 1/9th-scale models will be tested in deep water to both conventional high explosive and simulated-nuclear pressure pulses (Reference 3).

The effects of reloading due to the repeated explosion bubble pulses at these depths are not well known, and are generally much more severe for conventional charges than for nuclear detonations. Since most models to be tested are impulse sensitive, understanding the pulsation of the explosion bubble is becoming increasingly important, even for conventional depth charges. For deep underwater nuclear shock simulations using tapered charges, very little is known about the characteristics of the accompanying explosion bubble, and bubble reloading must be substantially reduced or eliminated (Reference 4).

Physics International Company (PI) participated in a research effort to examine explosion bubble growth and collapse from conventional explosives in deep water. Calculations were performed for both spherical and tapered high explosive charges, and methods were examined by which bubble pulsation might be eliminated, or at least substantially reduced. This report represents an initial effort to calculate and assess the effects of nonspherical bubble pulsation in deep water, a subject that may be of increased interest during the 1980s.

In Section 2 we review tapered charge designs, and present the "baseline" tapered charge geometry used in the two-dimensional calculations; in Section 3 we discuss the equation-of-state models. In Section 4 we review the literature concerning explosion bubbles from spherical explosive charges, and verify that bubble growth and collapse over the first bubble period can be accurately computed for this simple case. In Section 4 we also review what is known about nonmigrating, multiple bubble pulsation. In Section 5 we present the calculation of the tapered charge explosion bubble, and conclude that bubble pulsation will occur. Three methods of bubble pulse mitigation are then examined. In Section 6 we present the results of investigating the originally proposed method, that of supplying a propellant gas source to the explosion bubble to prevent, or at least cushion bubble collapse. In Section 7 we discuss two additional, more promising methods of bubble pulse mitigation.

SECTION 2

BASELINE TAPERED CHARGE DESIGN

Tapered charges have been used for more than 20 years to simulate nuclear shock waves in water. A typical nuclear shock wave in water is shown in Figure 2.1 (Reference 5). Tapered charges are long, slender explosive charges; Figure 2.2 (Reference 5) shows an example of such a charge. The charge is detonated at one end, and the time for complete detonation of the charge is controlled by the total charge length. Figure 2.3 shows water pressure and velocity for one such charge detonated in shallow water (Reference 5). The gages were located along the axis of the charge, off the charge end where the charge was detonated. A plateau pressure of 2 MPa (300 psi) was obtained; this pressure can be adjusted by varying the total explosive weight and/or the distance of the gage location from the charge (Reference 6).

Tapered charges have been built and expended with lengths from 0.6 to 10.7 m (2 to 35 ft) and total explosive weights of 4 to 4,500 kg (10 to 10,000 lb). The most common types have weights of 227 to 454 kg (500 to 1,000 lb), diameters of 0.3 to 0.46 m (12 to 18 in.), and lengths of approximately 6.1 m (20 ft) (Reference 7). An up-to-date listing of information on tapered charges fired in the past is maintained by Weidlinger Associates, Chesapeake, VA (Reference 4).

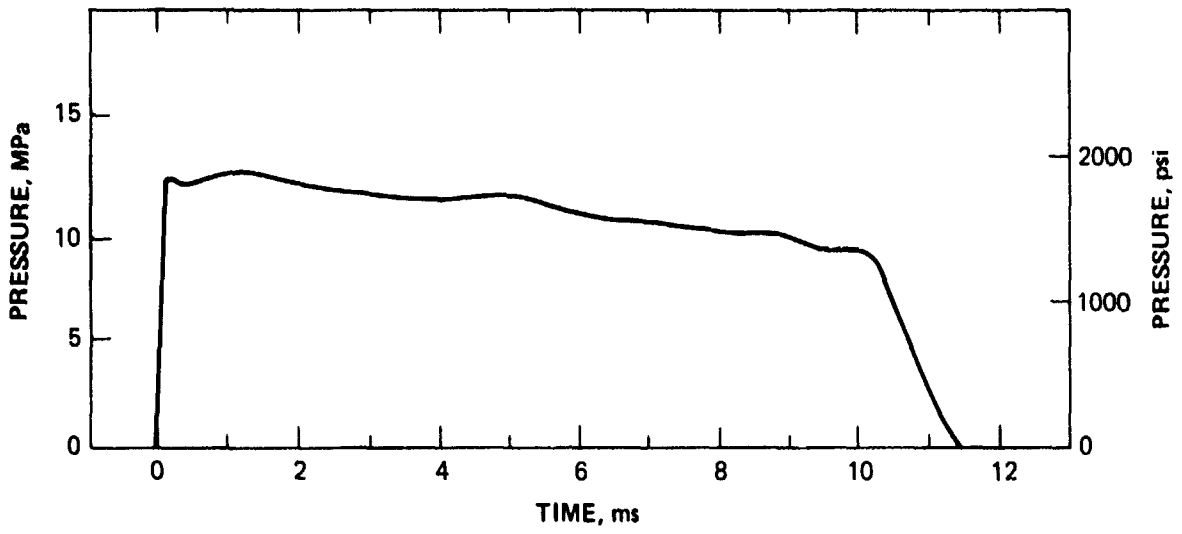

Figure 2.1 Measured nuclear underwater shock wave (courtesy of Mr. J. D. Gordon, UERD).

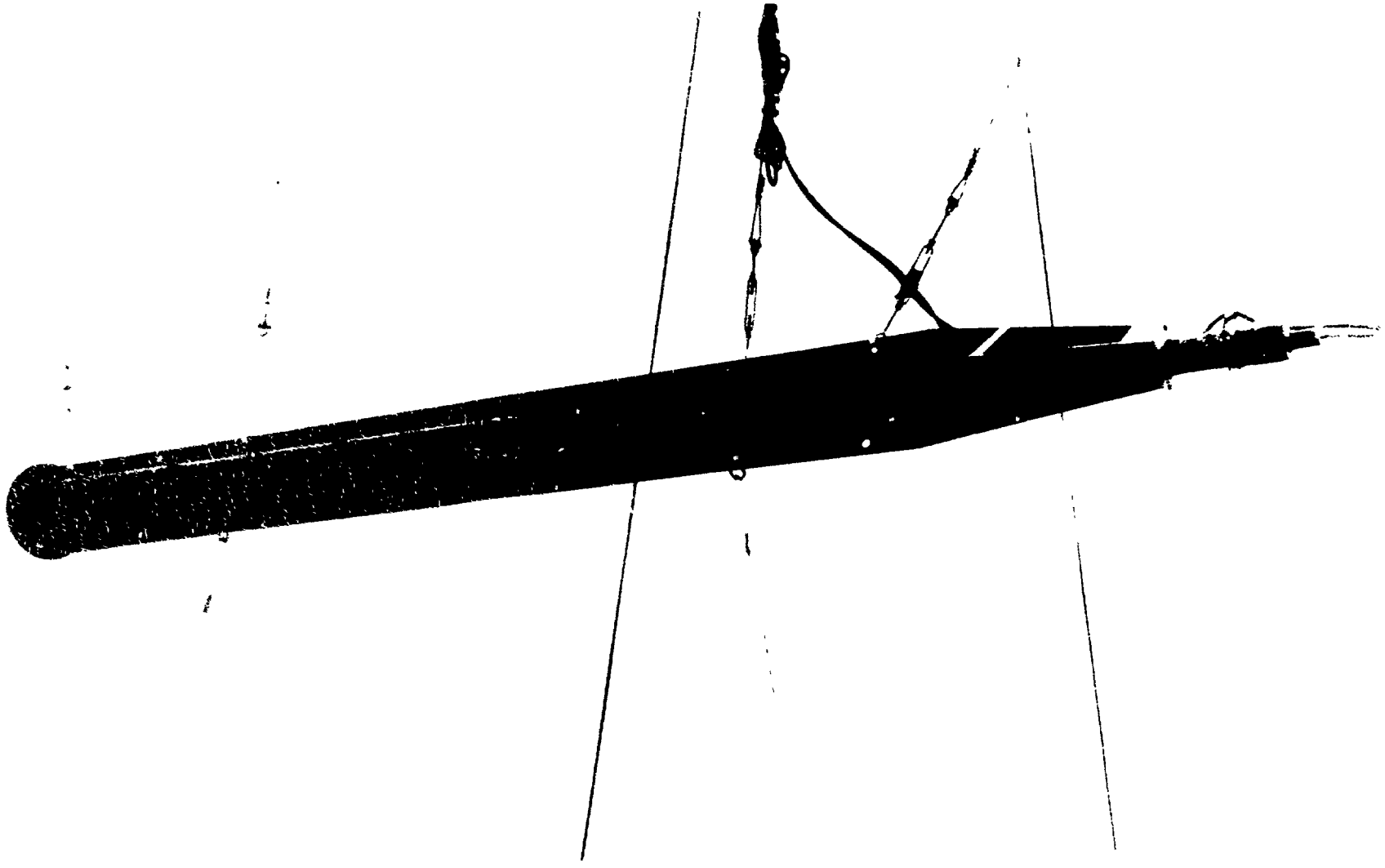

Figure 2.2 Tapered charge used in underwater nuclear shock wave simulation experiments (courtesy of Mr. John D. Gordon, UERD).

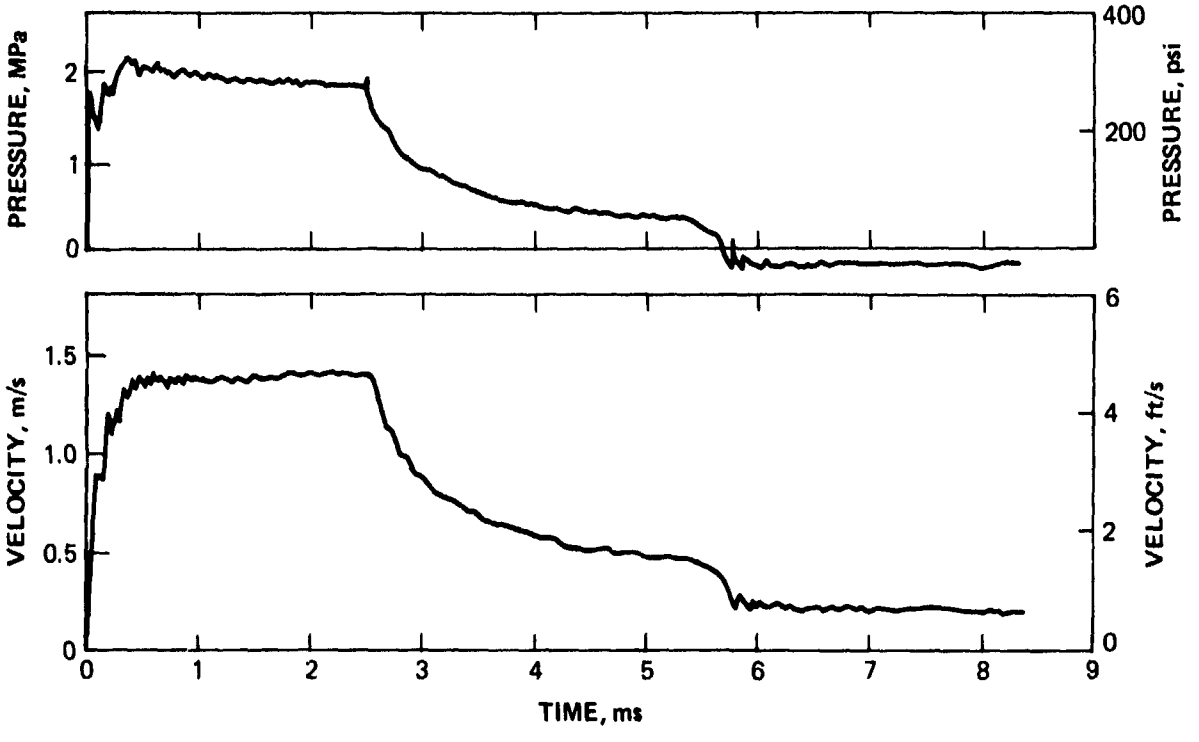

Figure 2.3 Water pressure and velocity from tapered charge detonated in shallow water (courtesy of Mr. John D. Gordon, UERD).

A typical design was obtained from personnel of the Underwater Explosions Research Division (UERD) of the David W. Taylor Naval Ship Research and Development Center, Portsmouth, VA (Reference 7). This design is shown in Figure 2.4; this charge was modeled in the two-dimensional (2D) calculations. A nominal water depth of 305 m (1,000 ft) was chosen for the depth of the detonation.

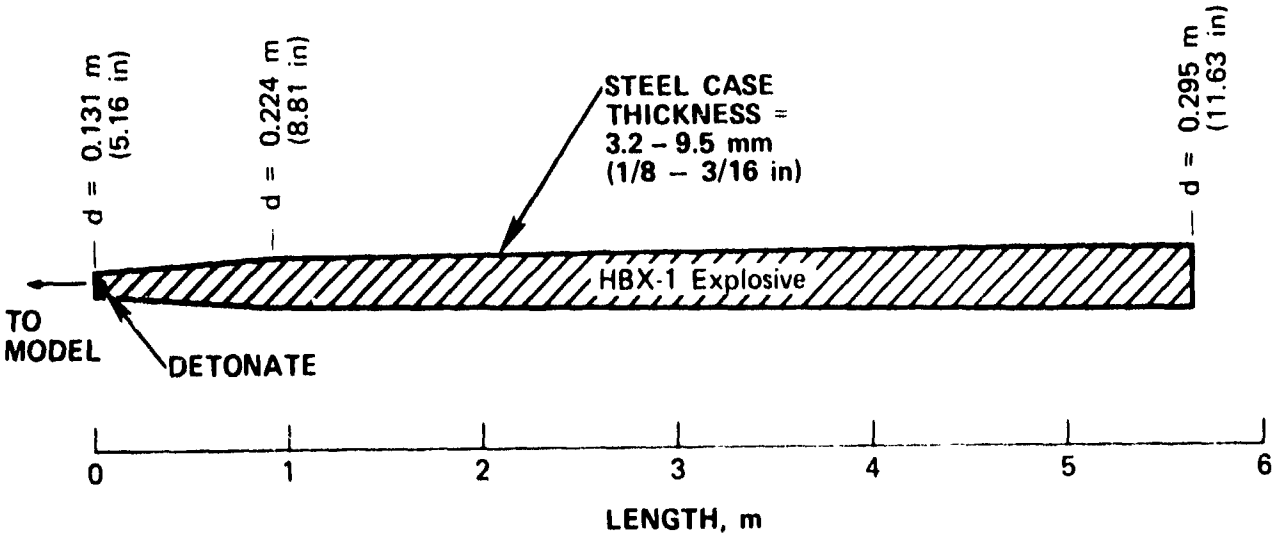

Figure 2.4 Representative design for a 454-kg (1000-lb) tapered charge (courtesy of Mr. J. Krezel, UERD).

SECTION 3

EQUATIONS OF STATE

To perform the calculations of bubble growth and shock wave propogation resulting from the detonation of a tapered charge under water, equations of state (EOSs) for High Blast Explosive-1 (HBX-1) and water were required. An EOS for TNT was also required for the 1D check problems performed to compare the bubble growth and shock wave parameters with the empirically predicted values. Because the existing HBX-1 EOS was found to be inadequate for underwater explosion bubble problems, the TNT EOS was used for the 2D calculational effort as well. This section presents the equations of state used for these materials.

3.1 EXPLOSIVES

The EOS for TNT is well described by the Jones-Wilkins-Lee (JWL) model (Reference 8). This EOS describes the adiabatic expansion of the explosion products for a wide range of explosives, including TNT. The JWL EOS form is widely accepted, and will not be described again here, as it is very well described in Reference 8. The TNT coefficients used are given in Table 3.1.

HBX-1 is an aluminized explosive, with constituents as shown in Table 3.2 (Reference 9). An EOS was developed for this explosive by Roslund and Coleburn of the U.S. Naval Ordinance Laboratory (Reference 10). The EOS form is a modified JWL form where

Table 3.1 JWL EOS coefficients for TNT.

A	=	3.712
B	=	0.0323
C	=	0.0104527
R_1	=	4.15
R_2	=	0.95
ω	=	0.30
E_o	=	4.46 X 10^3 J/g (0.07 Mbar-cm^3/cm^3)
ρ_o	=	1.56 Mg/m^3 (1.56 g/cm^3)
D	=	6.93 m/ms (0.693 cm/μs)

E_o: Total energy released per unit explosive mass

ρ_o: Initial explosive density

D: Explosive detonation velocity

Table 3.2 Constituents of HBX-1.

Constituent	Percent
RDX	40
TNT	38
Aluminum powder	17
D-2 wax	5
Calcium chloride	0.5

the pressure, P, in the explosive is given as a function specific volume, V:

$$P = \begin{cases} B \exp(-kV) + WG_1 V^{-(1+W)} & V < V_c \\ G_2 (V + V^*)^{-1} & V > V_c \end{cases} \qquad (3.1)$$

The constants of Equation 3.1 and Chapman-Jouguet (C-J) properties for HBX-1 are given in Table 3.3. These explosive properties were determined largely through tests in which the explosive products expanded into air. Figure 3.1 compares the TNT and HBX-1 adiabats. Because of the late-time contribution of the aluminum powder to the explosive energy release, the pressures at large relative volumes (greater than 100) are about seven times larger for HBX-1 than for TNT. It is the pressures at these large specific volumes that control the bubble growth at times when the bubble radius is close to the maximum radius.

3.2 WATER

The water EOS chosen was that due to Walker and Sternberg (Reference 11). This model gives pressure as a function of density and internal energy on the Hugoniot, and for adiabatic release off the Hugoniot for initial shock pressures up to 25 GPa (250 kbar). Table 3.4 summarizes the EOS in code units. Isentropes for this EOS are compared with those obtained from Butkovich (Reference 12) in Figure 3.2. The Walker and Sternberg EOS makes no attempt to model the production of steam below the saturation line, so the two models disagree below that point. Above the saturation line, however, the two models agree very well. The question of steam production is discussed in Section 4.

Table 3.3 EOS constants for HBX-1

$\rho = 1.712\ g/cm^3$

$\rho_o = 1.624\ g/cm^3$

$D = 7.307\ mm/\mu s$

$\gamma_{CJ} = 2.934$

$P_{CJ} = 22.04\ GPa\ (220.4\ kbar)$

$\mu_{CJ} = 1.858\ mm/\mu s$

$\rho_{CJ} = 2.178\ g/cm^3$

$dD/d\rho_o = 3800\ m/s/g/cm^3$

$\alpha = 0.1325$

$W = 0.3432$

$V_C = 1.15 cm^3/g$

$P_C = 0.3645\ GPa\ (3.645\ kbar)$

$k = 6.450\ g/cm^3$

$B = 418.7\ GPa\ (4.187\ Mbar)$

$G_1 = 0.397\ GPa\ (3.97\ kbar)$

$G_2 = 9.142 \times 10^9\ (cm/s)^2$

$V^* = 1.358\ cm^3/g$

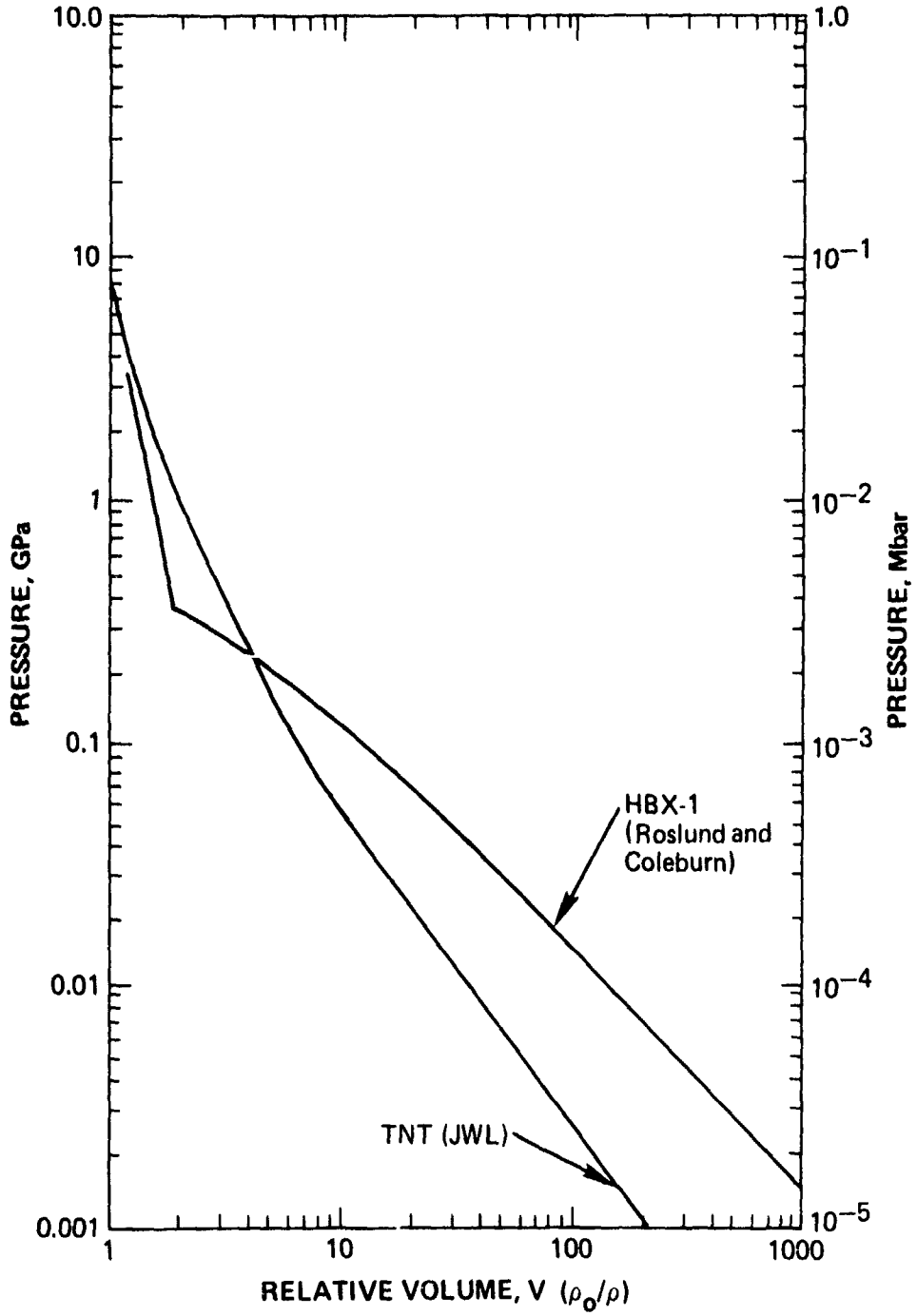

Figure 3.1 JWL TNT adiabat compared with the modified JWL adiabat for HBX-1.

Table 3.4 Summary of water EOS model of Walker and Sternberg.

$$p\ (\text{mbar}) = f_1 \rho + f_2 \rho^3 + f_3 \rho^5 + f_4 \rho^7$$

ρ = current density (g/cm^3); $\rho_o = 0.9982$ g/cm^3

$0 < E < 0.006$	$f_1 = 0.005722427 - 1.240522\ E + 50.42535\ E^2 - 1.400579 \times 10^3 E^3 + 4.137950 \times 10^6 E^4 - 2.726437 \times 10^8 E^5 - 1.295684 \times 10^{11} E^6 + 1.437988 \times 10^{13} E^7$
$0.006 < E < 0.017$ $(E' = E - 0.006)$	$f_1 = 0.001015091 - 0.3270122\ E' + 6.734616\ E'^2 + 1.552785 \times 10^4 E'^3 - 2.926440 \times 10^6 E'^4 + 2.139341 \times 10^8 E'^5 - 5.61538 \times 10^9 E'^6$
$0.017 < E$ $(E'' = E - 0.017)$	$f_1 = 5.607572 \times 10^{-4} + 0.1122840\ E'' + 5.27579\ E''^2 + 82.21745\ E''^3 - 147.1514\ E''^4 - 4.044093 \times 10^3 E''^5 - 3.130131 \times 10^4 E''^6$
$0 < E < 0.0032$	$f_2 = -0.02748180 + 1.691130\ E + 17.12981\ E^2 + 1.483364 \times 10^4 E^3 - 1.549072 \times 10^7 E^4 + 3.415591 \times 10^9 E^5 - 2.357818 \times 10^{11} E^6$
$0.0032 < E < 0.0245$ $(E' = E - 0.0032)$	$f_2 = -0.02215430 + 1.510990\ E' - 10.56299 E'^2 - 5.411856 \times 10^3 E'^3 + 6.176871 \times 10^5 E'^4 - 1.810118 \times 10^7 E'^5 - 6.205700 \times 10^8 E'^6 + 4.406075 \times 10^{10} E'^7 - 6.587460 \times 10^{11} E'^8$
$0.0245 < E$ $(E'' = E - 0.0245)$	$f_2 = 0.002499950 + 0.9374720\ E'' - 4.624610\ E''^2 - 44.52203\ E''^3 + 375.1364\ E''^4$
	$f_3 = 0.0268 - 0.4148\ E$
	$f_4 = -0.005 + 0.0741\ E$

E = internal energy in mbar-cm^3/g

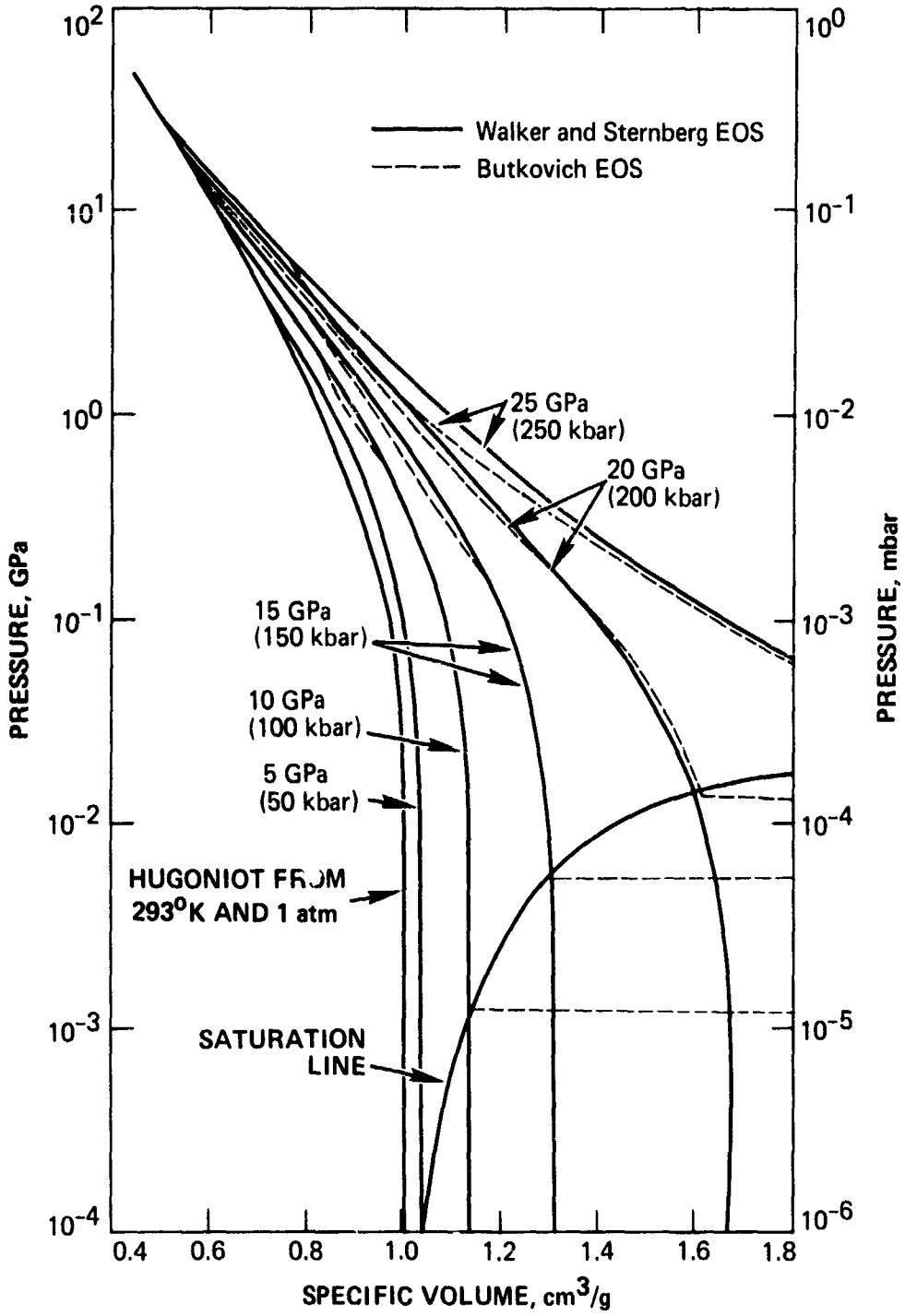

Figure 3.2 Water isentropes calculated using the Walker and Sternberg EOS model compared with those calculated by Butkovich.

SECTION 4

UNDERWATER EXPLOSION BUBBLE GROWTH AND COLLAPSE FOR SPHERICAL CHARGES

The purpose of the work discussed in this section was to verify that the calculational tools (i.e., computer codes, equations of state, initial condition, etc.) could calculate the case of the detonation of a spherical charge under water. Once the tools were validated, they could be used to compute the much more difficult problem of the detonation of a tapered charge under water. Section 4.1 reviews briefly what is known about explosion bubbles; Section 4.2 shows that the computed results for the spherical case* agree with empirical formulas; Section 4.3 discusses steam generation, and Section 4.4 discusses what is known about multiple bubble pulsation.

4.1 LITERATURE REVIEW

Experimental and theoretical research into the dynamics of explosion bubble growth and collapse began during World War I, reached a peak during World War II, and continued for 10 to 15 years after the end of World War II. It was found that upon detonation of a spherical or near-spherical charge in deep water, the initial shock wave was followed by a series of secondary shock waves. Theoretical treatments showed that the secondary shocks could be traced to a pulsating bubble that occupied the

*Detonation of a 454-kg (1000-lb) spherical TNT charge in water at a depth of 305 m (1000 ft).

region surrounding the explosive charge. Laboratory-scale experiments confirmed this. An excellent summary of early work is given in Reference 13, which is a compendium of British and American reports concerned with explosion bubble dynamics.

Upon detonation of a spherical explosive charge in deep water, a shock wave is transmitted to the water and propagates away from the source. After passage of the initial shock, the water retains a residual velocity. The detonation products expand into the approximately spherical void around the charge; the void is caused by the radial motion of the water away from the charge. Hydrostatic pressure halts the growth of the explosion bubble eventually, but the pressure within the bubble at this first bubble maximum radius (A_m) is far less than the hydrostatic pressure. This pressure imbalance is remedied through the collapse of the bubble, which recompresses the explosive products. The pressures reached within the bubble at the time of the first bubble minimum radius (T_1) exceed the hydrostatic pressure; this leads to a second shock propagation radially outward in the water as the bubble reexpands. This second shock is the bubble pulse. The process of bubble expansion and contraction can be repeated many times. Figure 4.1 (Reference 14) shows the bubble radius versus time for a specific case.

Theoretical models of bubble oscillation generally treat the water as an incompressible fluid. Cole (Reference 14) and Snay (Reference 15), among others, describe models that ignore the gas

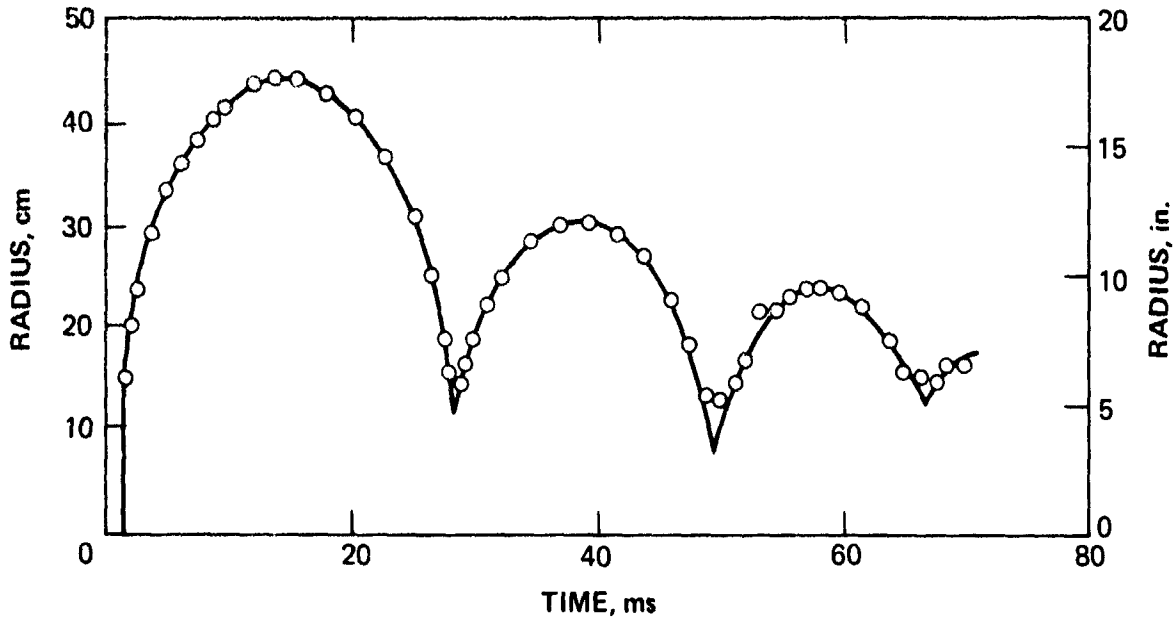

Figure 4.1 Radius of the gas sphere as a function of time for a 0.25-kg (0.55-lb) tetryl charge 91 m (300 ft) below the surface (from Cole, Reference 14).

pressure within the bubble. Pritchett (Reference 16) reviews similar models that include the bubble pressure, and gives an excellent summary of spherical bubble dynamics. In addition to the above analytic techniques, hydrodynamic calculations have been performed using incompressible flow computer codes (References 16-18). The incompressible approach cannot give correct results for the initial bubble expansion, or near the bubble minimum, because the pressures during those times are high enough that water is slightly compressible (Reference 15).

Formulas derived from the analytic models can be used to predict A_m and T_1. These are found to be a function of charge weight, W, the type of explosive used, and the hydrostatic pressure, P_o. P_o can be expressed in terms of Z, the charge depth plus the atmospheric head:

$$A_m = J \frac{W^{1/3}}{Z^{1/3}} , \qquad (4.1)$$

and

$$T_1 = K \frac{W^{1/3}}{Z^{5/6}} . \qquad (4.2)$$

The constants J and K depend on the units chosen, and on the type of explosive used. In m-kg-s units,

$$J = 3.50\ m^{4/3}/kg^{1/3} \qquad (4.3)$$

and

$$K = 2.11\ s\text{-}m^{5/6}/kg^{1/3} \qquad (4.4)$$

for TNT, and Z equals the water depth plus 10 m. Thus, for a 454-kg (1000-lb) spherical TNT charge detonated at a depth of 305 m (1000 ft), A_m = 3.95 m (13 ft) and T_1 = 134 ms. For HBX-1,

$$J = 3.95\ m^{4/3}/kg^{1/3} \qquad (4.5)$$

and

$$K = 2.41\ s\text{-}m^{5/6}/kg^{1/3}, \qquad (4.6)$$

so for a 454-kg (1000-lb) spherical HBX-1 charge detonated at the same depth, A_m = 4.46 m (14.6 ft) and T_1 = 153 ms. The above, and many other empirical formulas, are summarized in a recent report by Swisdak (Reference 19).

Thus, the dynamics of explosion bubble growth and collapse in deep water (i.e., where the hydrostatic gradient over the maximum bubble diameter is small) are treatable in one dimension using analytical tools, and these give results that agree very

well with experimental data over the first bubble period (Reference 20). Theoretical work concerning nonspherical explosion bubble expansion and collapse has been limited, although the analytic equations have been formulated (Reference 14). The main reason is that these equations are extremely difficult to solve for specific cases.

4.2 ONE-DIMENSIONAL VALIDATION CALCULATIONS

One-dimensional (1D) computer calculations were performed simulating the detonation of 454-kg (1000-lb) spherical charges of TNT and HBX-1 explosives at a depth of 305 m (1000 ft) in deep water. Figure 4.2 shows the zoning and initial conditions for these calculations. The zoning is the result of a series of preliminary 1D calculations in which finer zoning was used, both in the explosive and in the water.

Results of these calculations include the pressure and particle velocity at and behind the initial shock in the water at all ranges as a function of time, the pressure of the explosive products (within the explosion bubble) versus time, and the motion of the water/explosion products interface. For this effort, which concentrated on the behavior of the explosion bubble, the latter two results were of the greatest interest. Figures 4.3a and 4.3b show the computed explosion bubble radius and bubble pressure histories for the spherical TNT charge. The bubble radius reaches a maximum of 4.05 m (13.3 ft), and then decreases to a minimum radius of about 0.9 m (3 ft) at T_1 =145 ms. The internal bubble pressure decreases rapidly to a value much less than the hydrostatic pressure P_o. The minimum bubble

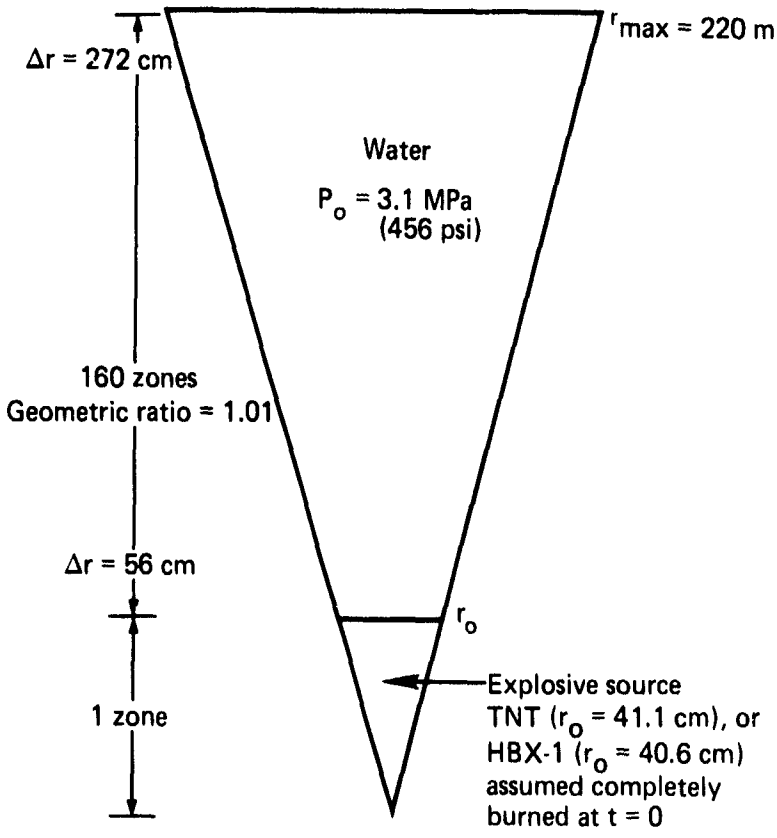

Figure 4.2 Zoning and initial conditions for 1D validation calculations.

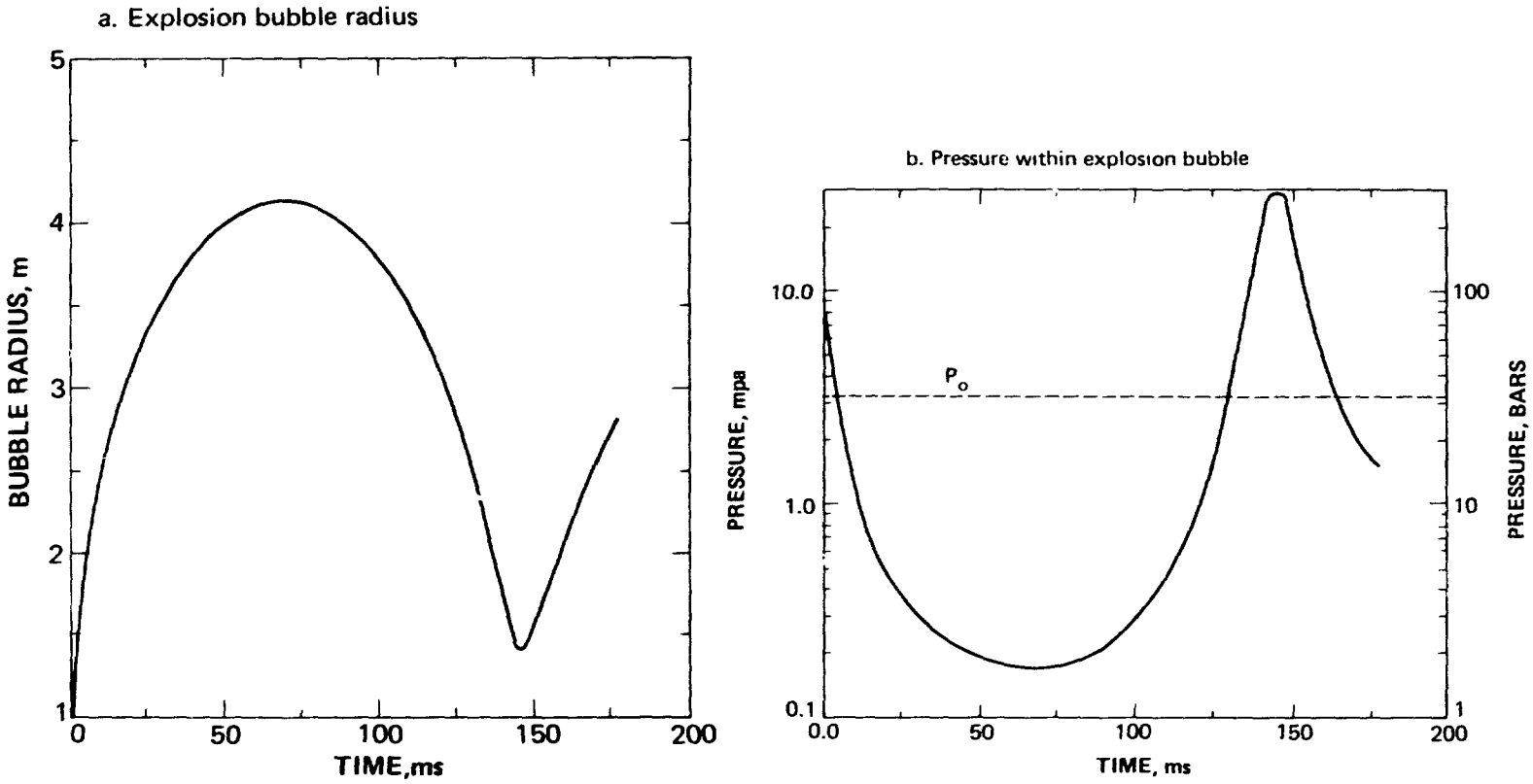

Figure 4.3 Calculated bubble parameters versus time for a 454-kg (1000-lb) spherical TNT charge detonated in water at a depth of 305 m (1000 ft).

pressure is about 0.2 MPa (29 psi), whereas P_o = 3.1 MPa (456 psi). Bubble collapse occurs because P_o reverses the radial velocity field in the water. Since the pressure within the bubble is much less than P_o, it initially offers very little resistance to the collapse process. As the bubble is recompressed during collapse, the internal pressure rises, and reaches a value of about 30 MPa (4400 psi) at T_1.

Table 4.1 compares computed and empirical (Reference 19) values of A_m and T_1 for TNT and HBX-1. For TNT, both A_m and T_1 agree very well with empirical formulas. This is not the case for HBX-1, however, where both A_m and T_1 are much larger than empirical formulas predict. After a detailed investigation, we concluded that current knowledge about the HBX-1 EOS is not adequate to enable calculation of explosion bubble growth and collapse. Since the computer simulations were validated for TNT, we concluded that all 2D calculations should be performed using TNT.

Similar calculations of explosion bubble growth and collapse have been performed by Mader (Reference 21) and Walker (Reference 22). For spherical Pentolite charges, Walker investigated explosion growth and collapse at water depths of 4267 m (14,000 ft) and 7010 m (23,000 ft) and found good agreement with empirical formulas. This work tends to support the contention that HBX-1 is not characterized well enough for this type of computational effort.

Computed results of the shock in the water were also examined in the 1D calculations. Figure 4.4 shows computed pressure

Table 4.1 Comparison of computed and empirical explosion bubble parameters for 454-kg (1000-lb) spherical TNT and HBX-1 charges detonated in deep water at a depth of 305 m (1000 ft).

	Swisdak (Empirical)	PISCES Calculation
TNT		
Maximum Bubble Radius (A_m)	3.95 m	4.05 m (+2.5%)
Time for First Bubble Period (T_1)	135 ms	145 ms (+7.4%)
HBX-1		
Maximum Bubble Radius (A_m)	4.46 m	5.7 m (+27.8%)
Time for First Bubble Period (T_1)	153 ms	225 ms (+46.2%)

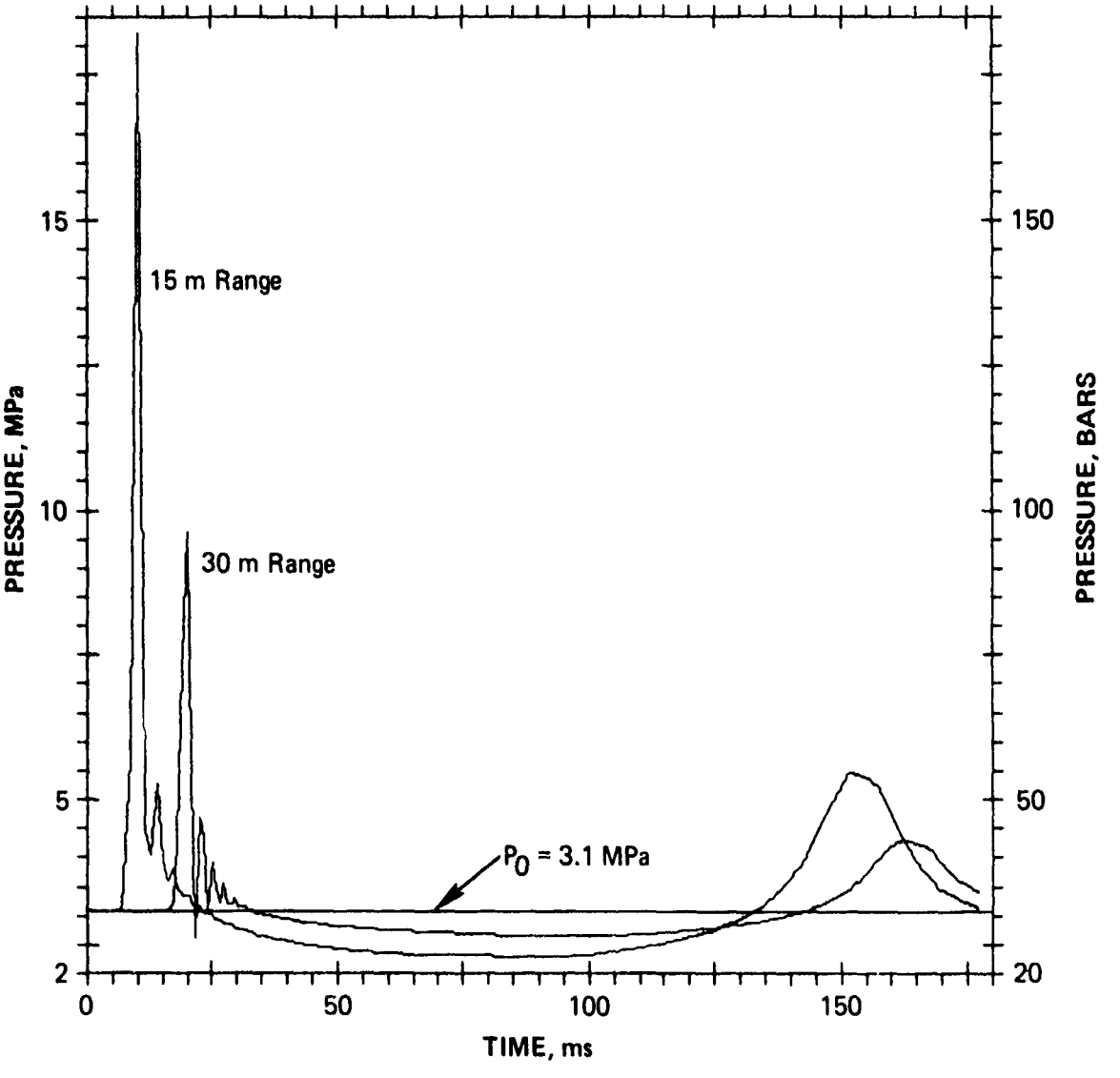

Figure 4.4 Calculated shock wave in water for a 454-kg (1000-lb) spherical TNT charge detonated at 305 m (1000 ft) depth in water.

versus time, 15-m (49-ft) and 30-m (98-ft) from a 454-kg (1000-lb) spherical TNT charge. The initial shock is followed by a "negative phase," where the water pressure is less than P_o, and this is followed by the bubble pulse. Figure 4.5 shows the general characteristics of the pressure pulse from a deep explosion, and defines terms. These characteristics can be predicted using empirical formulas (Reference 19), and the computed results are compared to the empirically predicted ones in Table 4.2. Computed maximum pressures are uniformly low compared with empirically predicted maximum pressures. This is to be expected because a finite-difference computer code will spread out the shock. Sternberg and Walker (Reference 23) found that a shock-following technique was required to accurately compute maximum shock pressures (P_{pp}) for an underwater detonation.

4.3 THE PROBLEM OF STEAM GENERATION

The water EOS of Walker and Sternberg does not compute the production of steam below the saturation curve. In their paper, Walker and Sternberg (Reference 11) examine the contribution of steam-generated pressure within the bubble for Pentolite explosive detonated in water. Their conclusion is that steam, even if generated, would not significantly raise the pressure within the bubble. For our tapered charge calculations, we decided to further investigate the problem of steam generation. A cylindrically symmetric 1D calculation was performed to examine the peak pressures close to the cylindrical charge. In the calculation, the explosive was detonated in over 10 zones, and the first water zone was mass-matched to the mass of the last explosive zone.

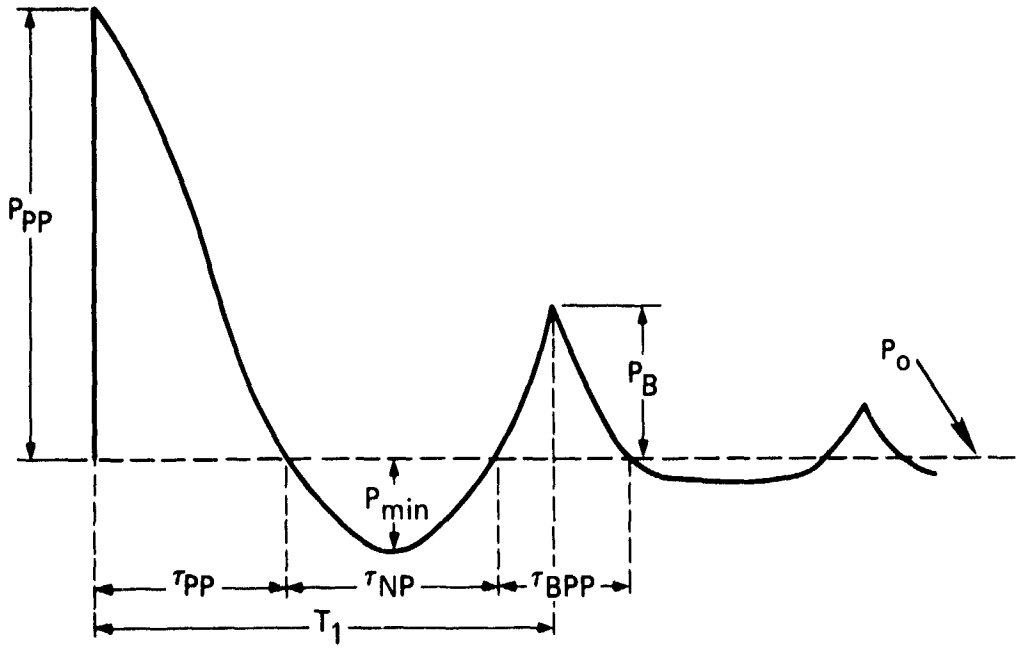

Figure 4.5 Pressure pulse characteristics of deep explosions (from Swisdak, Reference 19).

Table 4.2 Shock wave and bubble pulse comparsion for TNT [454 kg (1000 lb) at 305 m (1000 ft)].

Shock Wave Parameters	PISCES (Calculated)		Swisdak (Empirically Predicted)	
	15 m	30 m	15 m	30 m
Peak Overpressure, P_{pp}	15 MPa	6.5 MPa	24 MPa	11 MPa
Positive Phase Duration, τ_{pp}*	17 ms	17 ms	17 ms	17 ms
Negative Phase Duration, τ_{NP}*	108 ms	108 ms	124 ms	124 ms
Minimum Negative Phase Overpressure, P_{min}	-0.7 MPa	-0.4 MPa	-0.7 MPa	-0.35 MPa
Bubble Pulse Positive Phase, τ_{BPP}*	45 ms	45 ms	34 ms	34 ms
Bubble Pulse Peak Pressure, P_B	2.4 MPa	1.2 MPa	4.6 MPa	2.3 MPa

*These variables are independent of range.

The charge radius was set at 14.75 cm (corresponding to the thickest part of the cylindrical tapered charge), the first water zone was 2 cm thick, and an increasing zoning ratio of 2 percent was used from there on within the water.

Figure 4.6 plots the maximum shock pressure in the water versus range from the charge from this calculation. Only three zones show a maximum pressure of greater than 5 GPa (50 kbar); for less than that value, steam will not form, even in an equilibrium situation, according to the Butkovich water model. A cylindrical envelope surrounding the charge with an approximate thickness of 6 cm could possibly generate steam when the pressure within that region of shocked water falls below the corresponding pressure on the saturation curve. This corresponds to a pressure of approximately 1 MPa (10 bars), or about one-third of the hydrostatic pressure at a depth of 305 m. Thus, steam production can contribute (if it forms at all) only to the late-time pressure within the bubble, i.e., near the time when the bubble reaches its maximum radius. This means that it will not contribute significantly to the initial bubble growth. For these calculations, this is a conservative assumption.

This calculation was continued to investigate explosion bubble growth and collapse in cylindrical symmetry. This corresponds to an infinitely long cylindrical charge with a diameter of 0.30 m (1.0 ft). Figures 4.7a and 4.7b show the bubble radius and pressure versus time. If the baseline tapered charge were long enough that cylindrical symmetry dominated, one would expect these results to be valid. Although A_{max} is smaller than for the spherical charge (3.15 m versus 4.05 m), T_1 is much longer (250 ms versus 145 ms).

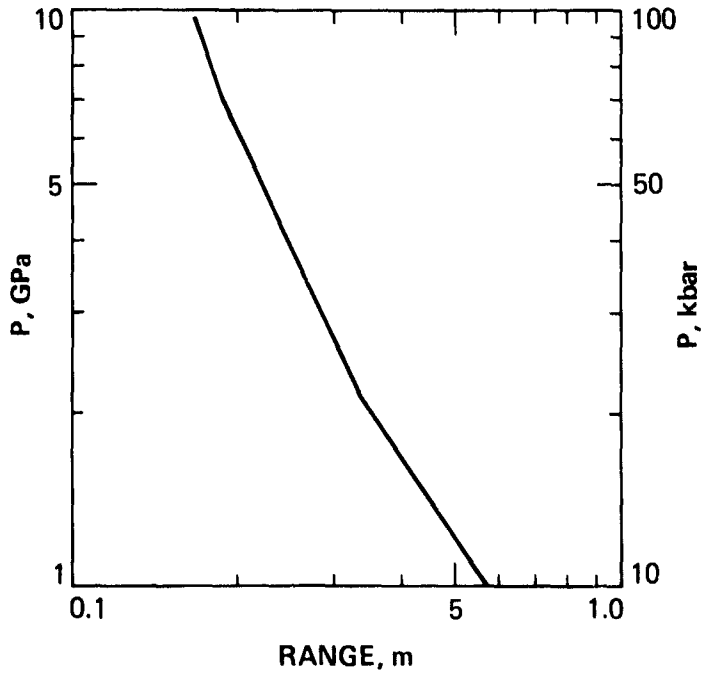

Figure 4.6 Maximum pressure versus range from a cylindrical TNT charge with an initial radius of 14.75 cm [the maximum radius of the chosen 454-kg (1000-lb) tapered charge].

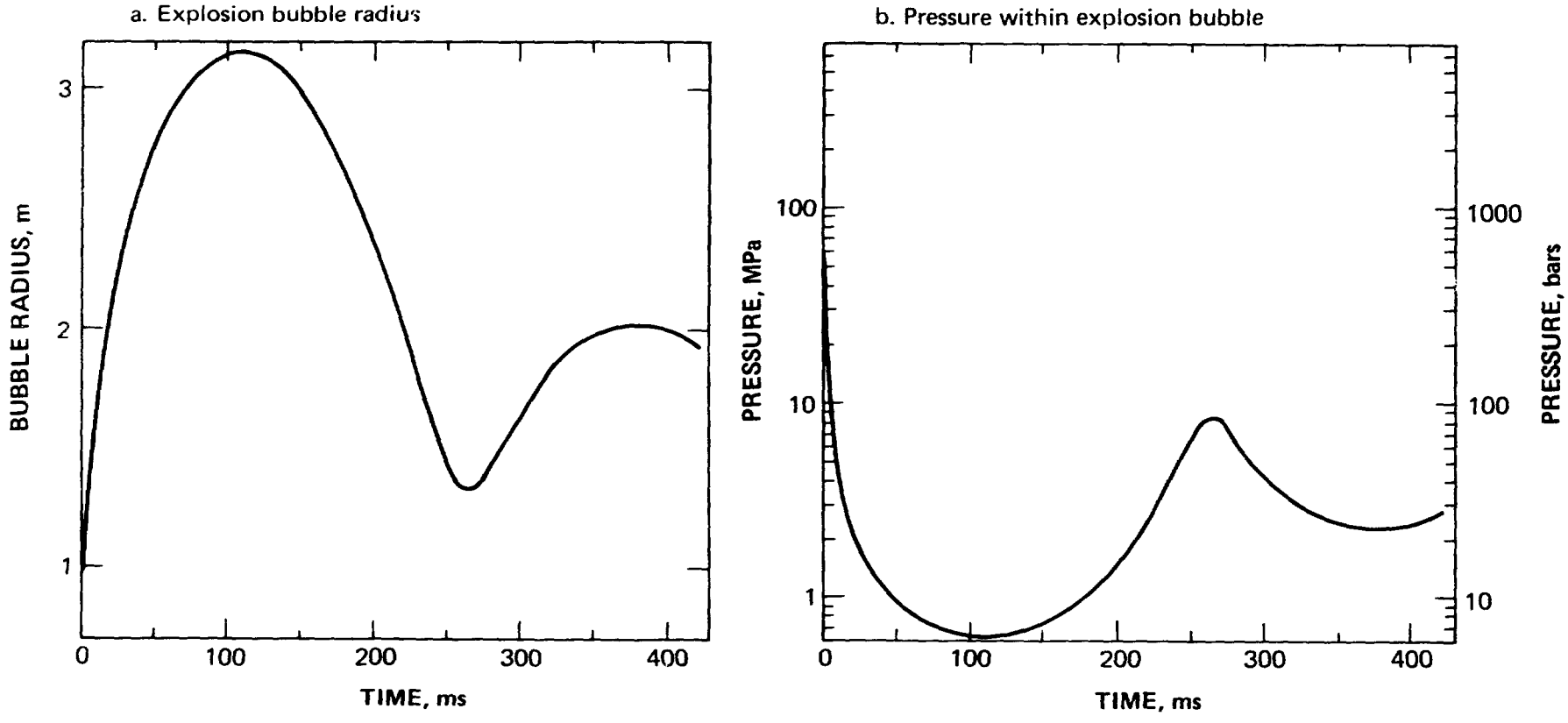

80-11-253

Figure 4.7 Calculated bubble parameters versus time for an infinitely long cylindrical TNT charge with a diameter of 0.30 m (1.0 ft) detonated in water at a depth of 305 m (1000 ft).

4.4 MULTIPLE BUBBLE PULSATION

Explosion bubble reexpansion after T_1 causes the bubble pulse to propagate in the surrounding water. This process removes internal energy from the bubble. Other loss mechanisms, such as heat conduction and turbulence, also tend to remove energy from the bubble by heating the surrounding water. Pritchett (Reference 16) provides an excellent discussion of these energy loss mechanisms.

In underwater high explosive detonations at deep depths, bubble oscillation can be followed through up to seven cycles before the bubble is reduced to a benign gas pocket, or to many small bubbles. In underwater nuclear detonations at deep depths, bubble reloading does not appear to be as effective because the energy loss per cycle from the bubble appears to be larger. Figure 4.8 qualitatively compares high explosive and nuclear bubble pulsation (Reference 16). The key difference between the two is that the nuclear-generated explosion bubble is filled primarily with steam (generated by the initial shock wave), while the high explosive bubble is filled primarily with noncondensible gaseous explosive products. This point is pursued later in this report.

Since the purpose of this work was to examine explosion bubble pulsation from high explosive charges, an effort was made to examine multiple bubble pulsation in order to estimate how much the bubble is degraded by each oscillation. Experimental data that give bubble radius versus time for more than one bubble period appear to be sparse. The best measurements, and the ones most often quoted, are derived from Swift and Decius (Reference 24). Figure 4.9 shows bubble radius versus time for a

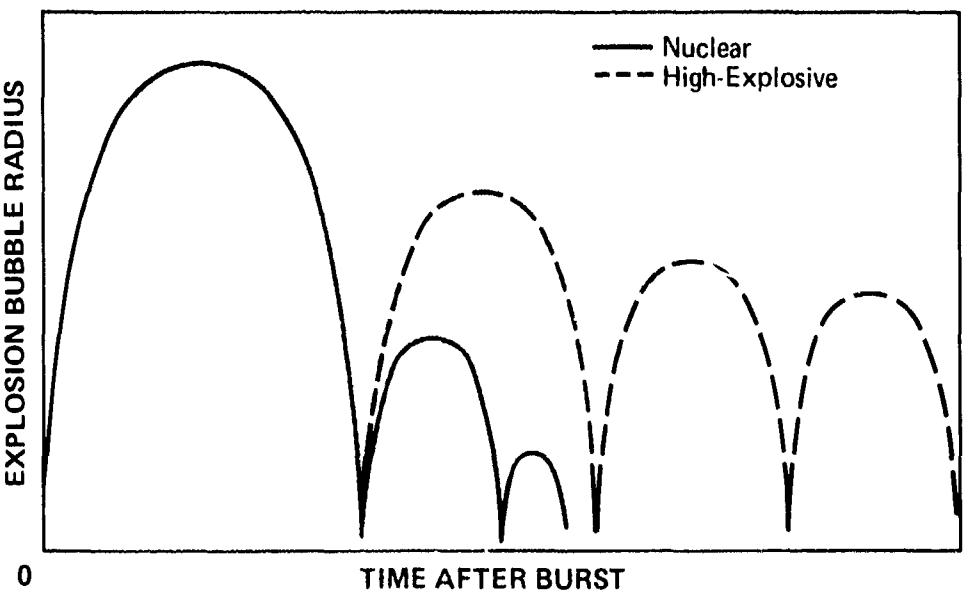

80-11-256

Figure 4.8 The effects of bubble energy loss--the nonmigrating case (from J. Pritchett, Reference 16).

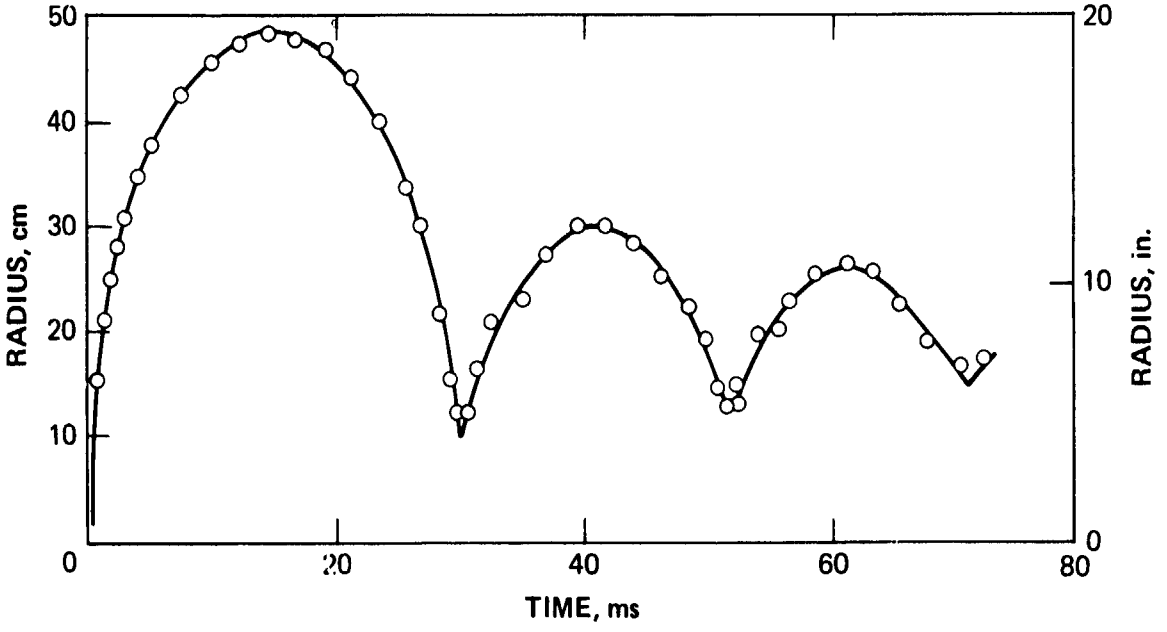

80-11-255

Figure 4.9 Explosion bubble radius versus time curve for a 0.3-kg (0.66-lb) TNT charge detonated in water at a depth of 91 m (300 ft) (from Reference 24).

0.3-kg (0.66-lb) TNT charge detonated in water at a depth of 91 m (300 ft). The first bubble radius and period are by far the largest, and a significant amount of the bubble energy appears to be absorbed in the first bubble collapse and reexpansion process.

Table 4.3 examines the TNT test data from Reference 22 for the first three periods of bubble oscillation. Average values of J and K (defined by equations 4.1 and 4.2) decrease with each oscillation. Figure 4.10 plots these average values versus period number, n. We are not certain if the power-law decay of J and K with period number is valid for $n > 3$, so the extrapolations to $n = 10$ are shown by dashed lines. Based on the valid part of the curves ($n = 1$ to 3), the effective bubble energy (W_{eff}) relative to the first period for a nonmigrating bubble can be calculated using cube root scaling; this is done in Table 4.3. W_{eff} for the second period is only about 40 percent of that on the first period, and on the third period is about 20 percent. If the extrapolation of Figure 4.9 is valid, W_{eff} is reduced to at most 10 percent of its first period value by the 6th period. Also, W_{eff} based on J and K give different values, possibly indicating that the partitioning of energy within the bubble region is different on each oscillation. Bubble period data from Slifko (Reference 25) for TNT charges were also analyzed, and the data are presented in Table 4.4. The data for the 3.6- and 86-kg (8- and 57-lb) charges generally agree with the data presented in Table 4.3; the 0.45-kg (1-lb) charges appear to be less efficient than the larger ones.

Bubble energy losses arise from two sources: the bubble pulse in the water due to the compressibility of water, and turbulence and related effects that operate near the bubble minimum. To assess the relative effects of these two loss

Table 4.3 Bubble parameter analysis and calculation of the effective bubble energy using experimental data (from Ref. 24).

Bubble Period	Avg J_n $m^{4/3}/kg^{1/3}$	Avg K_n $s\text{-}m^{5/6}/kg^{1/3}$	Effective Bubble Energy, W_{eff} Based on J_1	Based on K_1
First (n=1)	3.36 ± 0.01	2.10 ± 0.01	1.0	1.0
Second (n=2)	2.27 ± 0.05	1.55 ± 0.02	0.31 ± 0.03	0.40 ± 0.02
Third (n=3)	1.76 ± 0.03	1.32 ± 0.05	0.14 ± 0.01	0.25 ± 0.03

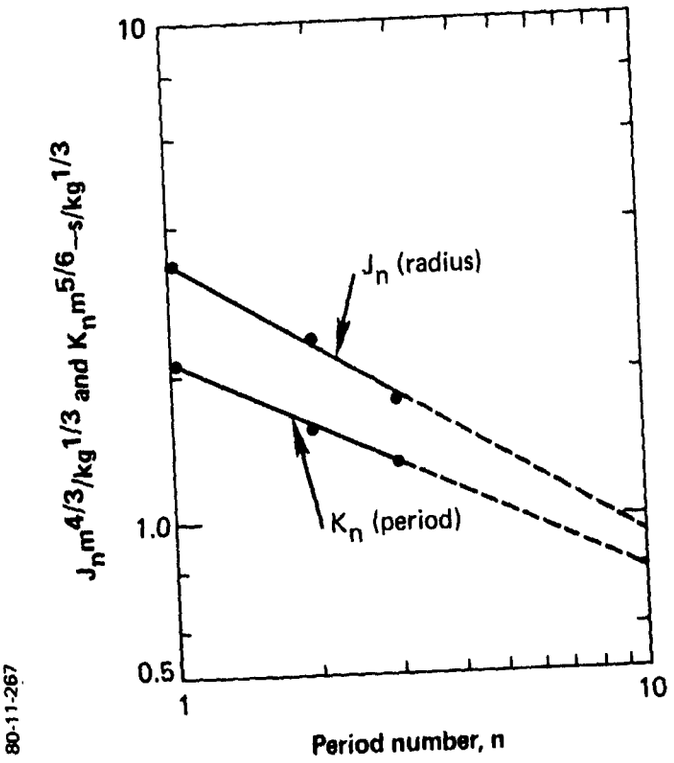

Figure 4.10 J_n and K_n versus n (data from Swift and Decius, Reference 24).

Table 4.4 Bubble period measurements from spherical TNT charges, and calculation of the effective bubble pulse energy on the second and third bubble periods relative to that on the first period (data from Reference 25).

Shot No.	Explosive Weight kg (lb)	Water Depth, m (ft)	n^{th} Bubble Period τ_n (ms)			Effective Bubble Energy	
			τ_1	τ_2	τ_3	$W_{eff}(2)/W_{eff}(1)$	$W_{eff}(3)/W_{eff}(1)$
67	0.45 (1)	282 (926)	14.52	10.71	7.98	0.40	0.17
42	0.45 (1)	363 (1191)	11.66	8.23	3.96	0.35	0.04
1	0.45 (1)	598 (1961)	7.86	5.76	4.25	0.39	0.16
27	0.45 (1)	621 (2036)	7.65	5.48	4.58	0.37	0.21
45	0.45 (1)	913 (2996)	5.41	4.06	3.12	0.42	0.19
10	0.45 (1)	934 (3063)	5.42	3.97	3.08	0.39	0.18
24	0.45 (1)	1354 (4444)	3.94	2.87	2.25	0.39	0.19
52	0.45 (1)	1382 (4535)	3.91	2.83	2.21	0.38	0.18
72	3.6 (8)	357 (1172)	24.28	17.97	14.50	0.41	0.21
21	3.6 (8)	580 (1904)	16.18	12.19	10.20	0.43	0.25
4	3.6 (8)	626 (2054)	15.72	11.84	9.35	0.43	0.21
35	3.6 (8)	629 (2064)	14.89	11.70	9.17	0.49	0.23
32	3.6 (8)	1322 (4338)	7.95	5.97	4.82	0.42	0.23
8	26 (57)	572 (1878)	30.55	22.20	--	0.38	--
20	26 (57)	1355 (4446)	14.84	11.56	8.68	0.47	0.20
3	26 (57)	2024 (6641)	10.10	7.27	4.67	0.37	0.10
79	26 (57)	2188 (7180)	10.20	7.52	5.96	0.40	0.20
62	26 (57)	4380 (14370)	5.53	4.28	3.38	0.46	0.23

mechanisms, the 1D spherical calculation of the detonation of a 454-kg (1000-lb) spherical TNT charge in water at a depth of 305 m (1000 ft) discussed in Section 4.1 was continued through the second bubble period. The results are given in Figure 4.11, which shows the computed bubble radius versus time. Calculation of W_{eff} for T_2 relative to T_1 shows that the relative bubble energy during the second period is 60 to 70 percent of that on the first bubble period. This, then, is the adiabatic energy loss due to the creation of the bubble pulse, since turbulence and heat conduction effects were not included in the calculation. Therefore, at least half of the bubble energy loss appears to be due to turbulence effects near the bubble minimum, and these act most effectively during the first bubble collapse. These results agree with the theoretical analysis given by Snay (Reference 15).

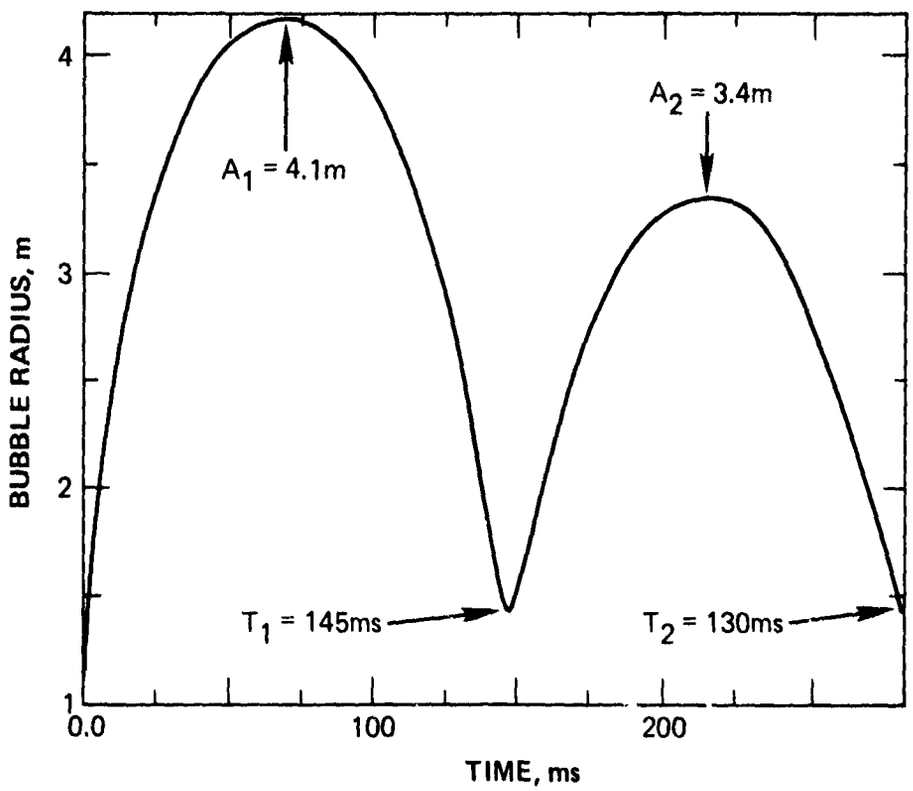

80-11-266

Figure 4.11 Computed explosion bubble radius versus time through the second bubble period for a 454-kg (1000-lb) spherical TNT charge detonated in water at a depth of 305 m (1000 ft).

SECTION 5

TWO-DIMENSIONAL CALCULATION OF THE EXPLOSION BUBBLE GROWTH AND COLLAPSE CAUSED BY THE DEEP UNDERWATER DETONATION OF THE BASELINE TAPERED CHARGE

A 2D calculation was performed for the baseline 454-kg (1000-lb) TNT tapered charge (Figure 2.4) using the PISCES 2DELK (Reference 26) continuum mechanics finite difference computer code. The basic geometry for the calculation is shown in Figure 5.1. Section 5.1 discusses the primary assumptions made, Section 5.2 presents the results, and Section 5.3 compares the computed average bubble parameters with those of an equal weight spherical TNT explosive charge.

5.1 CALCULATIONAL ASSUMPTIONS

The following assumptions were made in order to perform the 2D calculation in cylindrical symmetery with the tapered charge parallel to the sea surface:

1. The steel case enclosing the explosive was neglected. This may have an effect on the initial water shock produced by the charge, but should be relatively unimportant for the explosion bubble growth and collapse process.

2. The hydrostatic pressure, P_o was assumed constant over the vertical maximum dimensions of the bubble. The worst case would be if the tapered charge bubble had the same maximum vertical dimension as an equal weight spherical charge. From Section 4.1, A_m for a 454-kg (1000-lb) spherical charge detonated at 305 m (1000 ft) is about 4 m (13 ft). P_o at 305 m is about 3.1 MPa

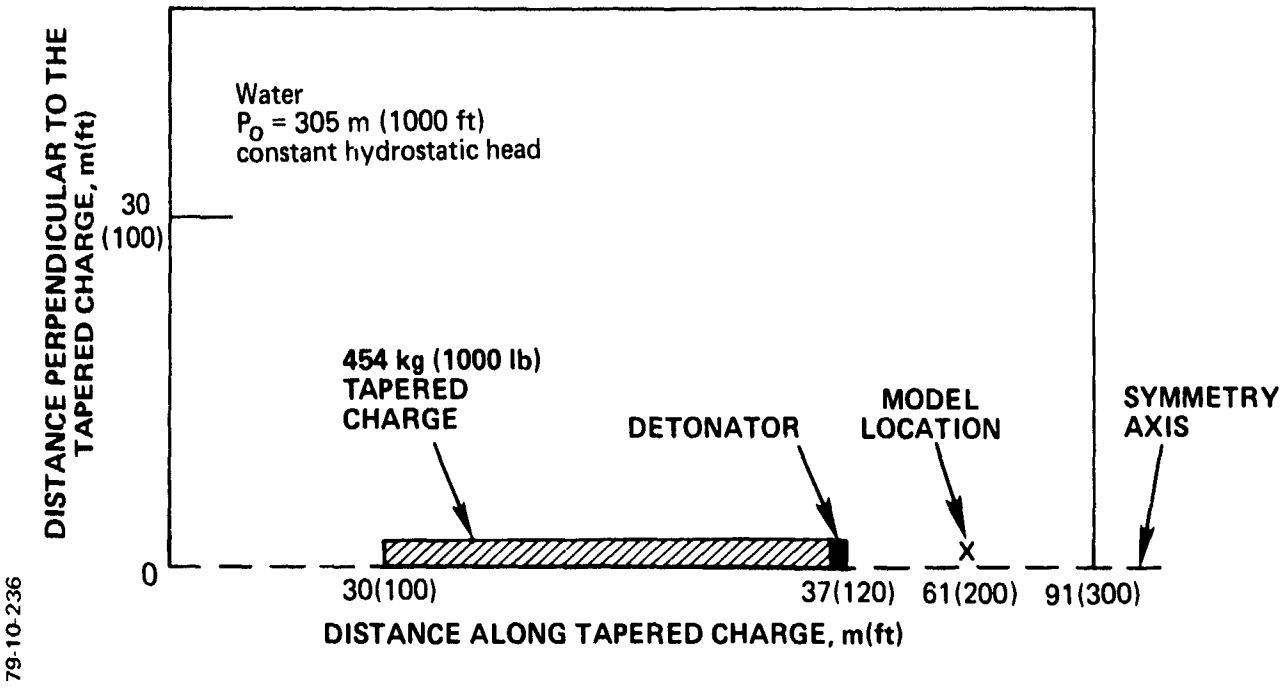

Figure 5.1 Geometry for 2D calculations.

(456 psi); the variation over the maximum bubble dimensions is 0.08 MPa (12 psi), or about 2.5 percent of P_o. Therefore, the gradient in the hydrostatic head can be neglected. Inclusion of this gradient would make the calculation fully three-dimensional.

3. Gravity was assumed to have little effect on the results, other than to produce the hydrostatic head. This essentially assumes that over the first bubble period the bubble is nonmigrating (Snay, Reference 15). Using analytic formulas, one can estimate the total amount of bubble migration, ΔZ, for a bubble caused by the detonation of 454 kg (1000-lb) of HBX-1 explosive at a depth of 305 m (1000 ft). This is about 0.9 m (3 ft), compared to an A_m of 4.4 m (14.5 ft). Therefore, the amount of bubble migration over T_1 is only 21 percent of the maximum bubble radius.

Figure 5.2 shows the initial zoning and material boundaries for the calculation. The coupled Eulerian-Lagrangian logic of PISCES 2DELK was used--the Eulerian grid described the high explosive of the tapered charge and the expansion cavity (the bubble); the Lagrangian grid described the water. The water had a constant hydrostatic pressure of 3.1 MPa (31 bars), consistent with a water depth of 305 m (1000 ft). Most of the Eulerian grid was initially covered by the Lagrangian grid as Figure 5.2 shows, and the tapered charge position is indicated. The total mass of the tapered charge was 449 kg (990 lb), and the total length was 5.3 m (17.5 ft).

5.2 RESULTS

The tapered charge was detonated from left to right, as indicated in Figure 5.2, and the detonation was completed at a time of about 0.8 ms. The shock wave was rapidly transmitted to the water, and the explosion bubble began to grow. Bubble growth

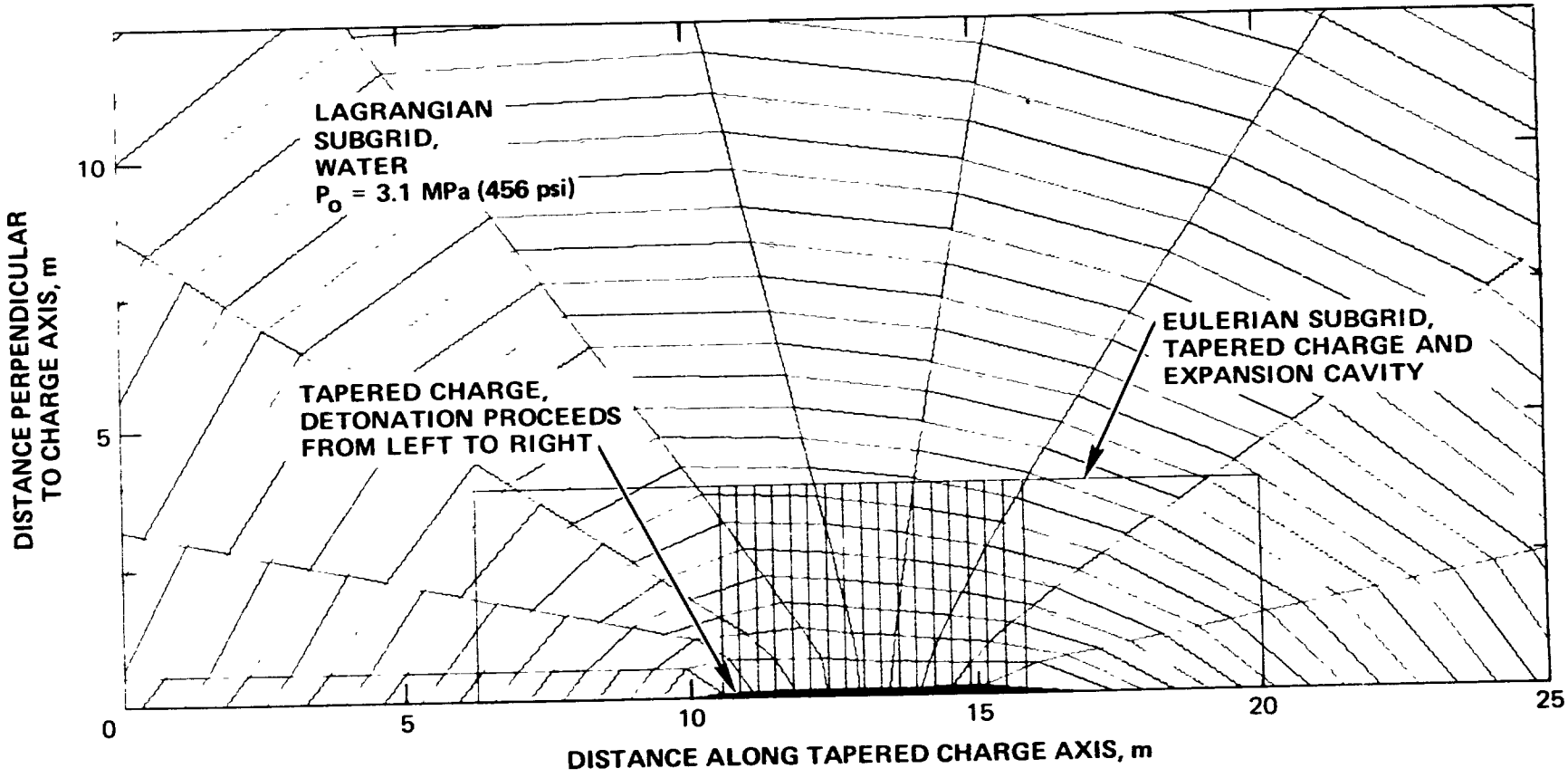

Figure 5.2 Initial zoning (t=0) of first PISCES 2DELK tapered charge calculation showing Eulerian subgrid containing the charge, and the surrounding Lagrangian subgrid containing the water.

to the time of the first bubble maximum (which occurs at about 75 ms) is shown in Figures 5.3, 5.4, and 5.5. At 75 ms, Figure 5.5 shows that the bubble is still somewhat elliptical, so the effect of the large length-to-diameter ratio of the tapered charge is retained by the bubble. After 75 ms, the hydrostatic pressure begins to collapse the bubble, as shown in Figure 5.6 and 5.7. Collapse to first minimum (T_1) occurs at approximately 133 ms.

Zoning effects were investigated by performing another calculation with twice the number of zones close to the charge to a time of 25 ms. Comparison of the computed results of the two calculations at that time revealed no essential differences, indicating that the original zoning was capable of resolving the initial bubble growth in sufficient detail.

5.3 COMPARISON OF THE TAPERED CHARGE AVERAGED EXPLOSION BUBBLE PARAMETERS WITH THOSE OF AN EQUAL WEIGHT SPHERICAL CHARGE

Figure 5.7 shows that at T_1 the explosion bubble is "almost spherical," while near the time of maximum growth of the bubble, the shape of the bubble was definitely elliptical. It was of interest to know whether the averaged bubble parameters were closer to those formed by a spherical charge detonated underwater, or to an infinitely long cylindrical charge. We had previously calculated both symmetries using 1D codes (see Section 4).

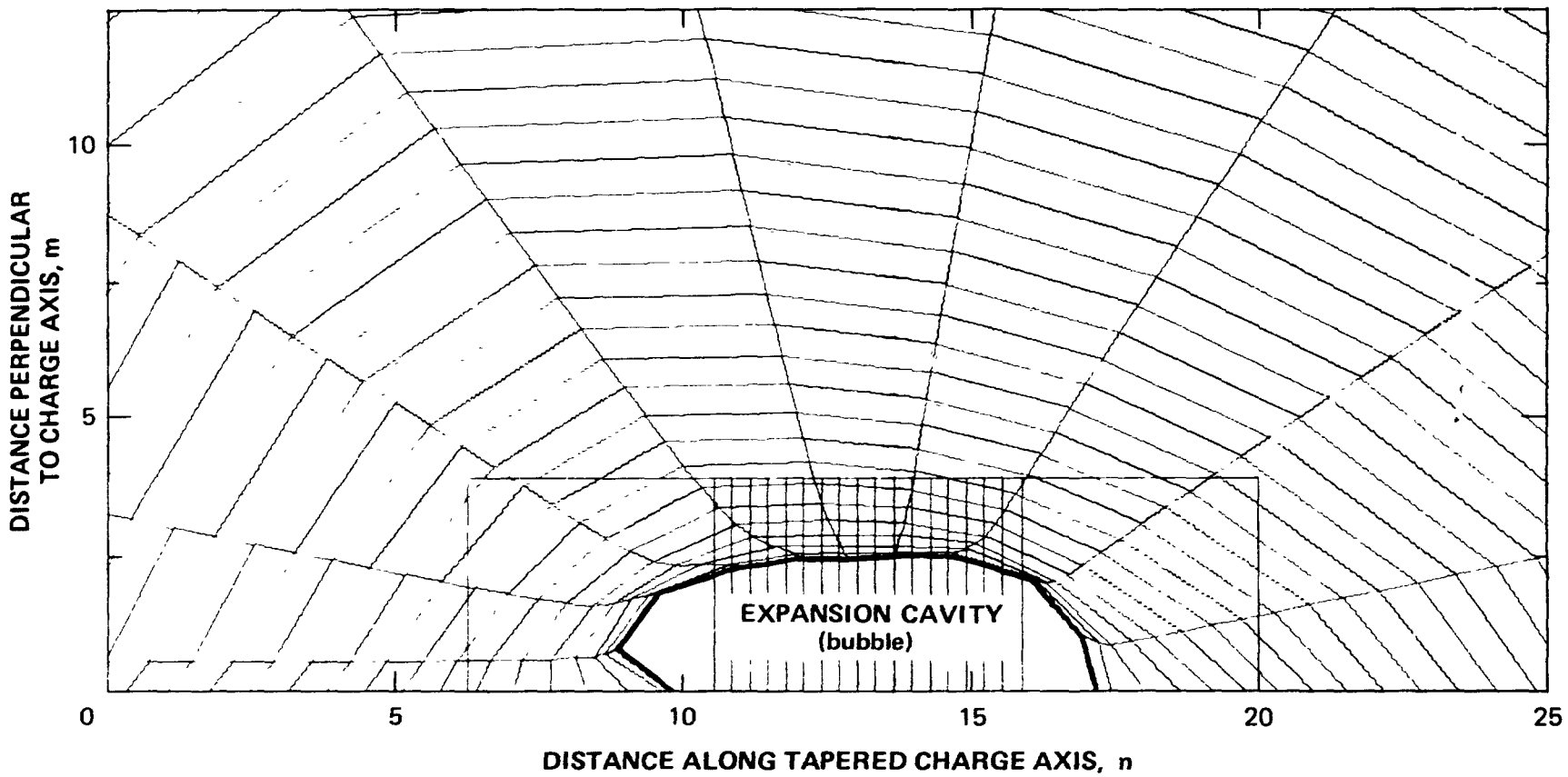

Figure 5.3 PISCES 2DELK first tapered charge calculation, t = 25 ms.

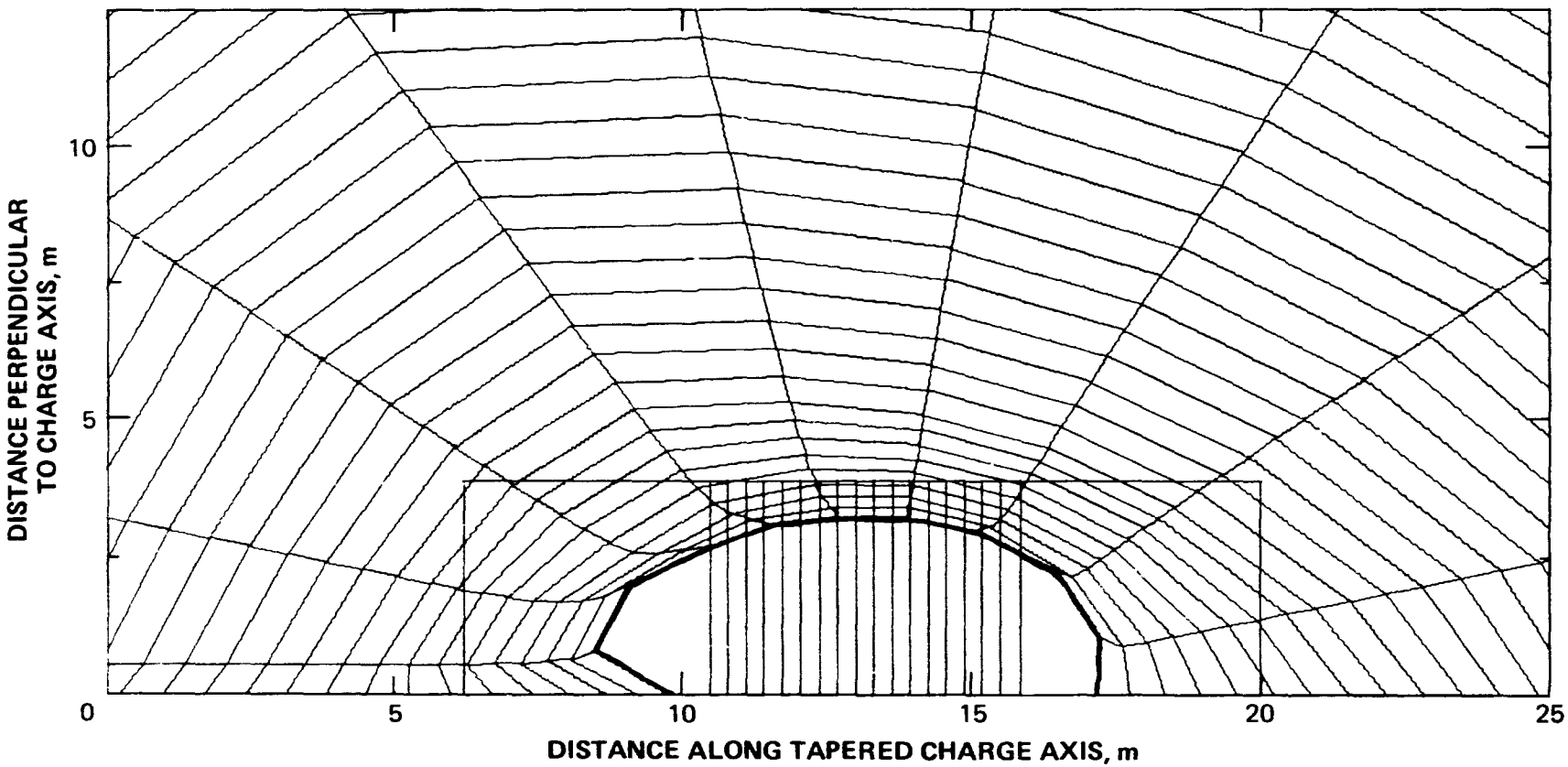

Figure 5.4 PISCES 2DELK first tapered charge calculation, t = 50 ms, continued expansion of bubble.

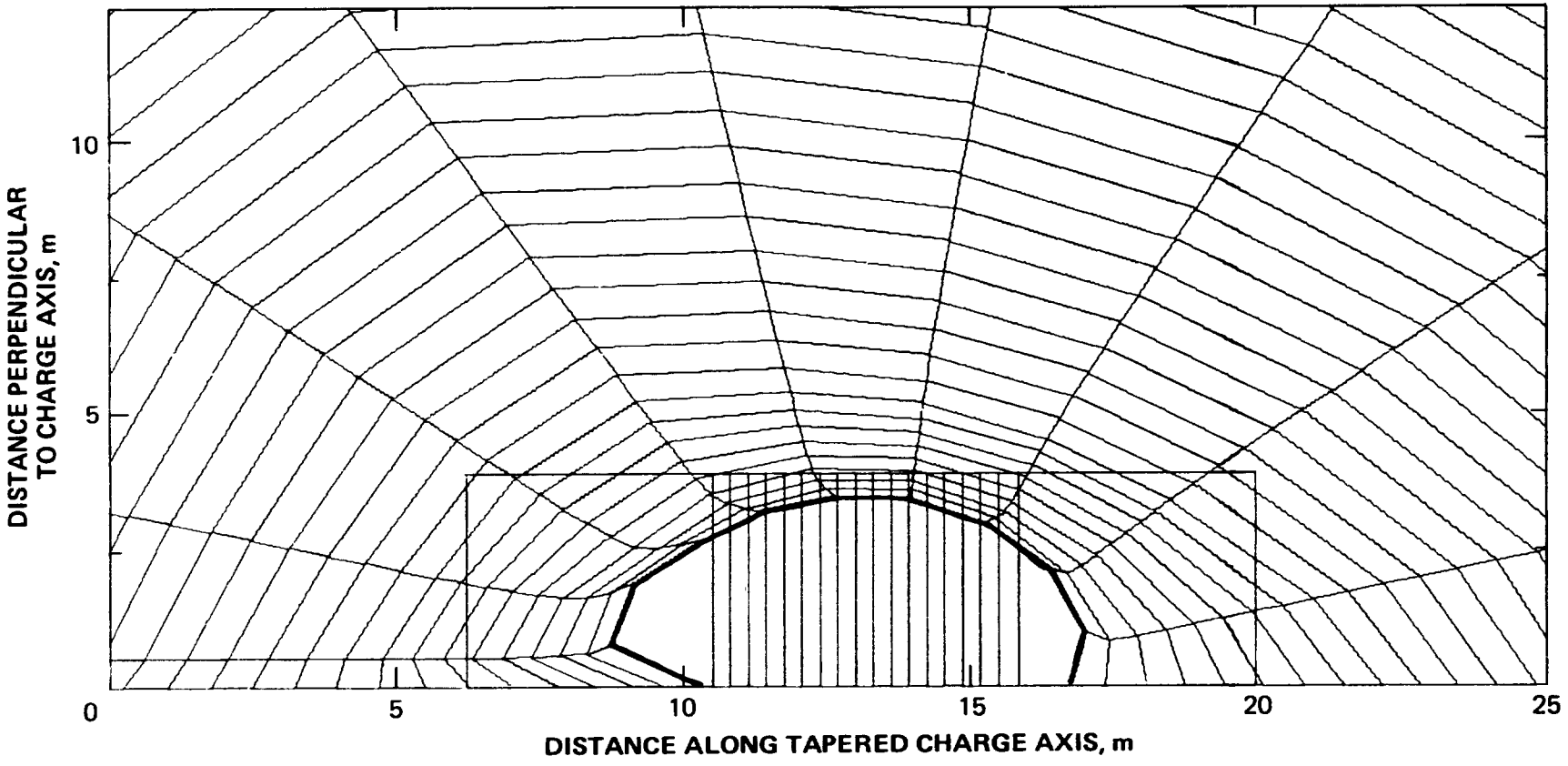

Figure 5.5 PISCES 2DELK first tapered charge calculation, t = 75 ms. This is the time of the first bubble maximum.

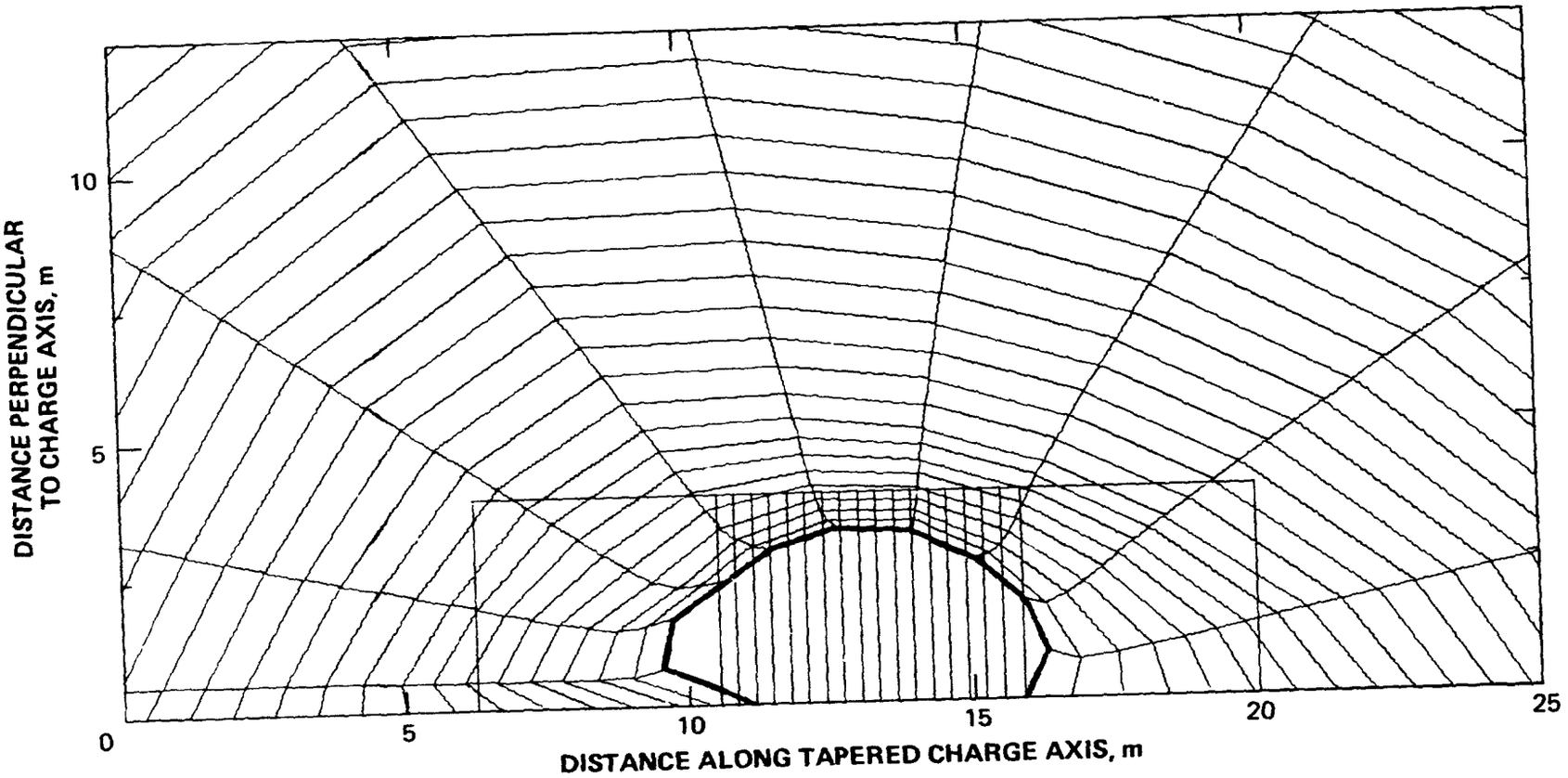

80-7-360

Figure 5.6 PISCES 2DELK first tapered charge calculation, t = 100 ms; bubble collapse is underway.

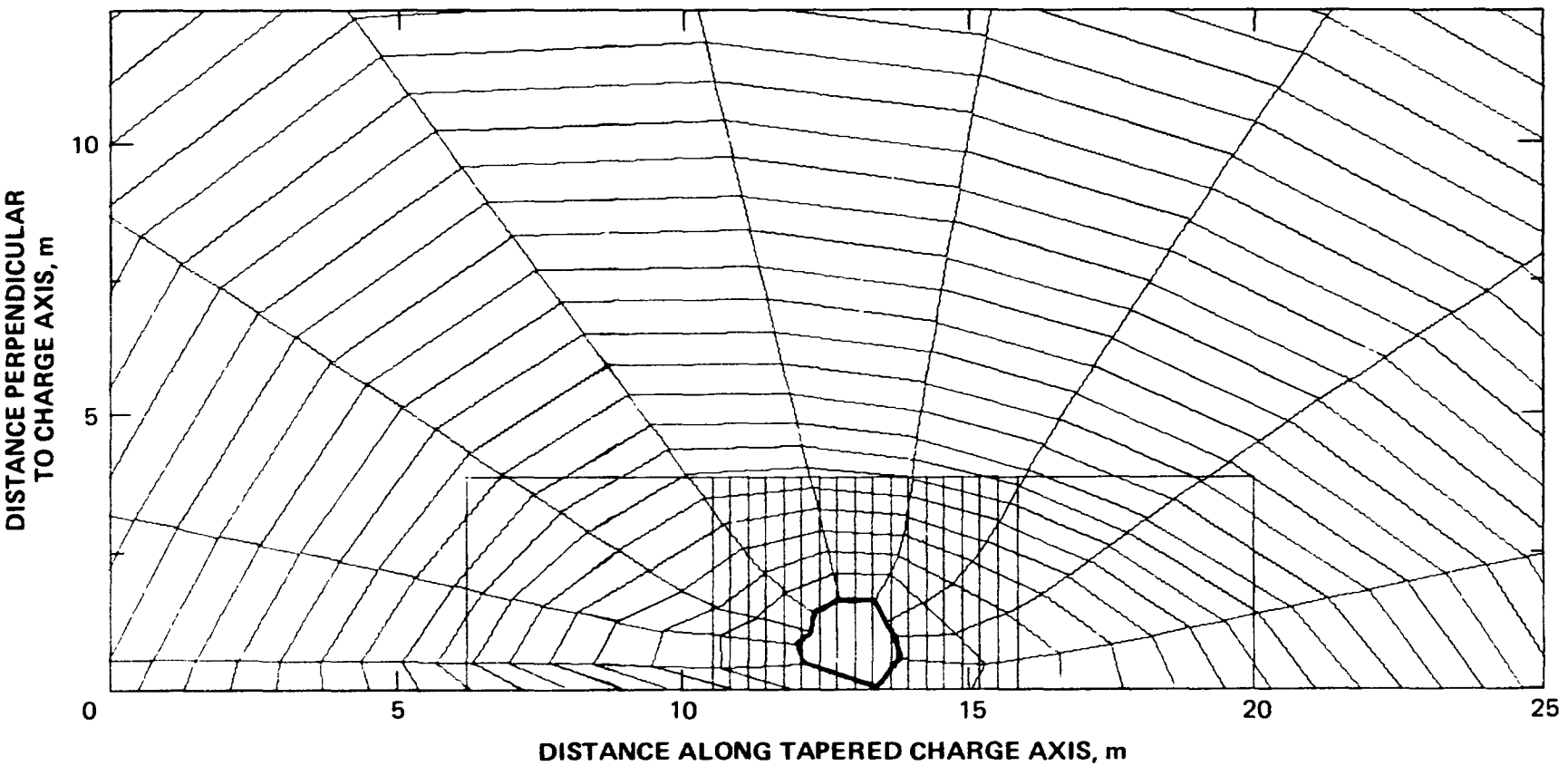

Figure 5.7 PISCES 2DELK first tapered charge calculation, t = 133 ms, the time of the first bubble minimum (T_1).

Both the total volume of the explosion bubble and the average pressure within the bubble were monitored in the calculation. From the volume, an average bubble radius was calcualted under the assumption that the bubble was spherical. Figure 5.8 compares this average spherized radius versus time with the bubble radii from an equal weight spherical charge, and the infinitely long cylindrical charge with equal charge weight per unit length.

The tapered charge average bubble radius appears to follow closely the behavior of the bubble for a 454-kg (1000-lb) spherical charge, but with a slightly smaller maximum radius (A_m = 3.8 m instead of 4.1 m for the spherical charge) and a slightly shorter bubble period (T_1 = 133 ms instead of 140 ms), consistent with the smaller maximum radius.

Figure 5.9 presents the averaged pressure within the explosion bubble versus time. The average pressure within the explosion bubble for the tapered charge is much closer to the pressure within the explosion bubble of the spherical charge than it is for the cylindrical charge. Also, it was seen in the 2D calculation that there was some variation of the pressure over the axial dimensions of the bubble (this variation is shown in the figure). The variation is much larger at the earlier times, i.e., during the bubble expansion, than it is after the bubble has reached its maximum radius and begun to collapse.

We concluded from this comparison that (at least to first order) the bubble from the tapered charge could be treated as a spherical charge, perhaps with the total energy of the equivalent

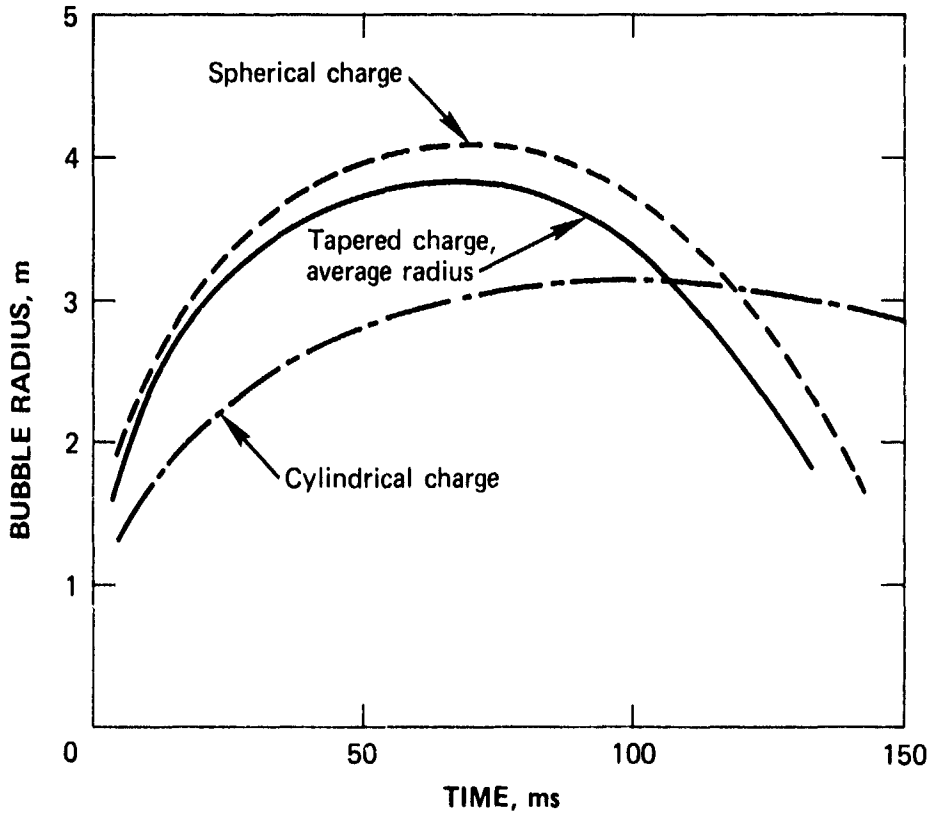

80-7-357

Figure 5.8 Explosion bubble radius versus time for a 454-kg (1000-lb) spherical TNT charge and cylindrical charge (diameter = 0.3 m) with volume-averaged radius of the bubble produced by the baseline 454-kg tapered charge (P_o = 305 m hydrostatic head).

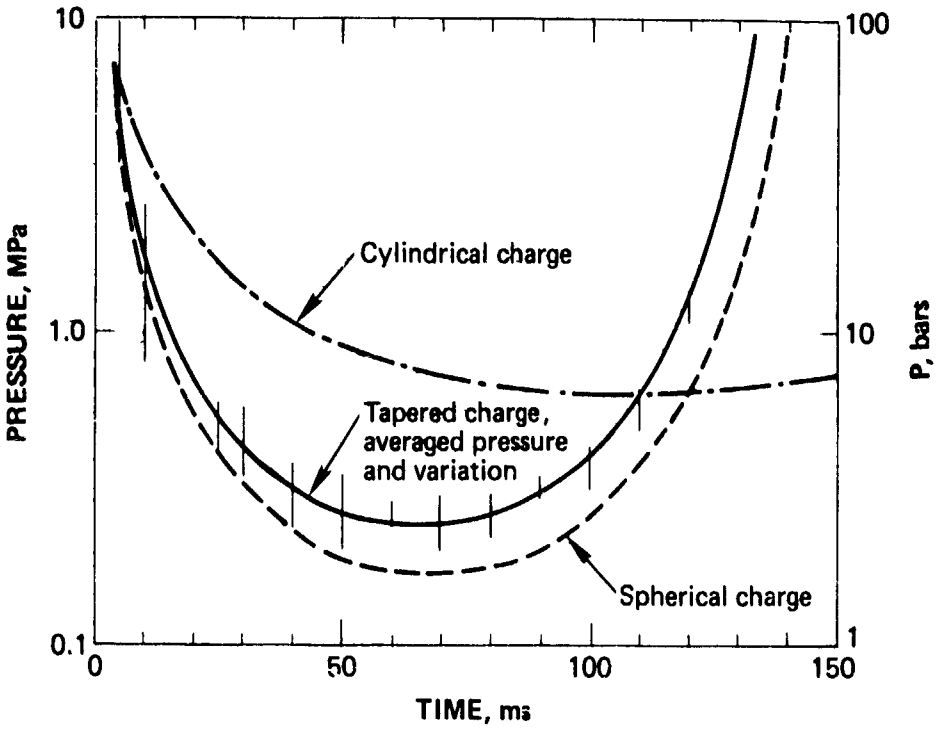

Figure 5.9 Pressure within the explosion bubble versus time for a 454-kg (1000-lb) spherical TNT charge and a cylindrical charge (diameter = 0.3 m) with the averaged bubble pressure produced by the baseline 454-kg tapered charge (P_o = 305 m hydrostatic head).

spherical charge slightly reduced (by about 20 percent). This assumption was useful for the next part of our effort, which concentrated on injecting propellant gasses into the explosion bubble in an attempt to mitigate the bubble collapse (see Section 6).

The fact that a tapered charge detonation deep under water appeared to produce an explosion bubble with characteristics very similar to those of an equal weight spherical charge leads one to suspect that such a detonation would produce at least one bubble pulse. This very important conclusion is corroborated by experimental data (Reference 27) from two tapered charges detonated in deep water.

SECTION 6

INVESTIGATION OF PROPELLANT-ASSISTED PREVENTION OF EXPLOSION BUBBLE COLLAPSE

At the beginning of the program, we thought that one way to eliminate the bubble pulse caused by the deep underwater detonation of a tapered charge (if bubble pulsation occurred) would be to prevent the bubble from collapsing. The calculation of the baseline tapered charge discussed in the preceding section showed that the explosion bubble caused by the detonation had characteristics very similar to the bubble caused by the detonation of a spherical charge of the same explosive weight. Therefore, one would expect the bubble pulses to be similar also. To prevent collapse of the bubble, we postulated that an additional propellant source might be used to supply gas to the bubble. Recalling the discussion of Section 4.1, the pressure within the explosion bubble is well below the hydrostatic pressure at the time of maximum bubble radius (Figure 4.3b); this pressure differential between the bubble interior and the surrounding water is the cause of bubble collapse. The purpose of the propellant source would be to raise the interior bubble pressure, thereby halting this process.

We realized early in the program that, because of the size of the explosion bubble, the amount of propellant required would be large. At maximum radius, the explosion bubble volume is about 270 m^3 (9500 ft^3). Previous work with propellants (Reference 28) was used to estimate how much propellant would be

required. Section 6.1 discusses this estimate; essentially, it was found that the mass of propellant required to raise the interior bubble pressure to the hydrostatic pressure level was prohibitively large. A series of 1D calculations was then performed to see if smaller amounts of propellant gas would substantially mitigate the bubble pulse. These are discussed in Section 6.2.

6.1 ESTIMATE OF THE AMOUNT OF PROPELLANT REQUIRED TO AVERT BUBBLE COLLAPSE

For a single propellant species burning in a volume, V_1, the pressure, P(t) is given by:

$$P(t) = \frac{\lambda(t)\ M\ F}{V - \frac{M}{\rho} + \lambda(t)\ M\left(\frac{1}{\rho} - C\right)}, \text{ where} \qquad (6.1)$$

M = mass of the propellant
F = propellant impetus (energy content)
C = covolume of the propellant gasses
ρ = initial density of the propellant
$\lambda(t)$ = fraction of the propellant burned.

Setting $\lambda = 1$ at $t = \infty$ gives

$$P_\infty = \frac{MF}{V - MC} \quad . \qquad (6.2)$$

Properties for a typical U.S. Navy gun propellant, SPDN (Reference 24) were used: $F = 9.35 \times 10^5$ J/kg, and $C = 9.33 \times 10^{-4}$ m^3/kg.

The amount of propellant required to raise the interior bubble pressure to the hydrostatic pressure, P_o, at the time of the first bubble maximum for the 454-kg (1000-lb) charge can be calculated as follows. First,

$$P_o = P_{bubble} + P_\infty \tag{6.3}$$

where P_{bubble} = 0.2 MPa (2 bars) at the time of first bubble maximum (see Figure 4.3b). This defines P_∞ as

$$P_\infty = 3.1 \text{ MPa} - 0.2 \text{ MPa} = 2.9 \text{ MPa} . \tag{6.4}$$

Next, the mass of propellant can be calculated using Equation 6.2:

$$M = \frac{VP_\infty}{F + CP_\infty}$$

$$= \frac{(270 \text{ m}^3)(2.9 \times 10^6 \text{ Pa})}{9.35 \times 10^5 \text{ J/kg} + (9.33 \times 10^{-4} \text{ m}^3/\text{kg})(2.9 \times 10^6 \text{ Pa})}$$

$$= 835 \text{ kg (1840 lb)}. \tag{6.5}$$

Thus, if propellant gas could be injected instantaneously into the explosion bubble at this time, 835 kg (1840 lb) would be required to raise the bubble pressure to the hydrostatic pressure at a depth of 305 m (1000 ft). This propellant weight is almost twice the weight of the 454-kg (1000-lb) explosive charge.

This is clearly a prohibitively large amount of propellant, and thus it did not appear feasible to completely arrest the bubble collapse process. Actually, this estimate is probably a lower bound, since some bubble oscillation might still occur.

6.2 CALCULATIONS AND ANALYSIS

Since it did not appear possible to avert bubble collapse with any reasonable amount of propellant, an effort was made to examine to what extent a reasonable amount of propellant could reduce the bubble pulse. This required running 1D spherical calculations well past the time of the first bubble minimum so that the bubble pulse could be examined at a reasonable range in water. The 1D calculations were adequate because of the similarity of the tapered charge explosion bubble to a spherical charge, discussed in Section 5.3.

Calculations were performed wherein propellant gasses were injected into the explosion bubble at constant rates. Figure 6.1 shows the computational method that we followed. In all calculations, a 454-kg (1000-lb) spherical TNT charge was initially detonated. The propellant source was placed within the explosion bubble using a special boundary condition to inject the propellant gas into the growing explosion bubble. Table 6.1 summarizes

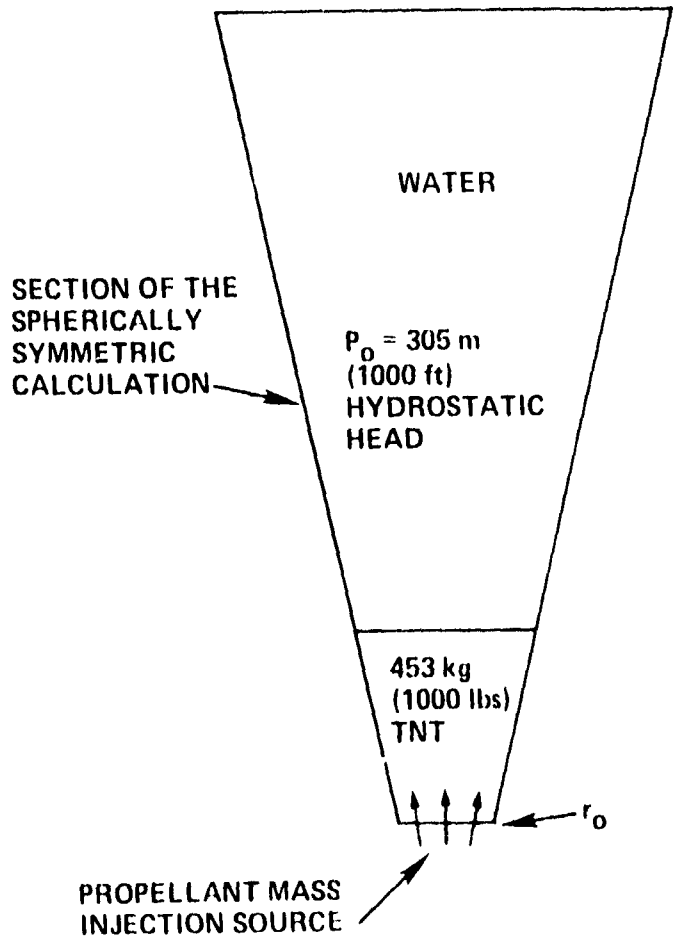

Figure 6.1 Sketch showing 1D computational method for adding a constant propellant gas source to the TNT explosion bubble.

Table 6.1 Summary of initial conditions for the 1D calculations with propellant gas mass addition.

Initial Conditions Used in All of the Calculations

TNT: 453-kg (1000-lb) charge

Water: Constant hydrostatic pressure, 3.1 MPa (460 psi)

Propellant Source

Density of gasses:	0.1 g/cc
Exit velocity of gasses:	1900 m/s (6200 ft/s)
Internal energy of gasses:	2570 J/g
Pressure of gasses:	7.7 MPa (1130 psi)

Initial Conditions Unique to Each Calculation

Calculation	r_o, cm	Mass Addition Rate kg/ms	Mass Addition Rate lb/ms
1	0.0	0.0	(0.0)
2	0.573	0.0784	(0.173)
3	1.146	0.3136	(0.691)
4	4.584	5.018	(11.06)
5	9.168	20.070	(44.25)

the initial conditions for these 1D spherical calculations. The propellant gasses were given a density, an exit velocity, an internal energy, and a pressure typical of those quantities for operating rockets (Reference 29). The mass injection rate was varied by varying the radius r_o, as indicated in Figure 6.1, over which the propellant source was injected into the explosion bubble. The mass injection rates ranged from 0.0 kg/ms (no mass addition at all) to 20.07 kg/ms, as shown in Table 6.1. We felt that this series of calculations would give us some indication of whether the addition of hot propellant gasses to the explosion bubble would contribute to mitigation of the bubble pulse.

Results of this series of calculations are given in Figure 6.2, which shows the computed bubble radius versus time. Some "cushioning" of the explosion bubble is seen, even with the lowest (0.0784 kg/ms) propellant injection rate. Too large a rate (20.07 kg/ms) leads to the formation of a much larger bubble, and this probably not useful. An injection rate of about 5 kg/ms appears to minimize bubble collapse, while not significantly enlarging the bubble maximum radius. This "optimized" injection rate leads to the addition of an even larger mass of propellant to the explosion bubble, about 1,000 kg (2200 lb) over one bubble period (220 ms). The constant mass injection rate is the most feasible method of supplying hot gasses to the explosion bubble; clearly, the "instantaneous" method of Section 6.1 is unrealistic. The gas is then allowed to contribute to bubble growth, however, thus lengthening the bubble period and requiring even more propellant.

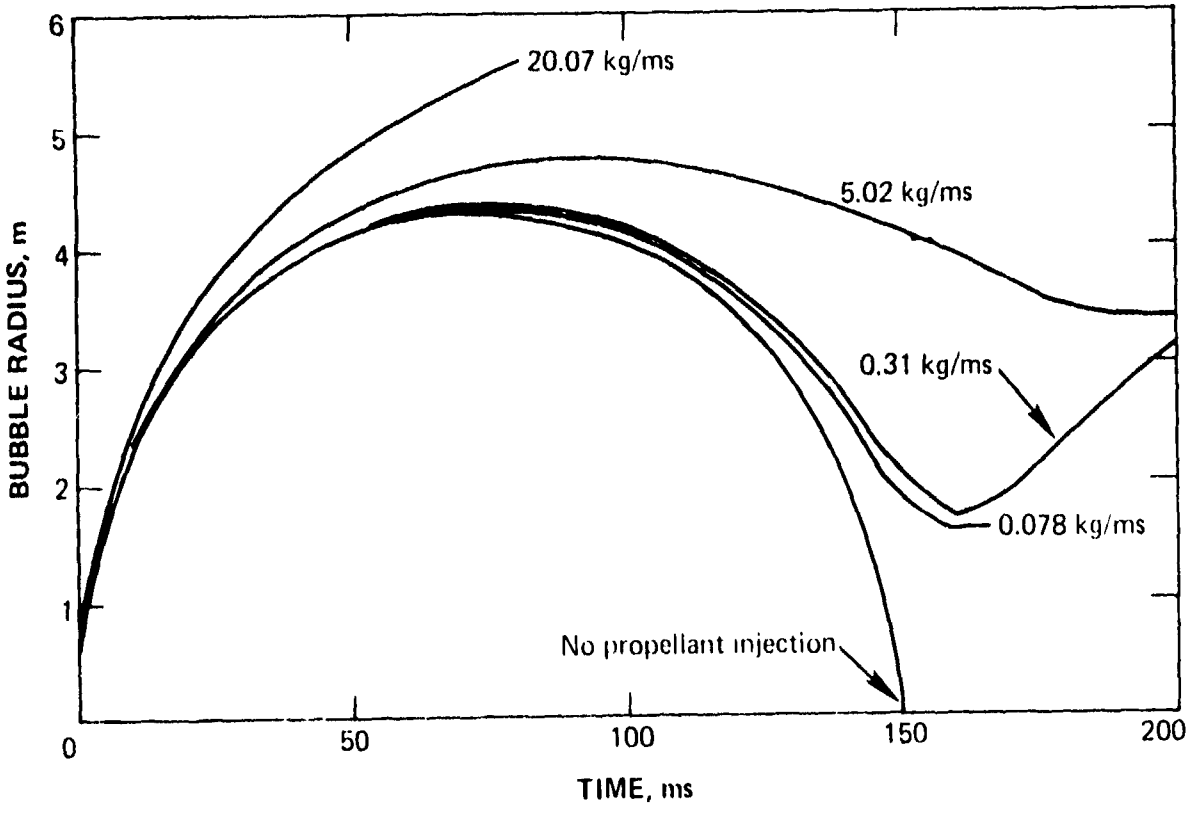

Figure 6.2 Explosion bubble radius versus time for a 453-kg (1000-lb) spherical TNT charge detonated at a depth of 305 m (1000 ft) in water; compared for various constant injection rates of propellant gasses into the explosion bubble.

Figure 6.3 shows pressure versus time at a range of 40 m for the case of no propellant gas injection, and the "optimized" case where 5.0 kg/ms (11.1 lb/ms) of propellant gas is injected into the explosion bubble. The initial shock wave is not affected by the propellant injection, but the bubble pulse peak overpressure is reduced from 0.7 MPa (105 psi) to 0.3 MPa (45 psi), more than a factor of two, by the propellant gas injection. Total positive phase impulse in the bubble pulse is decreased 22 percent from 22.2 MPa-ms (3330 psi-ms) to 17.4 MPa-ms (2600 psi-ms).

These results were encouraging, but they also showed that even to mitigate the bubble pulse is very difficult. Injection of propellants into the explosion bubble appears to cushion bubble collapse, thereby reducing the peak bubble pulse pressure in the surrounding water, but at the same time the bubble pulse positive phase is spread out over a longer period of time.

We concluded that propellant-assisted bubble pulse mitigation was not effective enough in reducing impulse, considering the large amount of propellant that would somehow have to be injected into the bubble during its expansion and collapse. Further, the discussion of the phenomenology of multiple bubble pulsation (Section 4.4) implies that by cushioning the first bubble collapse, one might actually increase the overall stability of the bubble. Thus, while decreasing the bubble pulse impulse per bubble period, one may actually increase the total number of bubble oscillations.

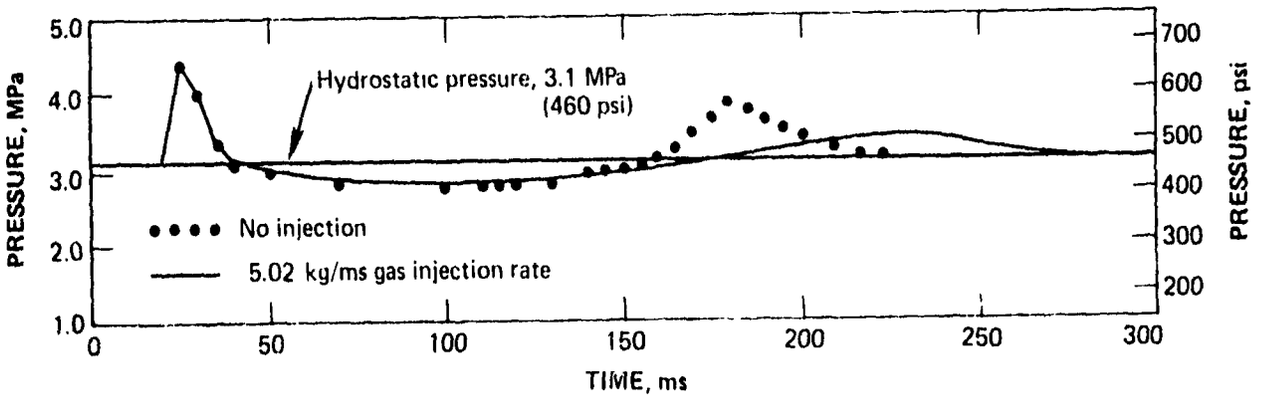

80-9-78

Figure 6.3 Calculated pressure versus time at the 40-m (131-ft) range from a 453-kg (1000-lb) spherical TNT charge detonated in water at a depth of 305 m (1000 ft) compared to that calculated for the TNT charge with a constant propellant gas injection source inside the explosion bubble.

SECTION 7

INVESTIGATION OF TWO POSSIBLE METHODS OF MITIGATION OF TAPERED CHARGE EXPLOSION BUBBLE PULSATION

We investigated two additional methods to see if bubble pulsation could be significantly reduced, even though it cannot be eliminated entirely. Both methods essentially employed the same principle of using the first bubble collapse to destroy the continuity of the explosion bubble. The first method was to make the explosion bubble from a conventional tapered charge sufficiently asymmetric at T_1 that turbulence would absorb more energy, leaving less for later pulsations. This is discussed in Section 7.1, along with an initial 2D calculation for a specific geometry.

The second method was to fill the explosion bubble with explosion products that are either condensible gasses (e.g., steam) or are solids soluble in water, by using a different explosive in the tapered charge. At T_1, these products would condense and/or dissolve into the water, preventing the rapid pressure rise that occurs with conventional charges, and thereby reducing bubble pulsation. Such explosives were developed about 10 years ago at the U.S. Naval Ordnance Laboratory, White Oak, MD. Section 7.2 discusses these explosives, and how they could be used to reduce bubble pulsation for simulated underwater nuclear detonations.

7.1 ASYMMETRIC BUBBLE COLLAPSE

Examination of explosively generated explosion bubbles (Section 4) revealed that the first bubble collapse and reexpansion removed the greatest amount of energy from the bubble (approximately 60 percent), and that turbulence and heat conduction effects were responsible for more than half of this energy loss. This is true for detonations in deep water: a non-migrating bubble is remarkably spherical over many periods of oscillation; i.e., it is dynamically stable. If the symmetry of the explosion bubble could be destroyed, particularly at T_1, instabilities might be enhanced, thereby making the energy loss mechanisms even more effective. This in turn would damp out bubble pulsation more rapidly.

An asymmetric bubble can be initiated by placing an air-filled "get lost" pipe directly behind the tapered charge, as shown in Figure 7.1. The initial water shock at the model location would not be affected, but explosive gasses will propagate down the air-filled pipe once the charge has completely detonated. Bubble growth would then proceed in an asymmetric manner, as illustrated in Figure 7.2. For this technique to work, the bubble must remain asymmetric through the collapse phase to the time of first minimum radius (T_1). This is illustrated in Figures 7.3a and b.

A 2D calculation was performed to further investigate this method of bubble pulse mitigation. We recognized that the entire concept could not be investigated because heat conduction and turbulence models were not included in the computational

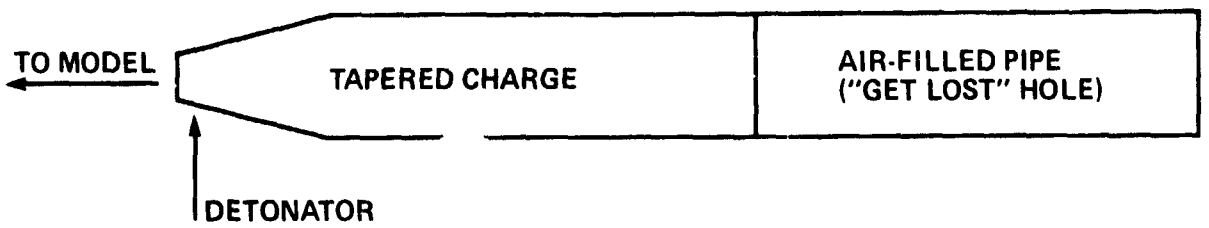

Figure 7.1 Tapered charge with pipe attached to introduce bubble asymmetry.

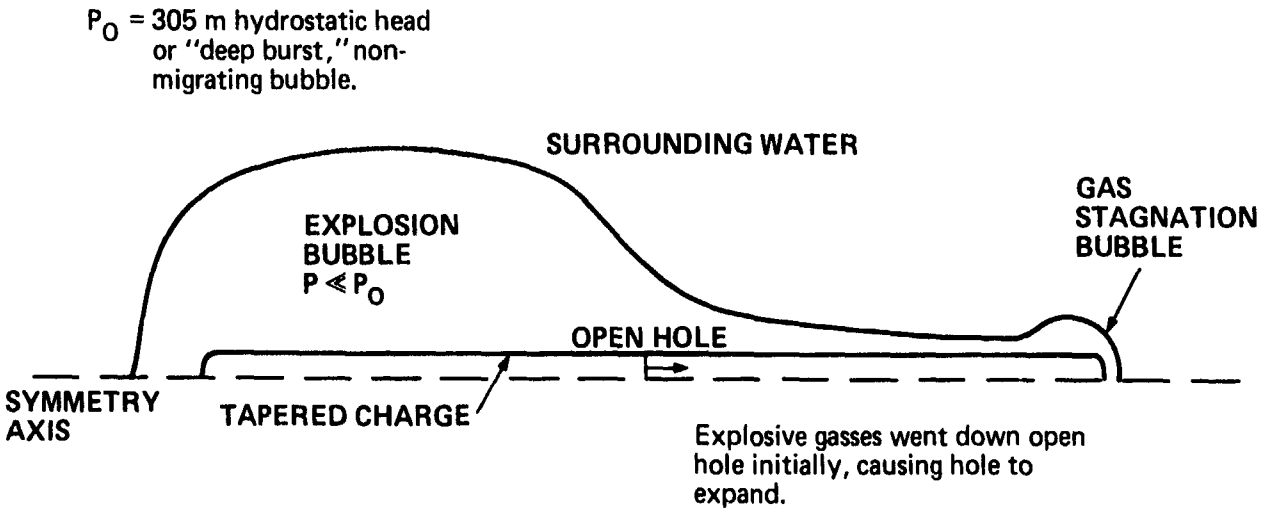

80-11-263

Figure 7.2 What asymmetric bubble might look like at first maximum.

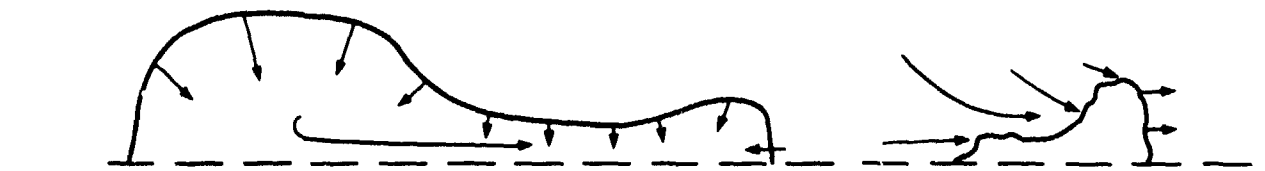

80-11-264

Figure 7.3 How bubble collapse might take place using this technique.

treatment. Therefore, the bubble collapse to T_1 could only be evaluated qualitatively to determine what effect the bubble asymmetry might have on the later oscillations of the bubble.

Figure 7.4 shows the initial zoning for this second PISCES 2DELK calculation. The air-filled pipe was assigned an initial diameter of 0.3 m (1 ft), the same as the maximum diameter of the tapered charge. The pipe itself was not modeled in the calculation, and the open region on the inside was treated as a void. Figure 7.5 shows the explosion bubble and the velocity field in the surrounding water at 5 ms. Explosive gasses had reached the end of the tube and stagnated, forming a second, smaller bubble and a "stagnation bubble." By 10 ms (Figure 7.6), the pipe region between the explosion bubble and the stagnation bubble had closed off due to the higher pressure in the surrounding water. At 25 ms (Figure 7.7), the stagnation bubble had ceased to expand. At that time, it contained about one percent of the TNT explosive products; the rest were sealed in the tapered charge explosion bubble.

Comparison of Figure 7.7 with Figure 5.3 shows that the explosion bubble was not significantly affected by the presence of the open pipe. The velocity vectors of Figure 7.7 show that the velocity field in the water is still roughly symmetric on each end of the tapered charge explosion bubble.

The above results led us to the conclusion that the pipe was too small in this calculation to significantly affect the growth of the explosion bubble. Therefore, it was terminated at 25 ms, and a third calculation was generated. This calculation was

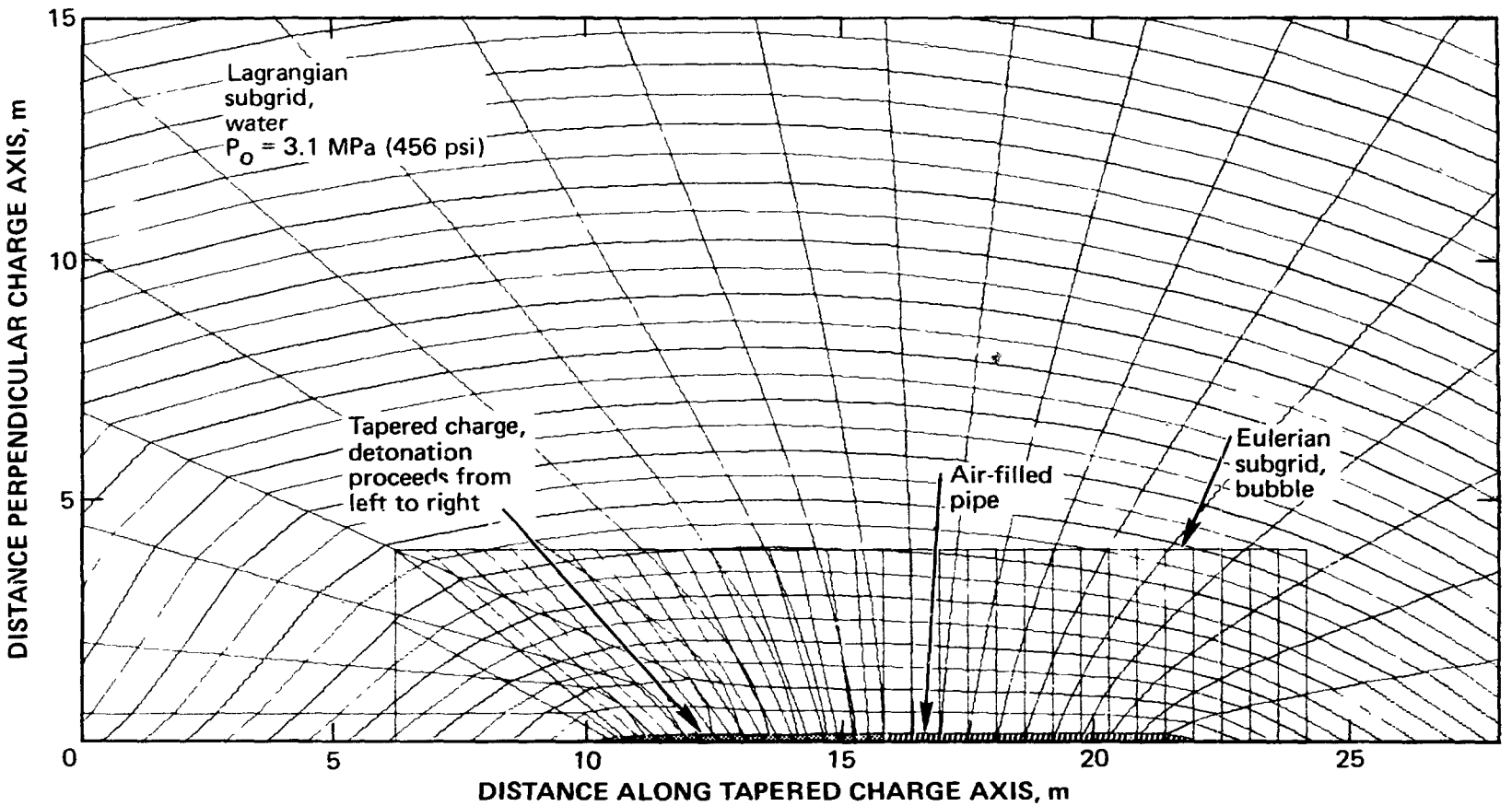

Figure 7.4 Initial zoning of the second tapered charge calculation showing the locations of the charge and the air-filled pipe.

80-11-241

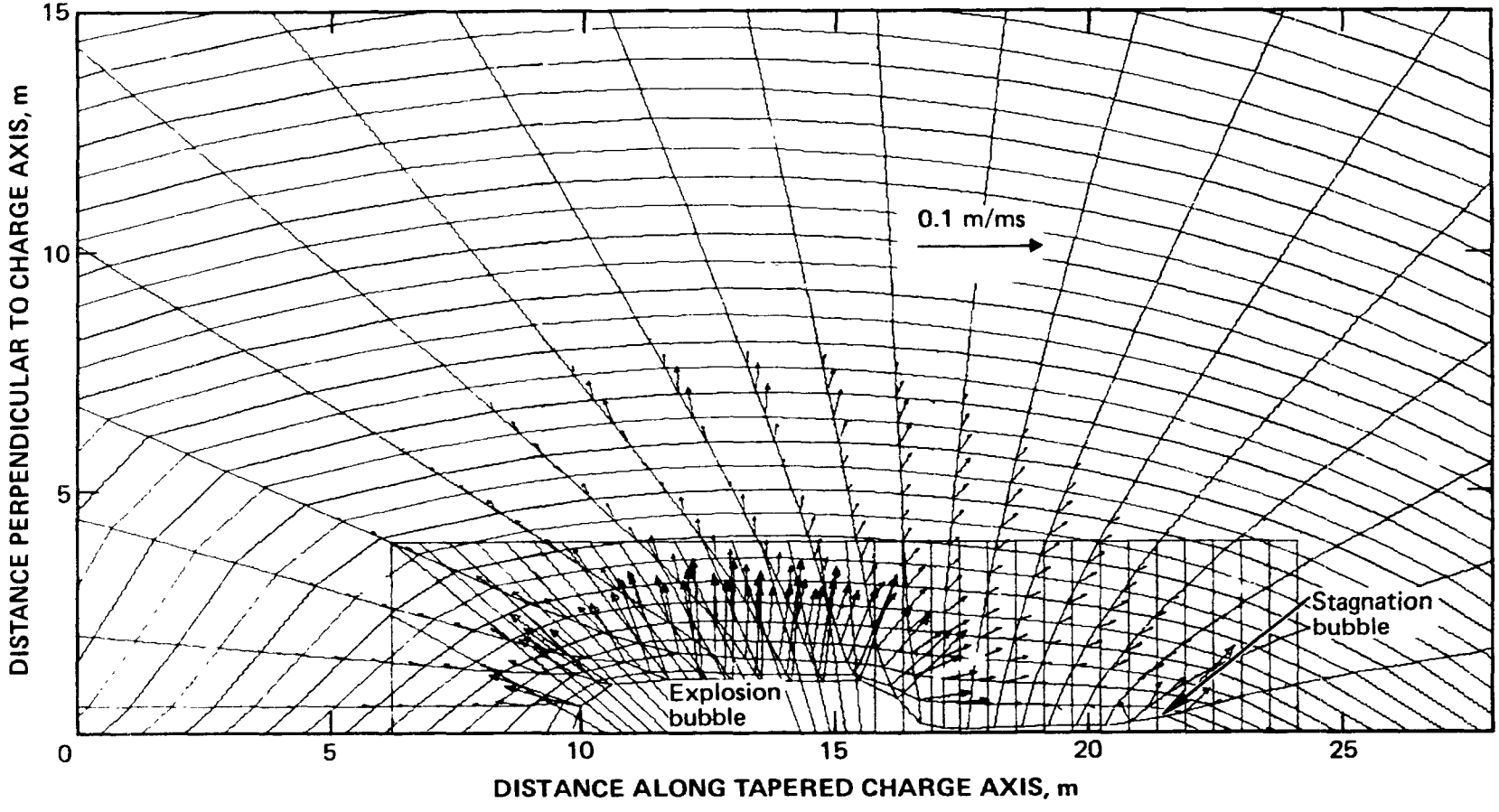

80-11 251

Figure 7.5 Material boundary and vector velocity plot from the second 2D tapered charge calculation at t = 5 ms.

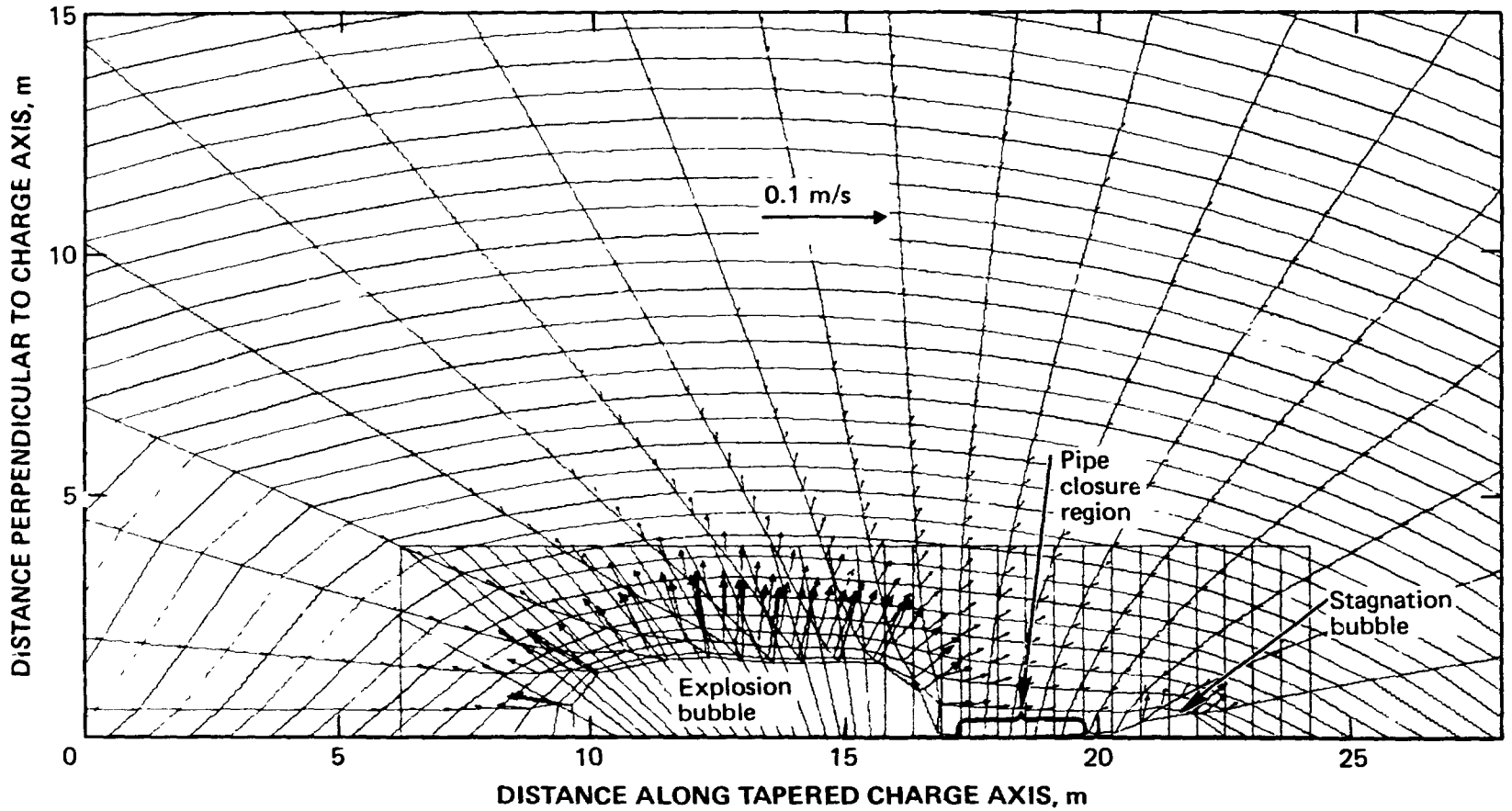

80-11-249

Figure 7.6 Material boundary and vector velocity plot from the second 2D tapered charge calculation at 10 ms.

81-8-22

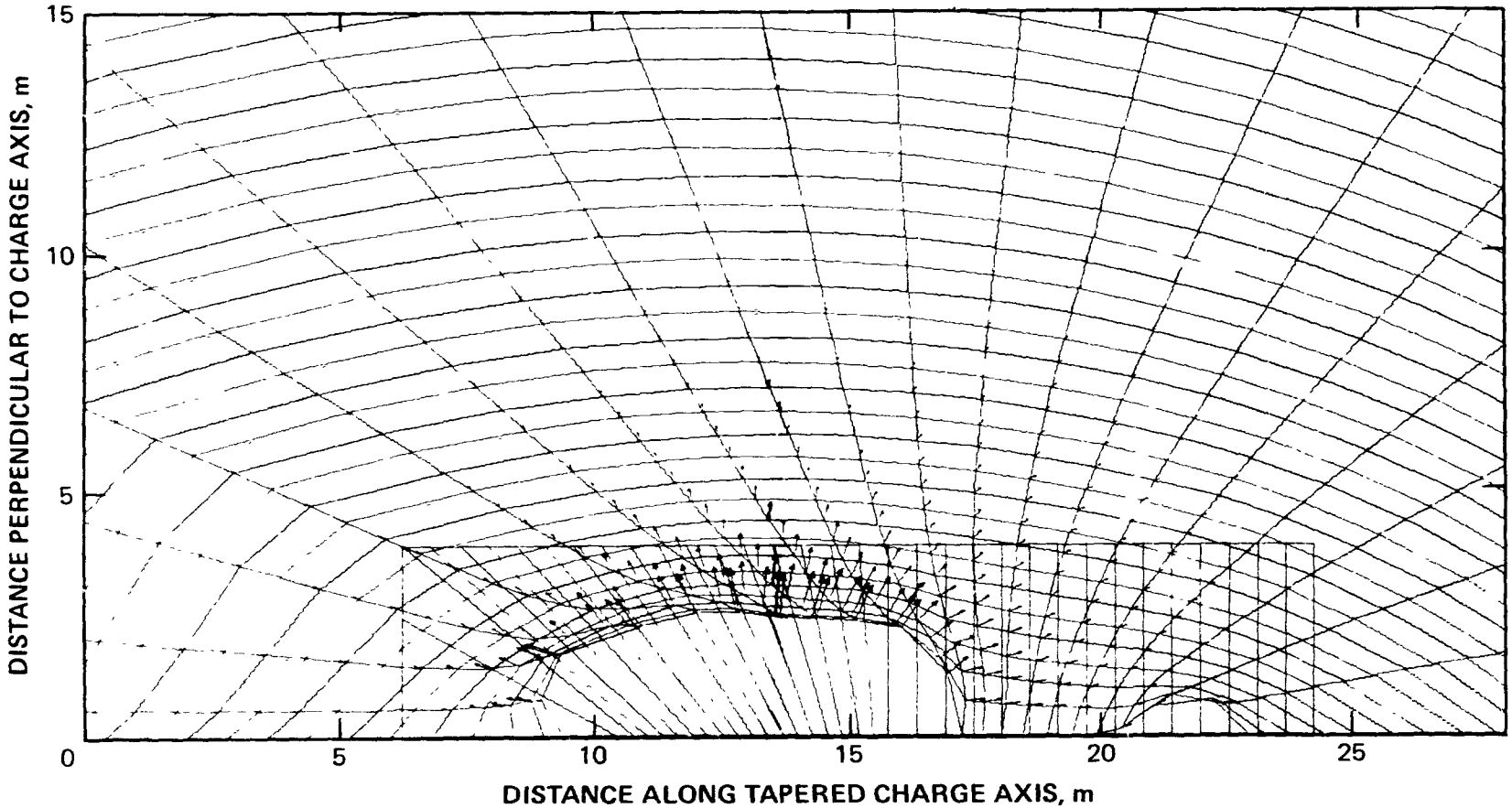

Figure 7.7 Material boundary and vector velocity plot from the second 2D tapered charge calculation at 25 ms.

similar, but the initial diameter of the air-filled pipe was doubled, to 0.6 m (2 ft), and then gradually tapered to a 0.3-m (1-ft) diameter. The length of the pipe was the same as in the second calculation. Figure 7.8 shows the geometry and zoning for this calculation. The intended purpose of the larger-diameter, air-filled pipe was to aid in generating a larger stagnation bubble, closer to the tapered charge explosion bubble.

Figures 7.9, 7.10, and 7.11 are computer-generated zoning, material boundary, and velocity vector plots at 25, 50, and 75 ms, respectively. A much larger stagnation bubble was formed (Figure 7.9) and was continuing to grow at 25 ms. It remained separated from the explosion bubble by a thin region of water, and contained about six percent of the explosive mass, clearly an improvement over the results of the second calculation. Figure 7.11 shows that the velocity field in the water is definitely asymmetric at approximately the time of the maximum size of the explosion bubble.

It was uncertain at this point whether or not the asymmetry created was sufficient, and so the calculation was continued through T_1 to the early portion of the bubble reexpansion. At 100 ms (Figure 7.12) a vortex was formed in the water between the expansion and stagnation bubbles. Whether or not the explosion and stagnation bubbles would truly be disconnected during the collapse phase is somewhat in doubt. For example, the pipe, or at least pieces of it (not modeled in this calculation) would still be contained in this region, which is less than 0.5 m thick. It would represent a major discontinuity there, causing the growth of instabilities.

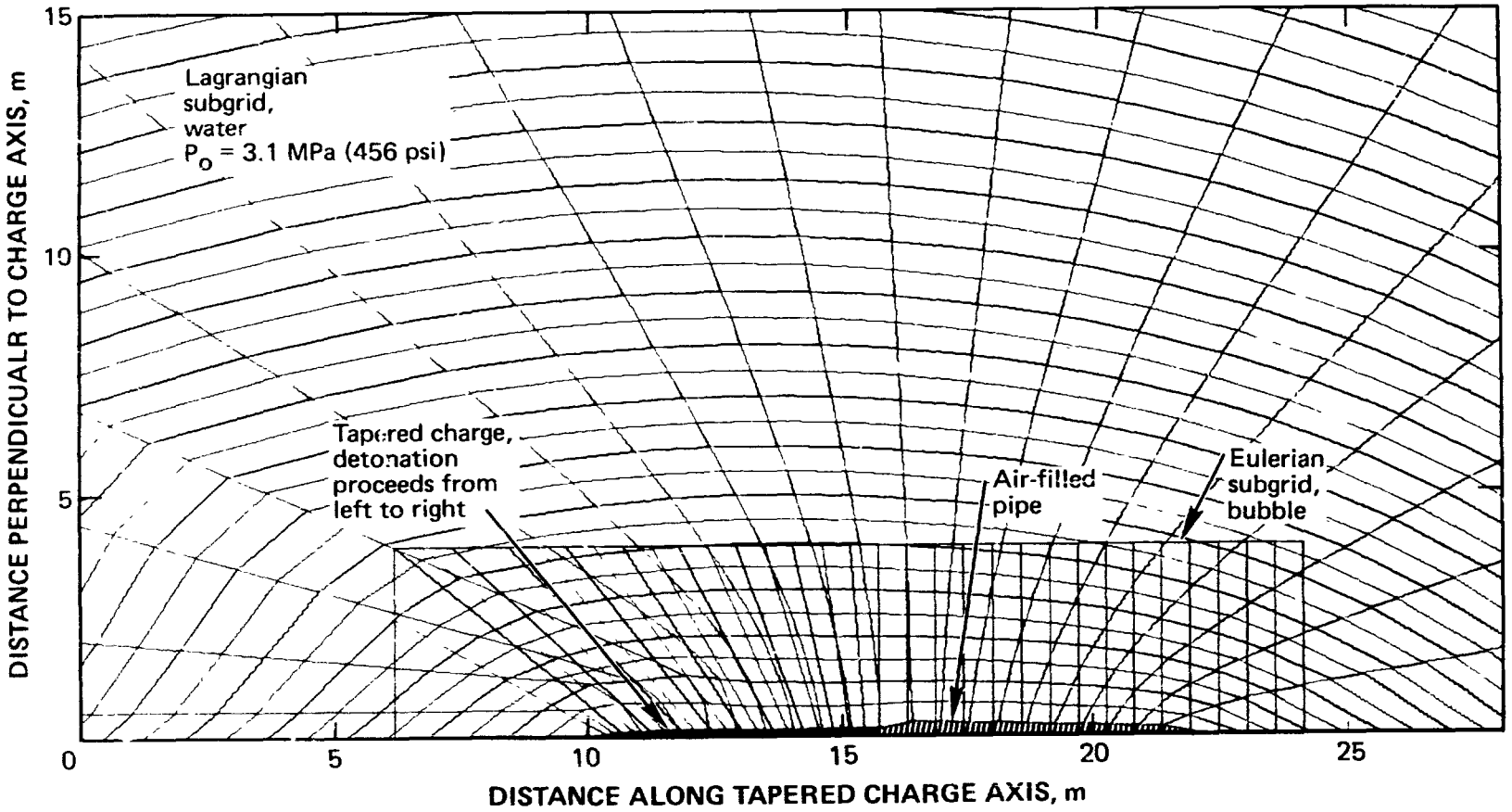

Figure 7.8 Initial zoning of the third tapered charge calculation showing the locations of the charge and the larger air-filled pipe.

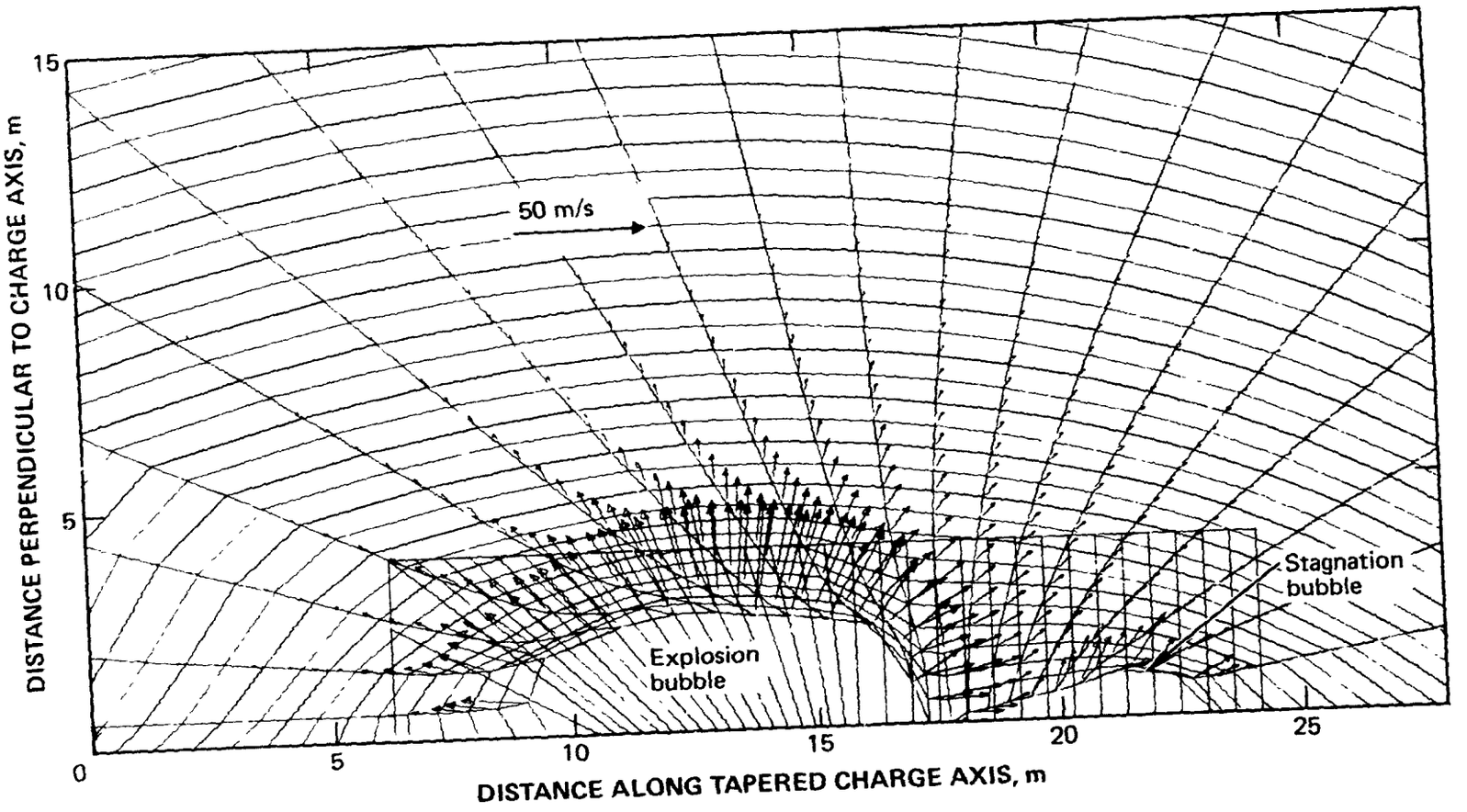

80 11-250

Figure 7.9 Material boundary and vector velocity plot from the third tapered charge calculation at 25 ms.

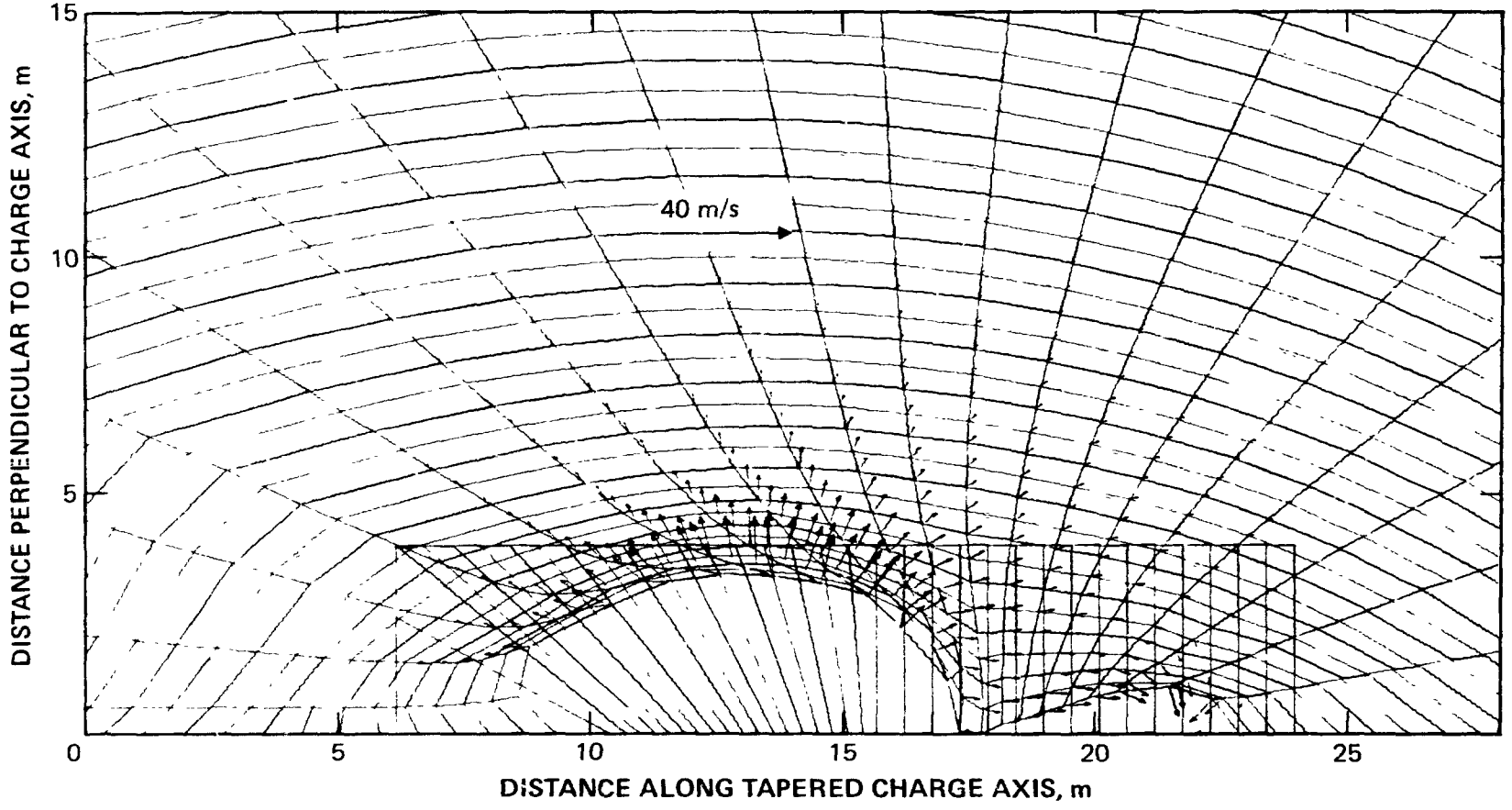

Figure 7.10 Material boundary and vector velocity plot from the third tapered charge calculation at 50 ms.

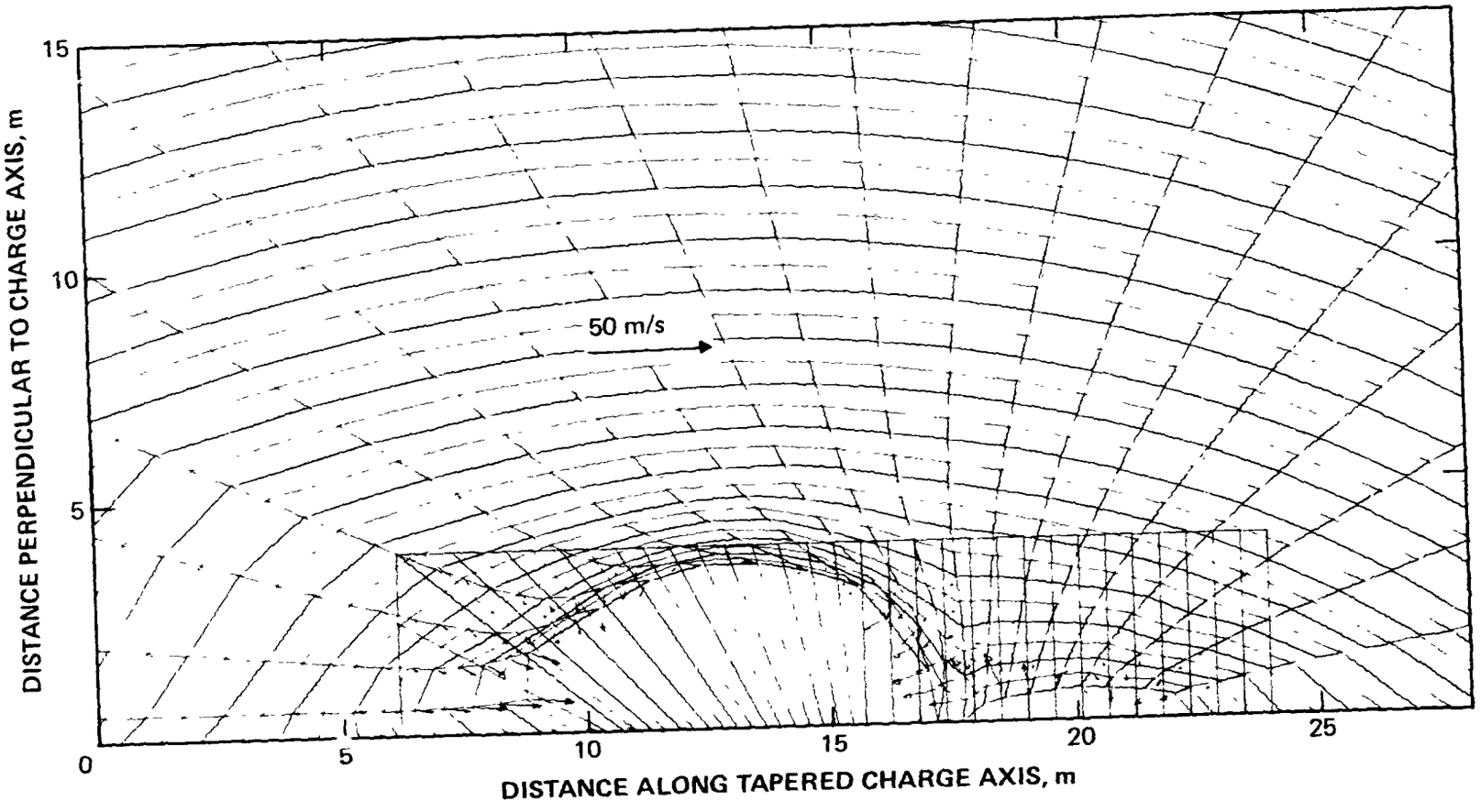

80-11-245

Figure 7.11 Material boundary and vector velocity plot from the third tapered charge calculation at 75 ms.

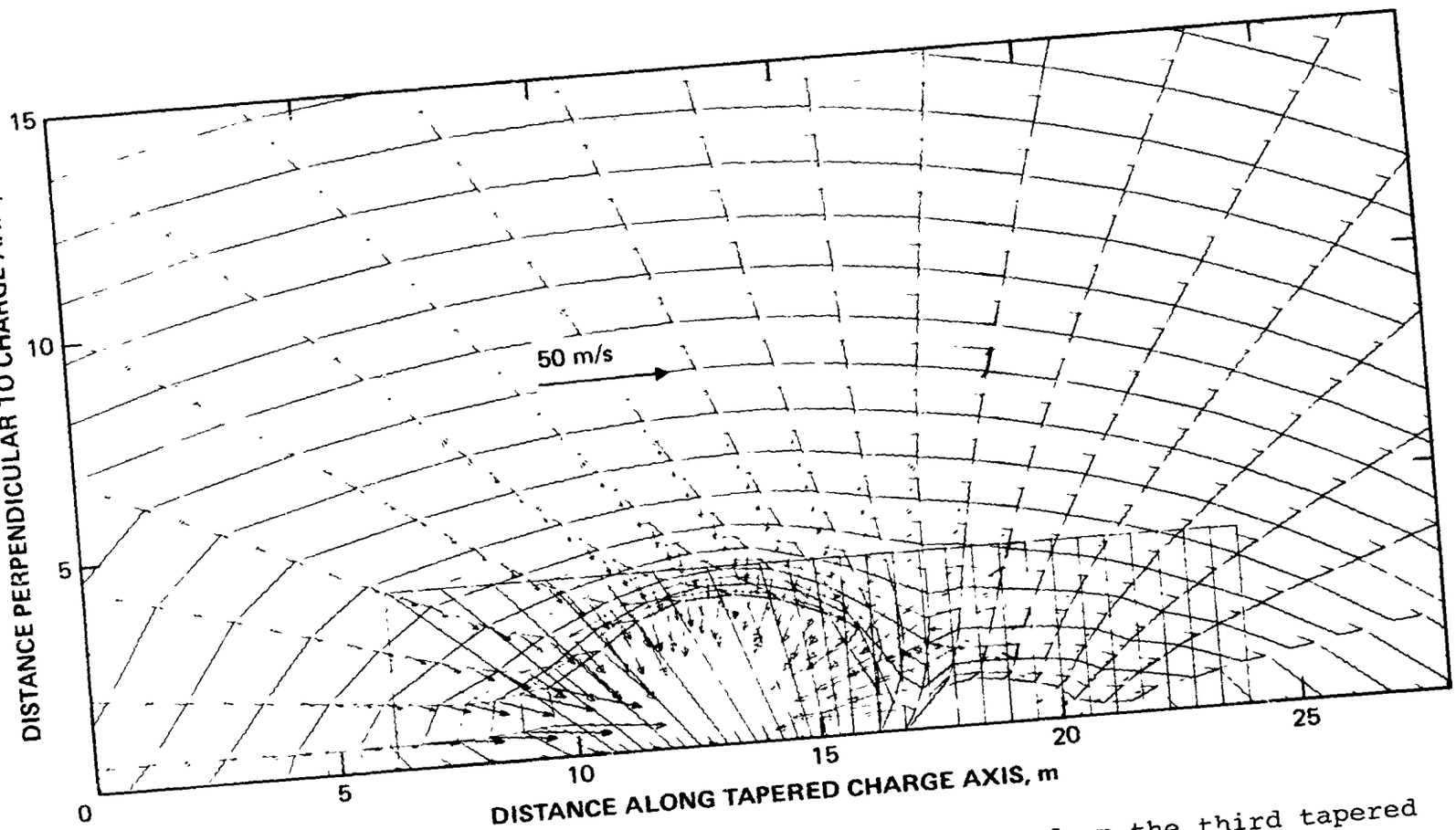

80-11-246

Figure 7.12 Material boundary and vector velocity plot from the third tapered charge calculation at 100 ms.

The results of the inviscid continuum calculation indicate that the collapse and reexpansion of the explosion bubble are controlled largely by the explosion bubble. Figure 7.13 shows the results at 125 ms, and Figure 7.14 shows the results at 140 ms, which is essentially T_1. The bubble collapse point appears to be located off-axis, indicating that the bubble might assume a toroidal shape for a short period of time. Bubble re-expansion is asymmetric, as shown in Figure 7.15 (158 ms).

It was obvious that one or two calculations were insufficient to entirely solve the problem of tapered charge bubble pulse mitigation; an additional effort will be required to address the more difficult problems of turbulent mixing. However, the results are encouraging. It appears that it is possible to enhance instabilities in this manner. Another way to further investigate this concept of bubble pulse mitigation would be to perform a test series using tapered charges in deep water, some with open pipes attached, and some without.

7.2 STEAM-PRODUCING EXPLOSIVES

Two steam-producing explosives were tested by the U.S. Naval Ordnance Laboratory, White Oak, MD (References 30,31). These explosives were aluminized lithium perchlorate ($LiClO_4 \cdot 3H_2O/Al$) and aluminized hydrogen peroxide (H_2O_2/Al). The basic detonation reactions are as follow:

$$3LiClO_4 \cdot 3H_2O + 8Al \rightarrow 3LiCl + 4\ Al_2O_3 + 9H_2O \qquad (7.1)$$

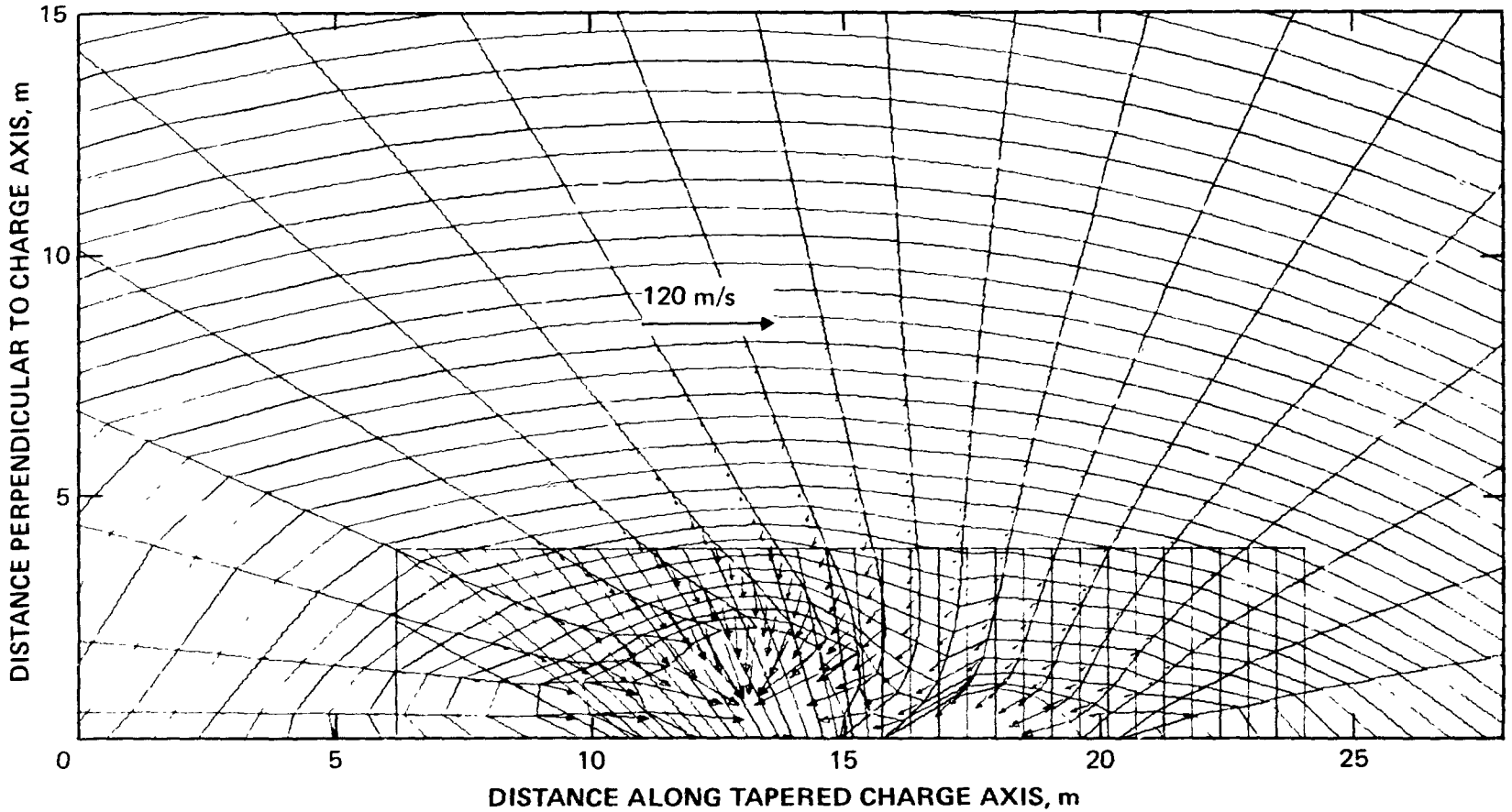

Figure 7.13 Material boundary and vector velocity plot from the third tapered charge calculation at 125 ms.

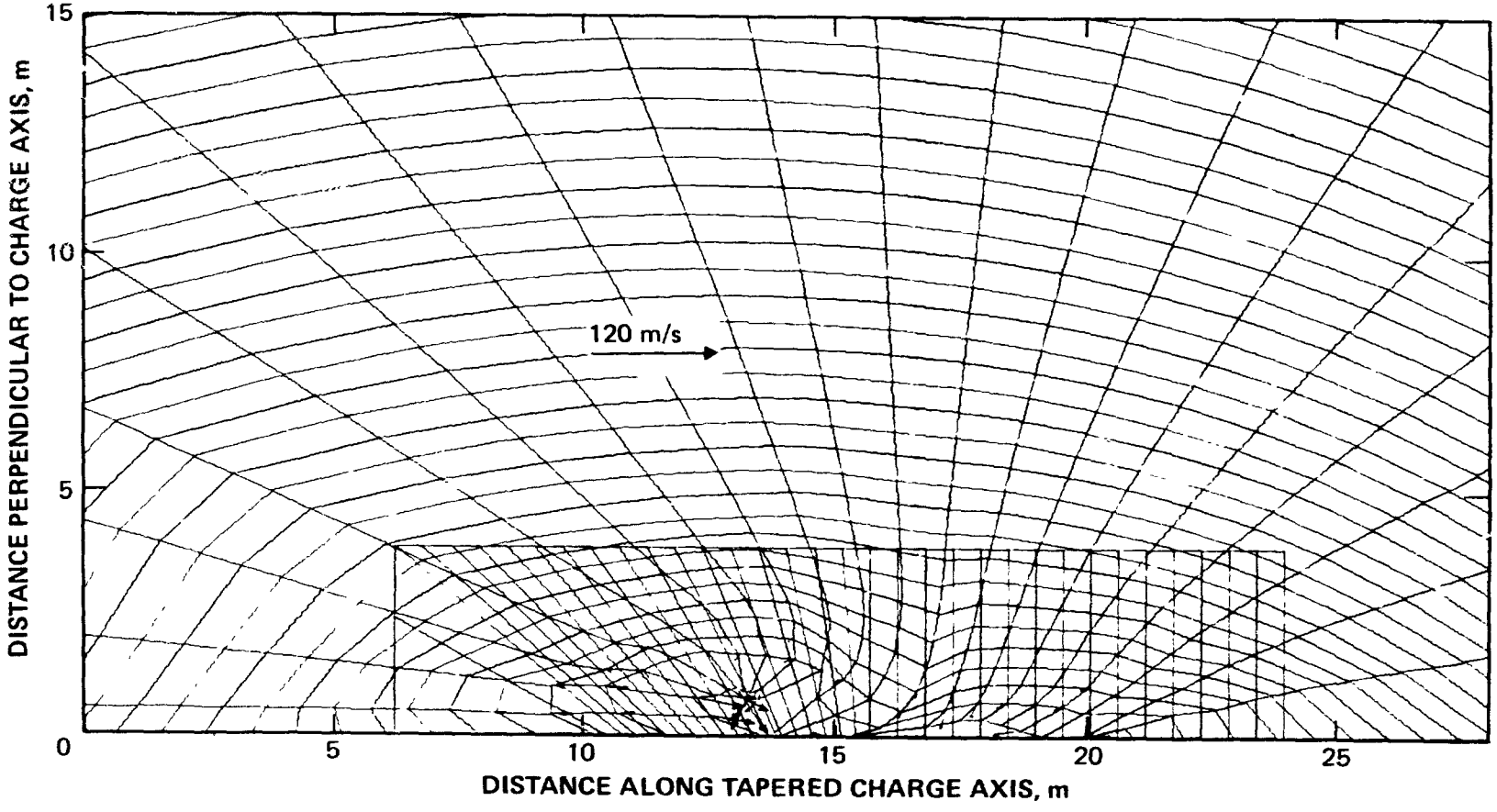

Figure 7.14 Material boundary and vector velocity plot from the third tapered charge calculation at 140 ms, the time of the first bubble minimum.

80-11-248

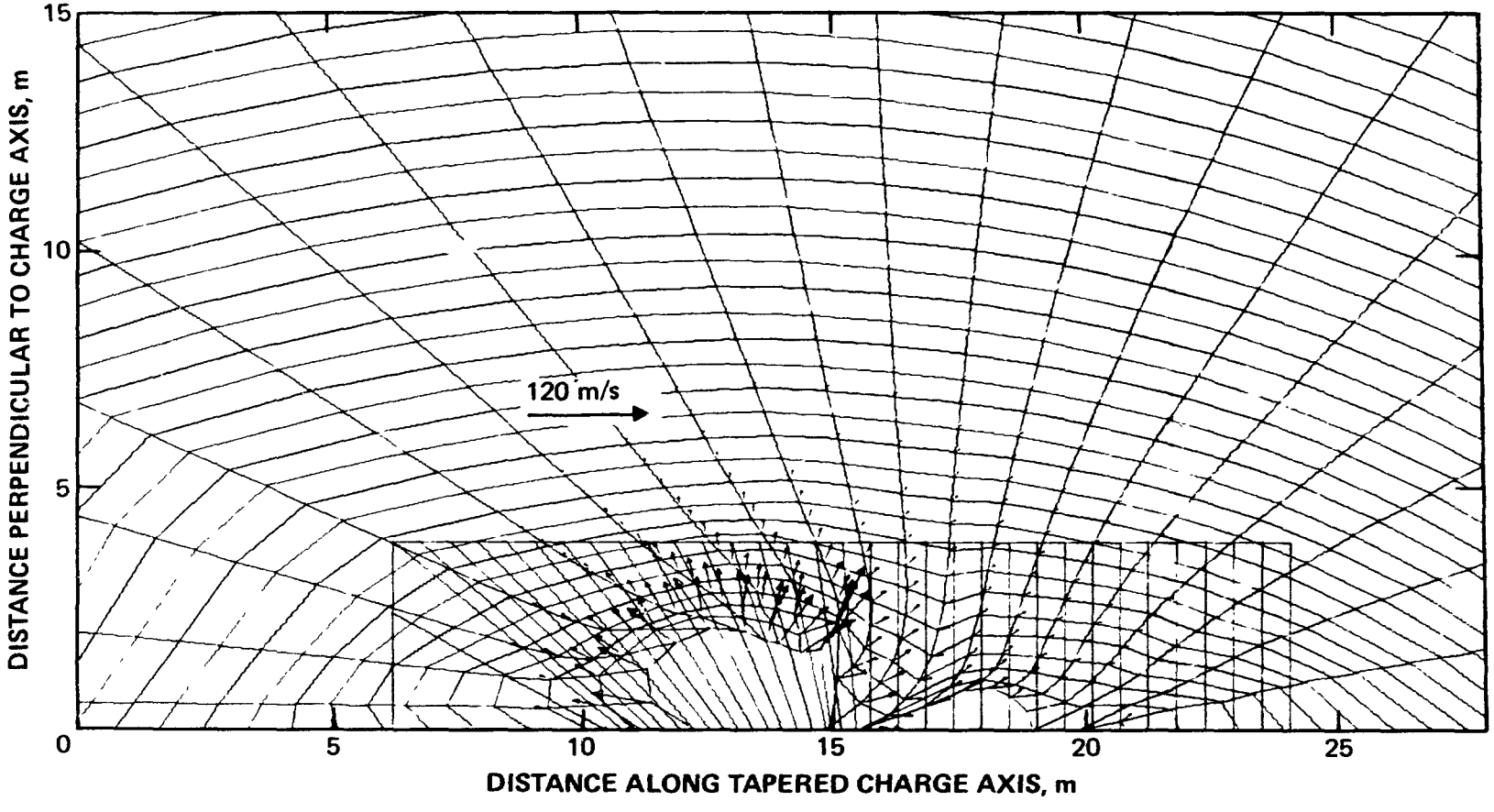

Figure 7.15 Material boundary and vector velocity plot from the third tapered charge calculation at 158 ms.

and

$$3H_2O_2 + 2Al \rightarrow Al_2O_3 + 3H_2O \ . \qquad (7.2)$$

The reaction products other than steam are either solid or are soluble in water; i.e., no noncondensible gasses are formed. The aluminized lithium perchlorate (Lithanol) was found to be by far the safer of the two explosives.

The purpose of the program was to develop an explosive that would generate a steam-filled bubble, as in a nuclear detonation. Bubble pulsation is substantially reduced in the nuclear case, as we discussed in Section 4.4. Small charge tests were performed to obtain values of underwater shock wave parameters in comparison with Pentolite (Reference 30). Larger charge tests, 22.6 kg and 136 kg (50 lb and 300 lb), were performed to examine bubble pulsation and migration characteristics (Reference 31). This section reviews the bubble pulsation characteristics of Lithanol.

Four experiments were conducted in which approximately 23-kg (50-lb) spherical charges of Lithanol were detonated in shallow (46-m-deep) water at a depth of about 30.5 m (100 ft). Four similar Pentolite experiments were also conducted. These test conditions are summarized in Table 7.1. Test results showed that the explosion bubbles formed in these tests were not strongly migrating.

Table 7.1 Experimental conditions for 23-kg (50-lb) spherical Lithanol and Pentolite charges detonated in water at a depth of 30.5 m (100 ft)(data from Reference 31).

Shot No.	Date	Explosive	Total [kg (lb)]	Depth of Burst [m (ft)]
PW-46	9/7/65	Lithanol	23.6 (52.0)	29.9 (98.0)
PW-47	9/7/65	Lithanol	24.2 (53.3)	30.2 (99.0)
PW-48	9/9/65	Lithanol	23.7 (52.2)	29.7 (97.5)
PW-49	9/9/65	Lithanol	23.7 (52.2)	29.7 (97.3)
PW-45	9/7/65	Pentolite	24.4 (53.8)	29.9 (98.1)
PW-50	9/9/65	Pentolite	24.4 (53.8)	29.6 (97.0)
PW-34	8/5/65	Pentolite	23* (50)	30.2 (99.0)
PW-35	8/12/65	Pentolite	23* (50)	30.5 (100.0)

*Nominal charge weight

Bubble pulses were recorded for at least four bubble periods for both Lithanol and Pentolite; Figure 7.16 compares the first three bubble pulses, as presented in Reference 31. As Phillips and Willey point out, "The shape of the first bubble pulse is essentially the same for both explosives. The second and third pulses are considerably different, the Lithanol showing many large spikes as opposed to the generally rounded appearance of the Pentolite pulses. In actuality, even more spikes were visible on the original playouts than could be shown on these tracings." The pressure spikes in the Lithanol waveforms were attributed to water jets impacting water on the opposite side of the bubble, much like the "water hammer" effect in the case of a migrating bubble.

Table 7.2 compares the first four measured bubble periods; the effective energies relative to the first period bubble energy (the cubes of the ratios of T_n to T_1, as in Section 4.4) are also compared. The Pentolite experiments indicate a second period bubble efficiency of about 60 percent; generally, bottom and surface effects appear to help the bubble retain more energy than it would in deep water. Even so, the relative efficiency of the Lithanol-produced bubbles (23-25 percent) is much less than the comparative Pentolite data, on the TNT data in deep water (about 40 percent, Table 4.4). The effects of steam condensation are even more effective on the later bubble periods.

Thus it appears that if Lithanol charges are fired in deep water, bubble oscillation will be damped out even more rapidly than indicated by the above data. Reducing the effective bubble energy by condensing the gasses and dissolving the rest of the

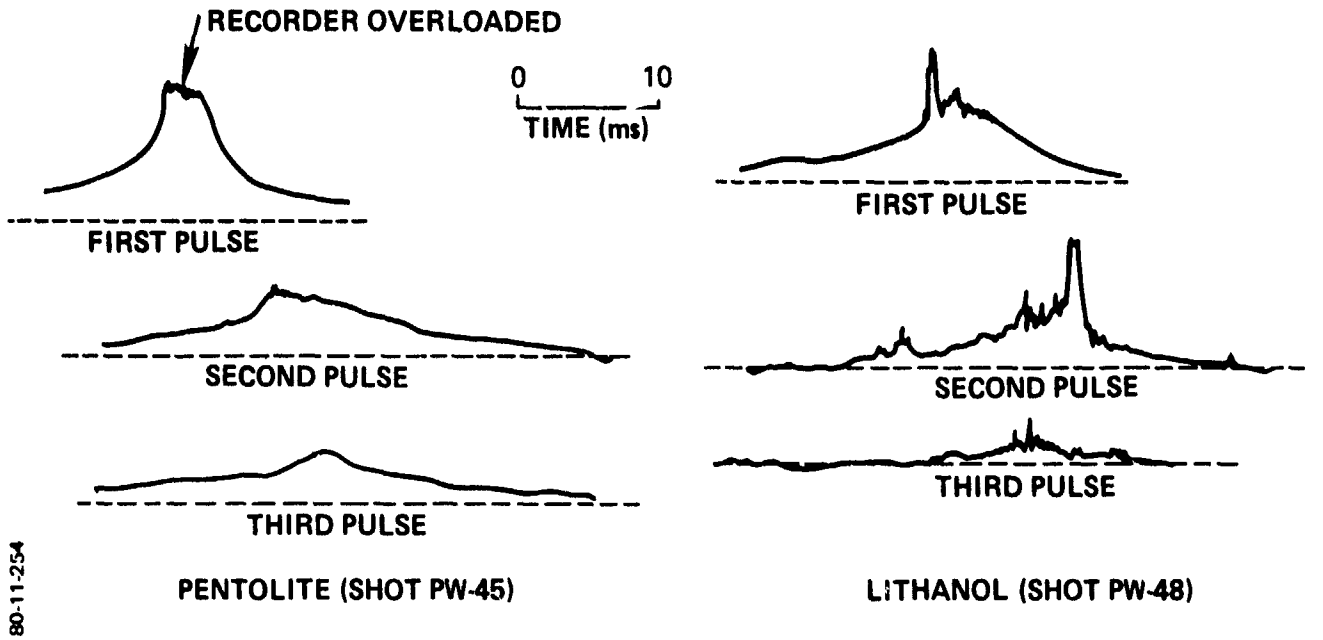

Figure 7.16 Comparison of bubble pulse resulting from a 23-kg (50-lb) spherical Pentolite and Lithanol charge detonation in water at a depth of 30 m (100 ft). The gage depth is 18 m (59 ft).

Table 7 2 Summary of bubble periods and effective bubble energies for 23-kg (50-lb) Pentolite and Lithanol charges detonated in shallow water at a depth of 30.5 m (100 ft).

Shot No.	Explosive	T_1(S)	T_2(S)	T_3(S)	T_4(S)	$\frac{W_{eff}(2)}{W_1}$	$\frac{W_{eff}(3)}{W_1}$	$\frac{W_{eff}(4)}{W_1}$
PW-34	Pentolite	0.273	0.230	0.205	0.176	0.60	0.42	0.27
PW-45	Pentolite	0.281	0.235	0.210	0.186	0.58	0.42	0.29
PW-50	Pentolite	0.283	0.240	0.210	0.188	0.61	0.41	0.29
PW-46	Lithanol	0.354	0.217	0.146	0.110	0.23	0.07	0.03
PW-47	Lithanol	0.360	0.225	0.148	0.116	0.24	0.07	0.03
PW-48	Lithanol	0.358	0.224	0.149	0.108	0.25	0.07	0.03
PW-49	Lithanol	0.358	0.226	0.149	0.096	0.25	0.07	0.02

bubble contents in water will lead to substantially mitigated bubble pulses. Lithanol is a safe, granular explosive, and it appears that tapered charges could be designed to use it. As with asymmetric bubble collapse, further calculations and experiments will be required to quantify this method of bubble pulse mitigation.

SECTION 8

SUMMARY, CONCLUSIONS, AND RECOMMENDATIONS

Physics International Company participated in a Defense Nuclear Agency-sponsored effort to examine bubble pulsation resulting from the deep underwater detonation of tapered high explosive charges. The objectives of the effort were to:

1. Determine if the explosion bubble formed by the deep underwater detonation of a tapered charge would produce bubble pulses.

2. Investigate methods of mitigating or eliminating these bubble pulses, should they occur.

During the effort, nonmigrating bubble pulsation from spherical charge detonations was examined in detail, as much information is available from past efforts. This information includes measurements of bubble pulsation that have resulted in reliable empirical formulas describing this behavior (at least over the first period of oscillation), and theoretical efforts that can predict the general features of bubble expansion and collapse. The current effort extended this work by calculating the expansion and collapse of a spherical explosion bubble from the time of detonation. The computed first bubble pulse compared very well with empirical formulas, even though turbulence, water jetting, heat conduction, and other energy loss mechanisms which operate during the bubble collapse phase were not modeled. Successful computation of spherical explosion bubbles made

the calculational method credible for the more difficult tapered charge explosion bubble calculations, and also provided a detailed look at bubble dynamics.

Major results of the effort, as related to the objectives, are as follow:

1. At least one bubble pulse will occur if a 454-kg (1000-lb) tapered charge is detonated at a depth of 305 m (1000 ft). The strength of this pulse should be almost as great as if the charge had been spherical.

2. Elimination or mitigation of the bubble pulse by injection of propellant gasses into the bubble does not appear feasible because the weight of propellant required would exceed the explosive charge weight by at least a factor of two.

3. Energy loss mechanisms operating during the period of the first bubble minimum absorb the greatest fraction of the bubble energy, even for conventional (i.e., non-nuclear) charges. Therefore, enhancement of bubble asymmetries and turbulence might mitigate further bubble pulsation. An air-filled pipe attached to the tapered charge is one way to encourage the creation of an asymmetric bubble.

4. Steam-producing explosives, developed by the U.S. Navy to simulate the characteristics of the nuclear explosion bubble, have already been shown to be effective in mitigating bubble pulses in shallow water. Analysis suggests that in deep water, use of such explosives would lead to even more effective bubble pulse mitigation.

The following recommendations are made as a result of this initial effort:

1. Turbulence and heat conduction effects must be incorporated into the calculational technique in order to accurately compute multiple bubble pulsation.

2. Deep water testing of small scale (~ 100-lb) tapered charges should be performed. Some of these tests might incorporate air-filled pipes; bubble pulse measurement will show how well this method of bubble pulse mitigation works.

3. Lithanol, a steam-producing explosive, should be further investigated for use in tapered charges.

REFERENCES

1. J. D. Gordon and V. D. Bloodgood, UERD, unpublished report, 1978.

2. J. Downs, "Navy Requirements," Defense Nuclear Agency Strategic Structures Div., Biennial Review Conference, 20-22 March 1979, SRI International, pp. I-13 to I-18.

3. R. E. Fuss, "Response of Submarine Models to Underwater Shock," Defense Nuclear Agency Strategic Structures Div., Biennial Review Conference, 20-22 March 1979, SRI International, pp. III-1 to III-16.

4. A. Misovec, Weidlinger Associates, private communication, July 1980.

5. J. D. Gordon, "Nuclear Underwater Shock Simulation," Defense Nuclear Agency Strategic Structures Div., Biennial Review Conference, 8-10 February 1977, SRI International, pp. V-1 - V-10.

6. P. Thompson, unpublished report, 1961.

7. J. R. Krezel, UERD, private communication, May 1980.

8. E. L. Lee, H. C. Hornig, and J. W. Kury, "Adiabatic Expansion of High Explosive Detonation Products," UCRL 50422, Lawrence Livermore Laboratory, May 1968.

9. ENGINEERING DESIGN HANDBOOK, Explosives Series, Properties of Explosives of Military Interest, AMCP 706-177, U.S. Army Materiel Command, January 1971.

10. L. A. Roslund and N. L. Coleburn, "Hydrodynamic Behavior of HBX-1 and Equation of State of the Detonation Products Below the Chapman-Jouguet State," NOLTR 70-133, United States Naval Ordnance Laboratory, November 1970.

11. W. A. Walker and H. M. Sternberg, "The Chapman-Jouguet Isentrope and the Underwater Shockwave Performance of Pentolite," Fourth Symposium on Detonation, Department of the Navy, Office of Naval Research, 1965.

12. T. R. Butkovich, "The Influence of Water in Rocks on Underground Nuclear Explosions Effects," UCRL-72558, Lawrence Radiation Laboratory, June 1970.

13. Underwater Explosion Research: A Compendium of British and American Reports, Vol. II, The Gas Globe, Department of the Navy, Office of Naval Research, 1950.

14. R. H. Cole, Underwater Explosions, Princeton University Press, 1948.

15. H. G. Snay, "Hydrodynamics of Underwater Explosions," Proc. Symp. on Naval Hydrodynamics, 24-26 September 1956, Publication 515, National Academy of Sciences, National Research Council, 1957, pp. 325-346.

16. J. W. Pritchett, "An Evaluation of Various Theoretical Models for Underwater Explosion Bubble Pulsation," IRA-TR-2-71, Information Research Assoc., April 1971.

17. C. A. Kot, "Intense Underwater Explosions," Astronautica Acta, 17, 4 and 5, 1972, pp. 421-433.

18. M. J. Vander Vorst and A. H. Van Tuyl, "Calculation of Incompressible Underwater Bubble Phenomena by the Marker and Cell Method," Proceedings of the First International Conference on Numerical Ship Hydrodynamics, 20-22 October 1975.

19. M. M. Swisdak, Jr., "Explosion Effects and Properties. Part II - Explosion Effects in Water," NSWC/WOL TR-76-116, Naval Surface Weapons Center, 22 February 1978.

20. L. C. Barrett and C. J. Thorne, "Oscillations of the Gas Bubble Produced by an Underwater Explosion," Technical Report No. 11, University of Utah, January 1952.

21. C. L. Mader, "Compressible Numerical Calculations of Underwater Detonations," LA-4594, Los Alamos Scientific Laboratory, 1971.

22. W. A. Walker, Naval Surface Weapons Center, White Oak Laboratory, private communication, November 1980.

23. H. M. Sternberg and W. A. Walker, "Calculated Flow and Energy Distribution Following Underwater Detonation of a Pentolite Sphere," Physics of Fluids, 14, 9, September 1971, pp. 1869-1878.

24. E. Swift, Jr. and J. C. Decius, "Measurement of Bubble Pulse Phenomena III, Radius and Period Studies," September 1947, in Underwater Explosion Research, A Compendium of British and American Reports, Vol. II, The Gas Globe, Department of the Navy, Office of Naval Research, pp. 552-599.

25. J. P. Slifko, "Pressure-Pulse Characteristics of Deep Explosions as Functions of Depth and Range," NOLTR 67-87, United States Naval Ordnance Laboratory, September 1967.

26. S. L. Hancock, "PISCES 2DELK Finite Difference Equations," TCAM 76-2, Physics International Company, April 1976.

27. M. Riley, "Capabilities for Nuclear UNDEX Simulation against Models at Deep Depths," presentation given at DNA Headquarters, Washington, DC, April, 1980.

28. J. M. Thomsen, F. M. Sauer, D. L. Orphal, and R. R. Franzen, "Simulation of Nuclear Explosion-Generated Stress Waves Utilizing Gun Propellants," Proceedings of the Sixth International Symposium on the Military Applications of Blast Simulation (MABS), 25-29 June 1979.

29. G. P. Sutton, Rocket Propulsion Elements, An Introduction to the Engineering of the Rockets, John Wiley and Sons, N.Y., 1967.

30. D. E. Phillips and T. B. Heathcote, "Underwater Explosion Tests of Two Steam Producing Explosion I. Small Charge Tests," NOLTR-66-79, U. S. Naval Ordnance Laboratory, May 1966.

31. D. E. Phillips and R. L. Willey, "Underwater Explosion Tests of Two Steam Producing Explosives II. 50- and 300-lb Charge Tests," NOLTR-67-7, U. S. Naval Ordnance Laboratory, March 1967.

DISTRIBUTION LIST

DEPARTMENT OF DEFENSE

Assistant to the Secretary of Defense
Atomic Energy
ATTN: Executive Assistant

Defense Intelligence Agency
ATTN: DT-2
ATTN: DB-4C, E. O'Farrell
ATTN: DT-1C
ATTN: RDS-3A
ATTN: DB-4C

Defense Nuclear Agency
2 cy ATTN: SPSS
4 cy ATTN: TITL

Defense Technical Information Center
12 cy ATTN: DD

Department of Defense Explo Safety Board
ATTN: Chairman

Field Command
Defense Nuclear Agency
ATTN: FCT
ATTN: FCP
ATTN: FCTMOF

Field Command
Defense Nuclear Agency
Livermore Branch
ATTN: FCPRL

Field Command Test Directorate
Test Construction Division
Defense Nuclear Agency
ATTN: FCTC

Interservice Nuclear Weapons School
ATTN: TTV

NATO School (SHAPE)
ATTN: U.S. Documents Officer

Under Secretary of Defense for Rsch & Engrg
ATTN: Strategic & Space Sys (OS)

DEPARTMENT OF THE ARMY

Chief of Engineers
Department of the Army
ATTN: DAEN-MCE-D
ATTN: DAEN-RDL

Deputy Chief of Staff for Rsch Dev & Acq
Department of the Army
ATTN: DAMA-CSS-N

Harry Diamond Laboratories
Department of the Army
ATTN: 00100, Commander/Tech Dir/TSO
ATTN: DELHD-I-TL
ATTN: DELHD-N-P

DEPARTMENT OF THE ARMY (Continued)

U.S. Army Ballistic Research Labs
ATTN: DRDAR-BLT, J. Keefer
ATTN: DRDAR-TSB-S
ATTN: DRDAR-BLT, W. Taylor
ATTN: DRDAR-BLV

U.S. Army Concepts Analysis Agency
ATTN: CSSA-ADL

U.S. Army Engr Waterways Exper Station
ATTN: WESSD, J. Jackson
ATTN: R. Whalin
ATTN: J. Strange
ATTN: Library
ATTN: WESSA, W. Flathau

U.S. Army Material & Mechanics Rsch Ctr
ATTN: DRXMR-TE, R. Shea
ATTN: Technical Library

U.S. Army Materiel Dev & Readiness Cmd
ATTN: DRXAM-TL

U.S. Army Missile Command
ATTN: RSIC

U.S. Army Mobility Equip R&D Cmd
ATTN: DRDME-WC

U.S. Army Nuclear & Chemical Agency
ATTN: Library

XVIII Airborne Corps
Department of the Army
ATTN: F. Ford

DEPARTMENT OF THE NAVY

David Taylor Naval Ship R & D Ctr
ATTN: CODE 1740.1
ATTN: Code 172
ATTN: Code 1844
ATTN: Code L42-3
ATTN: Code 1740.6
ATTN: Code 2740
ATTN: Code 174
ATTN: Code 17
ATTN: Code 11
ATTN: Code 173
ATTN: Code 1740.4
2 cy ATTN: Code 1740.5
2 cy ATTN: Code 1740.5, B. Whang
2 cy ATTN: Code 1770.1

Naval Civil Engineering Laboratory
ATTN: Code L08A
ATTN: Code L51, J. Crawford

Naval Coastal Systems Laboratory
3 cy ATTN: Code 741

Naval Electronic Systems Command
ATTN: PME 117-21

DEPARTMENT OF THE NAVY (Continued)

Naval Facilities Engineering Command
ATTN: Code 04B

Naval Material Command
ATTN: MAT 08T-22

Naval Ocean Systems Center
ATTN: Code 4471

Naval Postgraduate School
ATTN: Code 69NE
ATTN: Code 1424, Library

Naval Research Laboratory
ATTN: Code 8406
ATTN: Code 6380
ATTN: Code 8440, G. O'Hara
ATTN: Code 8445
ATTN: Code 8301
ATTN: Code 8100
ATTN: Code 2627

Naval Sea Systems Command
ATTN: SEA-0351
ATTN: SEA-09G53
2 cy ATTN: SEA-08
2 cy ATTN: SEA-323
4 cy ATTN: SEA-3221

Naval Surface Weapons Center
ATTN: Code R14, I. Blatstein
ATTN: Code R10
ATTN: Code R13
ATTN: Code F31
ATTN: Code F34
ATTN: Code R15
ATTN: Code R14

Naval Surface Weapons Center
ATTN: Tech Library & Info Svcs Br

Naval Weapons Center
ATTN: Code 233

Naval Weapons Evaluation Facility
ATTN: Code 210
ATTN: Code 10
ATTN: G. Binns

Naval Weapons Support Center
2 cy ATTN: Code 70553, D. Moore

New London Laboratory
Naval Underwater Systems Center
ATTN: Code 401, J. Kalinowski
ATTN: Code 401, J. Patel

Newport Laboratory
Naval Underwater Systems Center
ATTN: Code 363, P. Paranzino
ATTN: Code EM

Office of Naval Research
2 cy ATTN: Code 474, N. Perrone

DEPARTMENT OF THE NAVY (Continued)

Office of the Chief of Naval Operations
ATTN: OP 981
ATTN: OP 03EG
ATTN: OP 953
ATTN: OP 981N1
ATTN: OP 21
ATTN: OP 65
ATTN: OP 982
ATTN: OP 987
ATTN: OP 37
ATTN: OP 951
ATTN: OP 223
ATTN: OP 957E
ATTN: OP 225
ATTN: OP 605D5

Strategic Systems Project Office
Department of the Navy
ATTN: NSP-272
ATTN: NSP-43

DEPARTMENT OF THE AIR FORCE

Air Force Geophysics Laboratory
ATTN: LWW, K. Thompson

Air Force Institute of Technology
ATTN: Library

Air Force Systems Command
ATTN: DLW

Air Force Weapons Laboratory
Air Force Systems Command
ATTN: NTE, M. Plamondon
ATTN: NTES-C, R. Henny
ATTN: SUL
ATTN: DEX

Air University Library
Department of the Air Force
ATTN: AUL-LSE

Assistant Chief of Staff
Intelligence
Department of the Air Force
ATTN: INT

Ballistic Missile Office
Air Force Systems Command
ATTN: SYDT

Deputy Chief of Staff
Research, Development, & Acq
Department of the Air Force
ATTN: AFRDQI

Strategic Air Command
Department of the Air Force
ATTN: NRI STINFO, Library

DEPARTMENT OF ENERGY

Department of Energy
Albuquerque Operations Office
ATTN: CTID

DEPARTMENT OF ENERGY (Continued)

Department of Energy
ATTN: OMA/RD&T

Department of Energy
Nevada Operations Office
ATTN: Mail & Records for Technical Library

Lovelace Biomedical & Env Rsch Inst, Inc
ATTN: D. Richmond

OTHER GOVERNMENT AGENCIES

Central Intelligence Agency
ATTN: OSWR/NED

Federal Emergency Management Agency
National Sec Ofc Mitigation & Rsch
ATTN: Assistant Associated Dir

DEPARTMENT OF ENERGY CONTRACTORS

Lawrence Livermore National Lab
ATTN: Technical Info Dept, Library

Los Alamos National Laboratory
ATTN: MS 670, J. Hopkins
ATTN: MS 364

Sandia Laboratories
Livermore Laboratory
ATTN: Library & Security Classification Div

Sandia National Lab
ATTN: 3141

DEPARTMENT OF DEFENSE CONTRACTORS

Aerospace Corp
ATTN: Technical Information Services

Applied Research Associates, Inc
ATTN: N. Higgins
ATTN: J. Bratton

BDM Corp
ATTN: T. Neighbors
ATTN: Corporate Library

Boeing Co
ATTN: Aerospace Library

Bolt Beranek & Newman, Inc
ATTN: R. Haberman

California Research & Technology, Inc
ATTN: M. Rosenblatt

California Research & Technology, Inc
ATTN: D. Orphal

Columbia University
ATTN: H. Bleich
ATTN: F. Dimaggio

FG&G Wash. Analytical Svcs Ctr, Inc
ATTN: Library

Electromech Sys of New Mexico, Inc
ATTN: L. Piper

DEPARTMENT OF DEFENSE CONTRACTORS (Continued)

Electromech Sys of New Mexico, Inc
ATTN: R. Shunk

Eric H. Wang
Civil Engineering Rsch Fac
University of New Mexico
ATTN: N. Baum

General Dynamics Corp
ATTN: J. Mador
ATTN: J. Miller
2 cy ATTN: M. Pakstys

Geocenters, Inc
ATTN: E. Marram

H-Tech Labs, Inc
ATTN: B. Hartenbaum

IIT Research Institute
ATTN: Documents Library

Institute for Defense Analyses
ATTN: Classified Library

JAYCOR
ATTN: H. Linnerud

Kaman Avidyne
ATTN: Library

Kaman Sciences Corp
ATTN: Library

Kaman Tempo
ATTN: DASIAC

Lockheed Missiles & Space Co, Inc
ATTN: T. Geers
ATTN: Technical Library

Lockheed Missiles & Space Co, Inc
ATTN: TIC-Library

M & T Company
ATTN: D. McNaight

Martin Marietta Corp
ATTN: G. Freyer

University of New Mexico
ATTN: CERF, G. Leigh
ATTN: CERF, N. Baum

NAF Engineering Associates, Inc
ATTN: R. Belsheim

Pacific-Sierra Research Corp
ATTN: H. Brode

Pacifica Technology
ATTN: G. Kent

Physics Applications, Inc
ATTN: C. Vincent
ATTN: F. Ford

DEPARTMENT OF DEFENSE CONTRACTORS (Continued)

Physics International Co
ATTN: E. Moore
ATTN: Technical Library
ATTN: F. Sauer
4 cy ATTN: J. Thomsen
4 cy ATTN: S. Ruhl

R & D Associates
ATTN: R. Port
ATTN: Technical Information Center
ATTN: J. Lewis
ATTN: P. Haas

Science Applications, Inc
ATTN: J. Dishon

Science Applications, Inc
ATTN: Technical Library

Science Applications, Inc
ATTN: W. Layson
ATTN: J. Cockayne
ATTN: M. Knasel

Southwest Research Institute
ATTN: A. Wenzel
ATTN: W. Baker

SRI International
ATTN: G. Abrahamson
ATTN: B. Gasten
ATTN: A. Florence

DEPARTMENT OF DEFENSE CONTRACTORS (Continued)

Systems, Science & Software, Inc
ATTN: Library
ATTN: D. Grine

Tetra Tech, Inc
ATTN: L. Hwang

TRW Defense & Space Sys Group
ATTN: D. Baer
ATTN: Technical Information Center
2 cy ATTN: N. Lipner

TRW Defense & Space Sys Group
ATTN: P. Dai
ATTN: E. Wong

Weidlinger Assoc, Consulting Engrg
3 cy ATTN: M. Baron

Weidlinger Assoc, Consulting Engrg
ATTN: J. Isenberg

Weidlinger Assoc, Consulting Engrg
ATTN: A. Misovec